Vector bosons and jets in proton collisions

Paolo Azzurri[ORCID]

INFN Pisa, Largo B. Pontecorvo 3, 56127 Pisa, Italy

Marek Schönherr[ORCID]

Institute for Particle Physics Phenomenology, Durham University,
Durham DH1 3LE, United Kingdom

Alessandro Tricoli[ORCID]

Brookhaven National Laboratory, Upton, New York 11973, USA

(published 3 June 2021)

Events with vector bosons produced in association with jets have been extensively studied at hadron colliders and provide high-accuracy tests of the standard model. A good understanding of these processes is of paramount importance for precision Higgs physics, as well as for searches for new physics. In particular, associated production of γ, W, or Z bosons with light-flavor and heavy-flavor jets is a powerful tool for testing perturbative QCD calculations, Monte Carlo event generators, and can also constrain the parametrizations used to describe the parton content of the proton. Furthermore, events with a W or Z boson produced with two well-separated jets can be used to distinguish between electroweak and strong production mechanisms, and to set limits on contributions of physics beyond the standard model. This review summarizes the historical theoretical developments and the state-of-the-art in the modeling of vector-boson-plus-jet physics while focusing on experimental results by the LHC collaborations in run 1 and run 2 and including comparisons with recent measurements at the Tevatron.

CONTENTS

I. INTRODUCTION

Vector boson production associated with hadronic jets is one of the most important classes of processes that can be measured at hadron colliders. While the vector bosons, i.e., photons, Z, and W bosons, are the carriers of electroweak interactions, associated hadronic jets stem from the presence of strong interactions as a result of the process of fragmentation and hadronization of energetic partons (quarks and gluons). Figure 1 shows a proton collision event recorded by the CMS experiment with a Z boson produced in association with two jets. The two jets were identified as likely originating from charm quarks. Each jet is a spray of hadronic particles collimated in the general direction of the initial parton, carrying the bulk of its total energy and transverse momentum.

The study of $V +$ jets ($V = \gamma$, W, Z) events constitutes an ideal probe for testing quantum chromodynamics (QCD) and electroweak (EW) interactions as well as a major source of
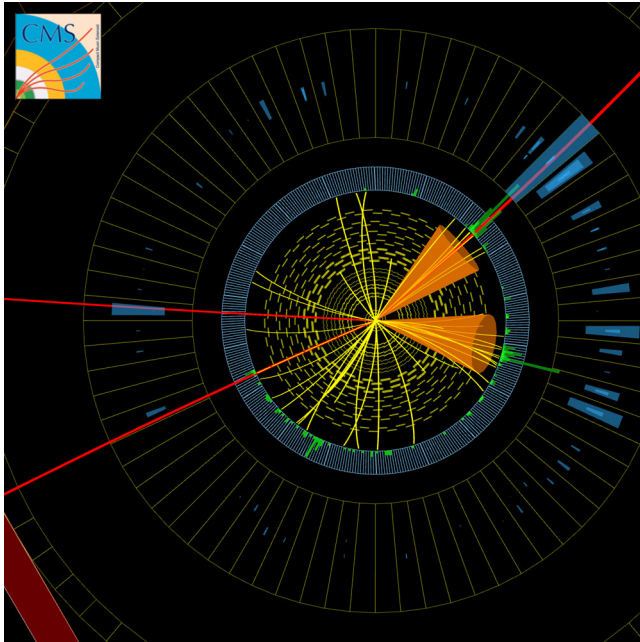
FIG. 1. A vector-boson-plus-jet event recorded by the CMS experiment in proton collisions at 13 TeV center-of-mass energy. The two solid lines on the left correspond to two reconstructed muons from the decay of a Z boson. The two cones on the right contain two collimated sprays of particles reconstructed as hadronic jets. The internal composition of the jets indicate that both are likely to have originated from charm quarks, and one of them contains a muon from a displaced hadronic decay. From CMS Collaboration, 2019a.

backgrounds to searches for new physics. Measurements of $V + $ jets also validate the adequacy of the approximations used in theoretical calculations and models used for background estimates in precision measurements. For example, the modeling of $V + $ jets has a significant impact on studies of the Higgs boson and top-quark sectors of the standard model (SM), or in searches for physics beyond the standard model. Thanks to their large cross sections, the colorless nature of the γ, W, and Z bosons as carriers of electromagnetic and weak forces, respectively, and their high sample purities, accurate studies of $V + $ jets are of paramount importance for the success of a hadron collider physics program.

More specifically, a precise understanding of $\gamma + $ jet production and its modeling plays an important role in new physics searches, as $\gamma + $ jets constitute a background to the production of high-mass resonances in the search for excited quarks in quark-compositeness models or quantum black holes in models of extra spatial dimensions, among others. Similarly, reliable $W/Z + $ jet calculations are important to correctly model the SM backgrounds in many searches of new particles in processes producing one or two charged leptons[1] with associated multijets, as they occur in supersymmetric theories, among others.

---

[1]In the review "charged lepton" refers to an electron or a muon, unless explicitly stated otherwise, since $W/Z + $ jet measurements have primarily focused on electronic and muonic decay channels of the W and Z bosons.

Vector boson production processes associated with jets containing heavy-flavor hadrons play important roles in several measurements at hadron colliders. From them, the dynamics of the underlying heavy-flavor quark processes can be inferred. In particular, they can give access to the heavy-flavor content of the proton, which is a limiting factor in several analyses at the Large Hadron Collider (LHC). In addition, a detailed understanding of heavy-flavor quark dynamics in these processes was of paramount importance to the recent observation of the Higgs boson decay into a b-quark pair (ATLAS Collaboration, 2018d; CMS Collaboration, 2018f) and is vital for many new physics searches.

In the last 30 years many measurements of $V + $ jet event properties have been carried out starting with the UA1 and UA2 experiments (Arnison $et\ al.$, 1983a, 1983b, 1983c, 1984a, 1984b; Bagnaia $et\ al.$, 1983, 1984; Banner $et\ al.$, 1983; Appel $et\ al.$, 1986) at the Super Proton–Antiproton Synchrotron (Sp$\bar{p}$S). Extensive measurements of such processes by the CDF and the D0 collaborations at the Tevatron have prompted significant development in the understanding of the underlying QCD dynamics, including new techniques for calculating high-precision theoretical predictions as well as nonperturbative modeling in Monte Carlo (MC) event generators. Tevatron data provided an important stepping-stone for $V + $ jet analyses at the LHC, despite the large difference in center-of-mass energies between the two colliders. The measurements carried out by the LHC collaborations, ATLAS, CMS, and LHCb, in LHC run 1 and run 2 have motivated further developments in the theoretical description of such processes in both the QCD and EW sectors. The wide range of center-of-mass energies, from 1.96 TeV in $p\bar{p}$ collisions at the Tevatron to 7, 8, and 13 TeV in pp collisions at the LHC, allows one to explore QCD dynamics in different energy regimes over a broad range of energy scales. The ranges of $V + $ jet cross sections at the LHC compared to inclusive vector boson production and other SM processes are shown in Fig. 2.

The underlying physics for the production of $V + $ jet processes at the LHC cannot be considered a simple rescaling of scattering processes at the Tevatron. The differing beam types and center-of-mass energies between the two colliders lead to a different relative importance of the various underlying production mechanisms and their associated phenomenology. More specifically, the LHC reaches far larger energy scales Q than the Tevatron thanks to the higher beam energies, while it can simultaneously probe a lower Bjorken-x range. The inclusive production of a W boson at the LHC is dominated by events with a Bjorken x in the range 10^{-4}–10^{-1} and $Q^2 \approx M_W^2$, while the exclusive production of a W boson and at least one jet is shifted to larger values of x, with the majority of events in the x range of 10^{-2}–3×10^{-1} and larger Q^2 values.

As a consequence the two colliders are sensitive to particulars of the parametrizations of the parton densities inside the proton, and their collision events are subject to different production mechanisms. For instance, at the Tevatron $V + $ jet processes have a significant valence-quark contribution from $q\bar{q}$ interactions, where the quark (q)
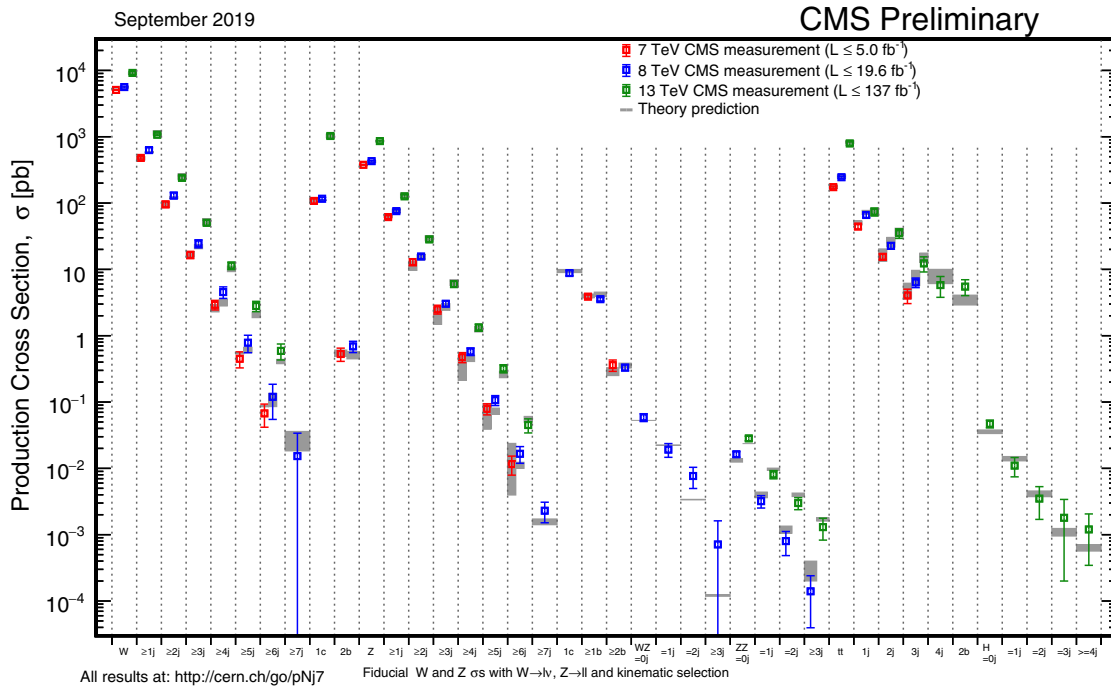
FIG. 2.   Summary of production cross sections for processes with a W or Z boson produced in association with light- or heavy-flavor jets studied at different center-of-mass energies at the LHC, and their cross sections compared to other SM processes. From CMS Collaboration, 2020f.

originates from the colliding proton and the antiquark ($\bar{q}$) originates from the colliding antiproton. On the other hand, at the LHC there are significant gluon (g) and sea-quark contributions, including $\bar{q}g$, qg, and gg interactions. For example, the $Z + 2$ jet production, i.e., the $qg \to Z + qg$ process, contributes around 75% at the LHC, but only around 25% at the Tevatron. At the LHC the relative fraction of subprocesses initiated by $qq/q\bar{q}/\bar{q}\,\bar{q}$, $gq/g\bar{q}$, and gg interactions varies with the number of associated jet production in the final state. In $W +$ jet processes the fraction of $qq/q\bar{q}/\bar{q}\,\bar{q}$ ($gq/g\bar{q}$) subprocesses increases (decreases) from 18% (82%) with one jet to 21% (73%), 23% (70%), and 25% (67%) with two, three, and four jets, respectively, while for gg subprocesses it increases from 0% with one jet to 6%, 7%, and 8% with two, three, and four jets; see Kom and Stirling (2010).

As a result of the LHC sensitivity to large contributions of sea-quark and gluon densities, $V +$ jet cross sections are far larger at the LHC than at the Tevatron. For example, the $W + 4$-jet cross section at the LHC is 500 times larger than that at the Tevatron with a similar kinematic selection, while the inclusive $Z + b$ cross section at the LHC is 50 times larger than that at the Tevatron (Campbell et al., 2004).

This review examines the evolution of the theoretical developments in the description of $V +$ jets physics for the Tevatron and the LHC, focusing on the recent achievements for LHC run 1 and run 2. An overview of experimental analysis techniques to identify $V +$ jet events and reconstruct their kinematics is given together with a selection of measurements at different center-of-mass

energies. The review of experimental results of $W/Z +$ jets focuses on the leptonic decays of the W and Z bosons. Comparisons between experimental measurements and cutting-edge theoretical predictions are highlighted. This review starts with a discussion of the production of vector bosons associated with light-flavor jets in Sec. II, followed by a presentation of the EW production of vector bosons in Sec. III and the associated production of a vector boson and heavy-flavor jets, i.e., $V + b$ or c jets, in Sec. IV. Each of these sections starts with a discussion of the theoretical predictions for the different $V +$ jet production modes, specifically highlighting the most recent developments on higher-order calculations and MC event generators, then proceeds with the discussion of the experimental results and their comparison with the theory. In this review we do not attempt to accomplish the arduous task of exhaustively presenting all available measurements but strive to highlight selected examples of measurements that give specific insight into $V +$ jet production dynamics. The numerous measurements of $V +$ jets make it difficult to select a representative set of results; therefore, we choose to provide a balanced representation of the different types of measurements and the different experiments at the Tevatron and the LHC. Section V illustrates some examples of analyses and interpretations of experimental $V +$ jet results, for example, for tuning of MC generators, constraining the proton parton densities, and setting limits on anomalous contributions to SM interactions. The review concludes in Sec. VI with a summary and an outlook for $V +$ jet analyses at future LHC runs and future colliders.
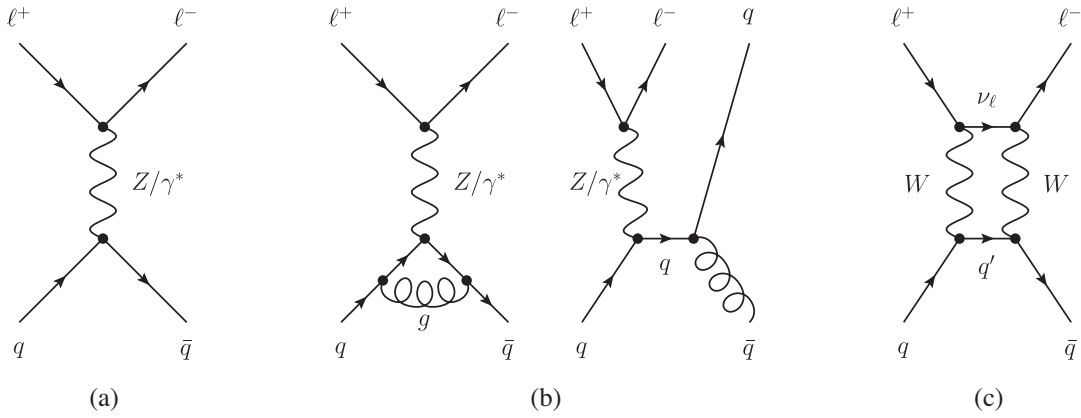
FIG. 3.   Representative Feynman diagrams for the production of a pair of charged leptons (a) at LO, and representative contributions at (b) NLO QCD and (c) NLO EW.
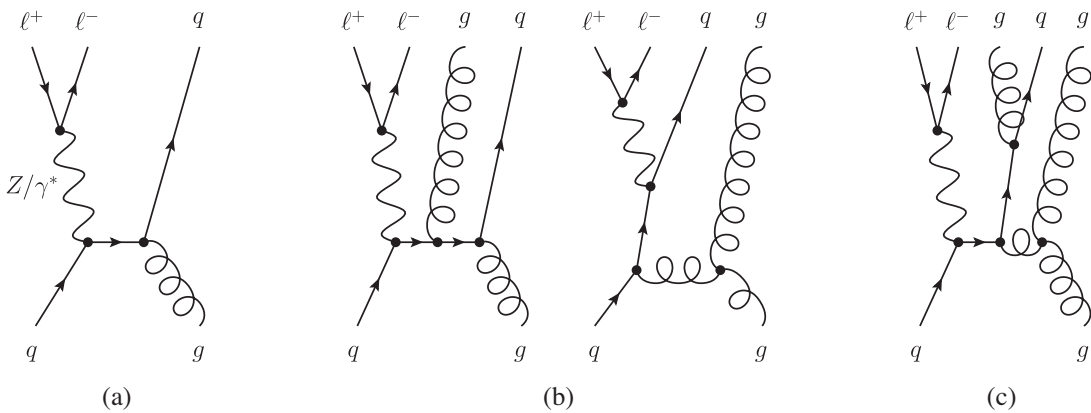

FIG. 4.   Representative Feynman diagrams for the production of a pair of charged leptons associated with (a) one jet, (b) two jets, and (c) three jets at LO.

II. ASSOCIATED PRODUCTION OF A VECTOR BOSON AND LIGHT-FLAVOR JETS

A. Theoretical predictions

The production of a single vector boson, γ, W, or Z, is the class of processes with the largest cross sections among the electroweak processes at hadron colliders. While the massive vector bosons W and Z can be produced by simple quark-antiquark annihilation without additional final-state partons at leading order (LO), photons, as the massless gauge boson of QED, are measurable only when they have finite transverse momentum and therefore always need at least one parton to recoil against.

To set the stage, the Feynman diagrams of the dominant leading and next-to-leading order (NLO), in both the strong and the electroweak couplings α_s and α, production processes of inclusive massive gauge bosons are detailed in Fig. 3. A substantial fraction of all events with single massive vector bosons are accompanied by additional hadronic jet activity. These processes are of specific interest due to their clean signature and the relative precision with which they can be calculated in the standard model. Representative leading-order Feynman diagrams are shown in Fig. 4.

Single-photon production, on the other hand, is always accompanied by hadronic recoil, as previously discussed. Figure 5 shows representative diagrams of photon production associated with jets.

1. Higher-order computations

The effort to increase the available accuracy of the theoretical predictions[2] for inclusive W- and Z-boson production processes started early. While the first results beyond leading-order accuracy date back 40 years (Altarelli, Ellis, and Martinelli, 1979), the current standard sees the inclusive cross sections determined at next-to-next-to-leading order (NNLO) in QCD with NLO EW corrections, i.e., NNLO QCD + NLO EW (Hamberg, van Neerven, and Matsuura, 1991; Anastasiou *et al.*, 2004; Melnikov and Petriello, 2006a, 2006b; Catani *et al.*, 2009; Gavin *et al.*, 2011; Li and Petriello, 2012). The NNLO QCD-EW mixed contributions of $\mathcal{O}(\alpha_s \alpha)$ are known in the pole approximation (Dittmaier, Huss, and Schwinn, 2014), which is valid in the region where the invariant mass of

---

[2]Theoretical uncertainties are typically estimated by varying all unphysical scales of the calculation, e.g., the renormalization and factorization scale. The resulting quoted error estimate has, however, no statistical interpretation.
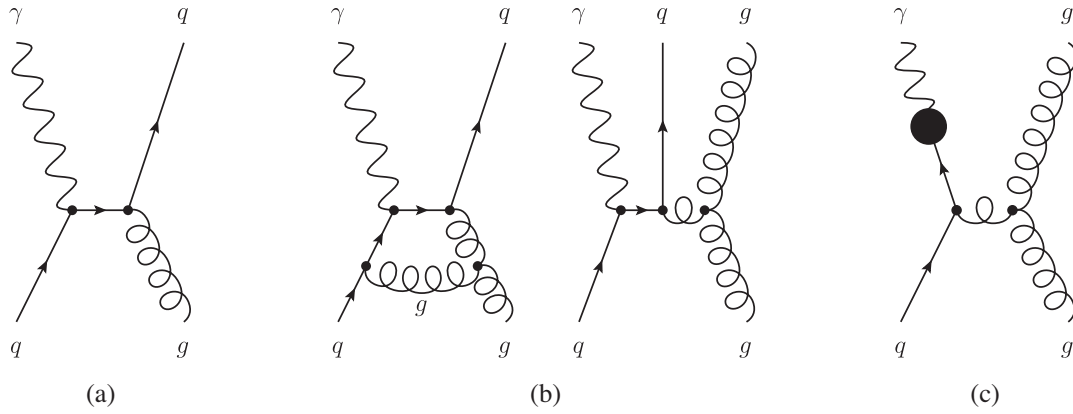
FIG. 5.   Representative Feynman diagrams for (a) the production of a photon at LO, (b) representative contributions at NLO QCD, and (c) photon production from quark fragmentation that enters at the same order.

the charged-lepton pair is close to the respective gauge boson's mass. Figure 6 (left panel) displays such a state-of-the-art calculation for the inclusive transverse momentum of the positively charged lepton in the inclusive production of a charged-lepton pair, showing the relatively large corrections received through the higher-order QCD corrections with respect to the leading-order calculation.

Another key inclusive experimental observable is the transverse-momentum distribution of the vector boson itself. Its description, however, depends on an accurate description of its recoil. It thus vanishes identically at leading order and starts only at $\mathcal{O}(\alpha_s)$ or $\mathcal{O}(\alpha)$. Its precise description is further complicated by large logarithms in the small-transverse-momentum region, as a result of an infrared divergence at $p_T = 0$, which spoil the convergence of the perturbative expansion in the coupling parameters. As the same logarithms reappear order by order, however, they can be resummed, and the respective results are detailed in Sec. II.A.2. In the medium- to large-transverse-momentum region, a fixed-order expansion is sufficient to achieve percent-level accuracy.

While the QCD two-loop amplitudes have been available for some time (Garland *et al.*, 2002a, 2002b; Moch, Uwer, and Weinzierl, 2002), the inception of novel subtraction formalisms (Kosower, 1998; Gehrmann-De Ridder, Gehrmann, and Glover, 2005; Catani and Grazzini, 2007; Currie, Glover, and Wells, 2013; Boughezal, Focke, Giele *et al.*, 2015; Gaunt *et al.*, 2015; Catani *et al.*, 2019) along with the computational frameworks that are able to deal with the complexity of the infrared structure of such a calculation have only recently become available. They paved the way for precise NNLO QCD calculations for this kinematic region (Boughezal, Focke, Liu, and Petriello, 2015; Gauld *et al.*, 2017; Boughezal *et al.*, 2016; Boughezal, Liu, and Petriello, 2016a, 2016b; Gehrmann-De Ridder *et al.*, 2016a, 2016b, 2016c, 2018, 2019; Campbell, Ellis, and Williams, 2017b), as is detailed in Fig. 6 (right panels).

At the same time, the electroweak corrections for both the vector boson transverse momentum and vector-boson-plus-jet production in general are also known (Denner *et al.*, 2011; Kühn *et al.*, 2005a, 2007, 2008; Kühn, Lindert,
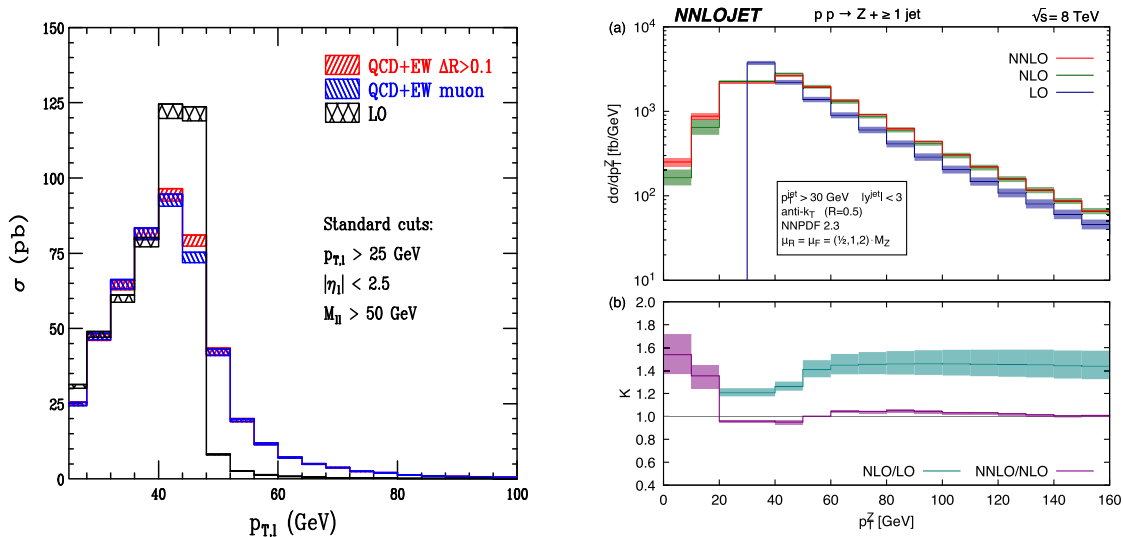

FIG. 6.   Left panel: charged-lepton transverse momentum in the inclusive production of two charged leptons at NNLO QCD plus NLO EW. From Li and Petriello, 2012. Right panels: transverse momentum of two charged leptons in the production of two charged leptons associated with at least one jet at LO, NLO, and NNLO QCD. From Gehrmann-De Ridder *et al.*, 2016b.

Pozzorini *et al.*, 2005; Actis *et al.*, 2013; Denner *et al.*, 2013, 2015; Hollik *et al.*, 2015; Kallweit, Lindert, Maierhöfer *et al.*, 2015; Kallweit, Lindert, Pozzorini *et al.*, 2015; Kallweit *et al.*, 2016; Lindert *et al.*, 2017). In their combination with the higher-order QCD corrections, two schemes are typically followed. They can be combined additively, corresponding to a strict next-to-leading-order expansion, commonly denoted as NLO QCD + EW. Or they can be combined multiplicatively, referred to as NLO QCD × EW, which assumes a factorization of both effects and is especially suitable if the typical scales of both processes are well separated. The difference is formally of higher order and can be used to estimate the potential size of the mixed QCD − EW NNLO corrections.

Conversely, the inclusive photon production cross section, as it is always accompanied by hadronic activity, starts at $\mathcal{O}(\alpha_s \alpha)$ at the Born level and is thus of the same level of complexity as $W/Z + 1$-jet production. Hence, all pieces of the calculation at NNLO accuracy in the strong coupling were

computed only recently (Campbell, Ellis, and Williams, 2017a, 2017b; Chen *et al.*, 2020), while the NLO EW corrections have been known for a slightly longer period (Kühn *et al.*, 2006; Kallweit, Lindert, Pozzorini *et al.*, 2015; Lindert *et al.*, 2017).

In addition, owing to their nature as massless gauge bosons, photons can both be produced promptly by the hard inter-action and emerge from a fragmentation process; see Fig. 5. Thus, unless the photon is identified using the smooth cone isolation procedure (Frixione, 1998), which completely removes the fragmentation component by construction, such additional fragmentation processes have to be considered starting at the next-to-leading order (Glück *et al.*, 1994; Aurenche *et al.*, 2006). We note that smooth cone isolation cannot be adopted by the experiments due to finite detector resolution, while the standard cone isolation that is typically used experimentally necessitates the use of fragmentation functions in theoretical calculations. Thus, for all calculations using smooth cone isolation the correspondence of its
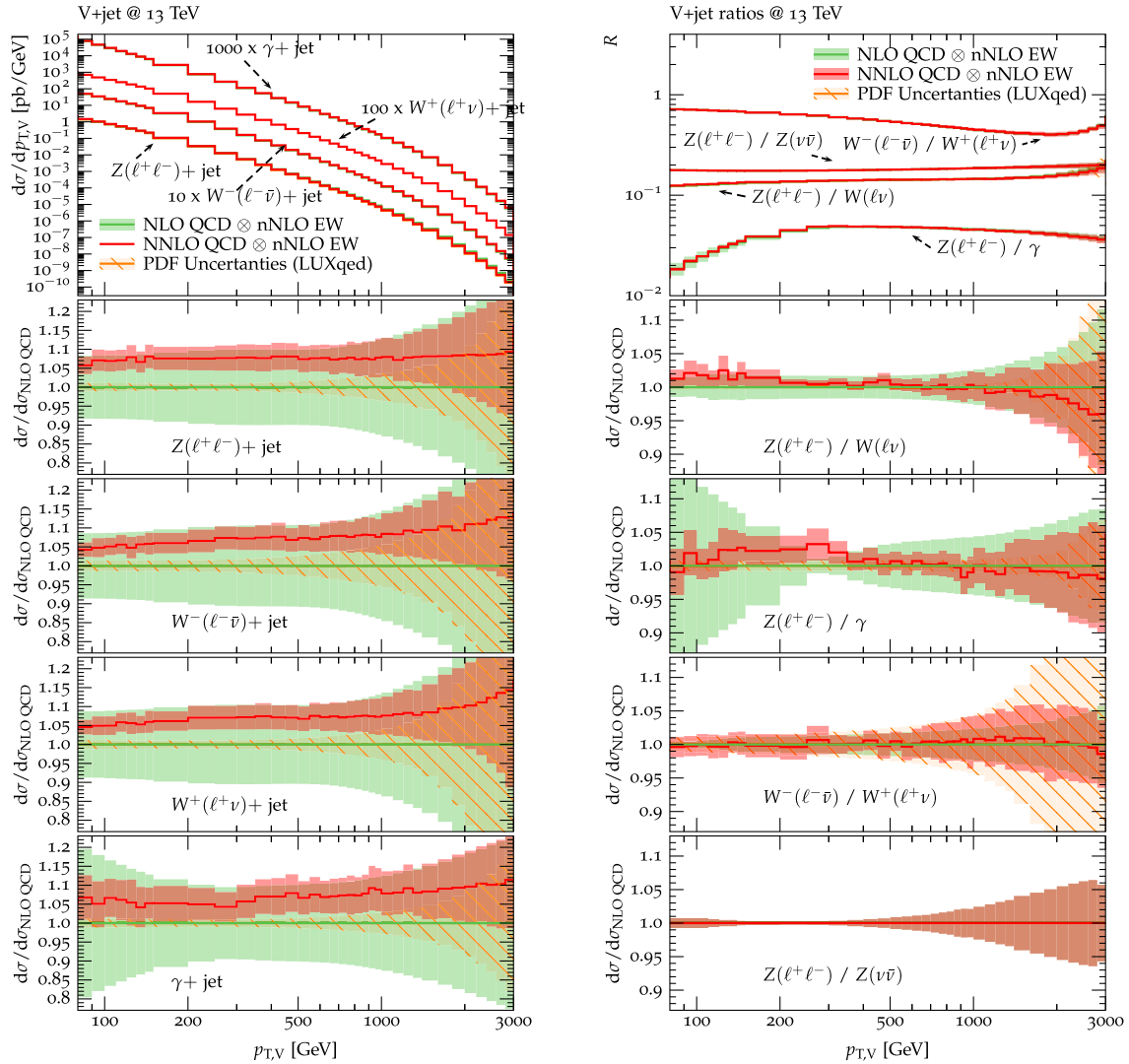
FIG. 7.   Left panels: transverse momentum of the reconstructed vector boson (from top to bottom: Z, W^-, W^+, and γ) in inclusive vector boson production at NLO and NNLO QCD plus nNLO EW. From Lindert *et al.*, 2017. Right panels: pairwise ratios of the differential cross section in the transverse momentum of the reconstructed vector bosons in inclusive vector boson production at NLO and NNLO QCD plus nNLO EW. From Lindert *et al.*, 2017.
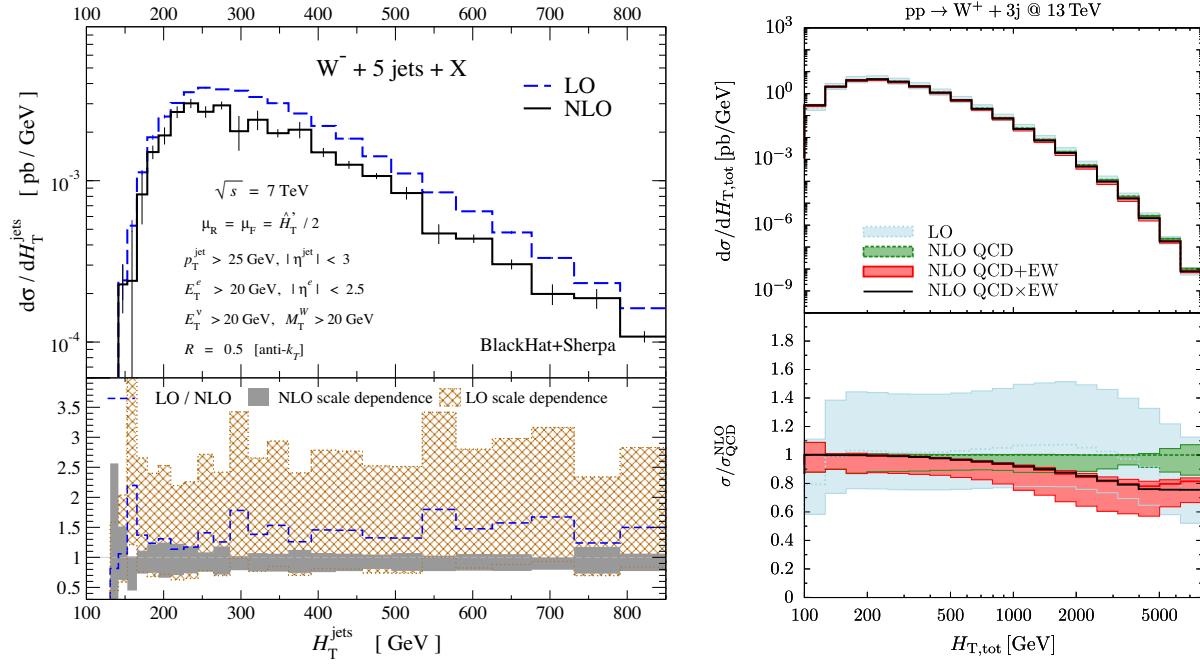
FIG. 8. Left panels: scalar sum of jet transverse momenta in single charged-lepton production associated with missing transverse momentum and at least five jets at LO and NLO QCD. From Bern *et al.*, 2013. Right panels: scalar sum of jet transverse momenta in single charged-lepton production associated with missing transverse momentum and at least three jets at LO and NLO QCD plus NLO EW. From Kallweit, Lindert, Maierhöfer *et al.*, 2015.

parameters to approximately match the experimentally used ones needs to be confirmed. Mixed schemes, such as a smooth or standard cone hybrid (Siegert, 2017), can be used to mediate such differences.

The transverse-momentum distribution of a Z boson decaying into neutrino pairs is of particular interest for new physics searches at the LHC, such as a background to searches for dark matter, as it has a similar topology and features particles that are invisible to the LHC detectors. Because of this fact, however, measuring this standard model background independently proves to be challenging. Typically it is indirectly inferred by measuring the transverse momentum of a leptonically decaying Z or W boson or a photon instead, relying on theoretical predictions to estimate to the sought-after $Z \rightarrow \nu\bar{\nu}$ distribution. The needed ratios of production cross sections of the different processes can now be predicted with high precision (Bern *et al.*, 2011; Campbell, Ellis, and Williams, 2017b; Lindert *et al.*, 2017; Gehrmann-De Ridder *et al.*, 2018; Bizoń *et al.*, 2019) thanks to the recently available accurate NNLO QCD plus NLO EW predictions, as discussed, and an understanding of the correlations across processes. Figure 7 details the predictions for these ratios, which are found to have percent-level accuracy for vector boson transverse mementa up to around 1 TeV, growing to 5%–10% in the regions beyond.

Finally, vector boson production associated with multiple jets is also of interest. Not only are such final states frequently measured at the LHC, but they also often constitute backgrounds to searches for particular new physics models. With the adoption of the anti-k_t-jet definition (Cacciari, Salam, and Soyez, 2008), a sequential recombination algorithm of the longitudinally-invariant-k_t family

(Catani *et al.*, 1993; Dokshitzer *et al.*, 1997; Ellis and Soper, 1993), by the LHC experiments as their default jet definition, long-standing issues around the compromised infrared safety of the Tevatron era jet algorithms (Blazey *et al.*, 2000) were resolved. This allows for high-precision higher-order calculations to be made for the precise observable that is measured.

The NLO QCD predictions are available for W plus up to five jets (Campbell and Ellis, 2002; Berger *et al.*, 2009, 2011; Ellis, Melnikov, and Zanderighi, 2009; Bern *et al.*, 2013) and Z plus up to four jets (Campbell and Ellis, 2002; Berger *et al.*, 2010; Ita *et al.*, 2012), and approximate NNLO corrections, named n̄NLO, can be calculated through the LOOPSIM method (Rubin, Salam, and Sapeta, 2010; Maître and Sapeta, 2013). At the same time, NLO EW corrections are known for fully off-shell production only up to two jets (Denner *et al.*, 2015; Kallweit *et al.*, 2016), and in the on-shell approximation for up to three jets (Kallweit, Lindert, Maierhöfer *et al.*, 2015; Chiesa, Greiner, and Tramontano, 2016). The effect of these corrections is detailed in Fig. 8. Processes with up to nine jets can be calculated at LO accuracy (Höche, Prestel, and Schulz, 2019).

2. Resummation calculations

Fixed-order calculations fail to yield reliable cross-section predictions in phase-space regions where large, typically logarithmic, terms appear at every order of the perturbative expansion. Consequently, a truncation of the perturbative series fails to converge quickly enough after the first, second, or third order. To render a truncation after any finite number of orders meaningful, a resummation of the terms spoiling the
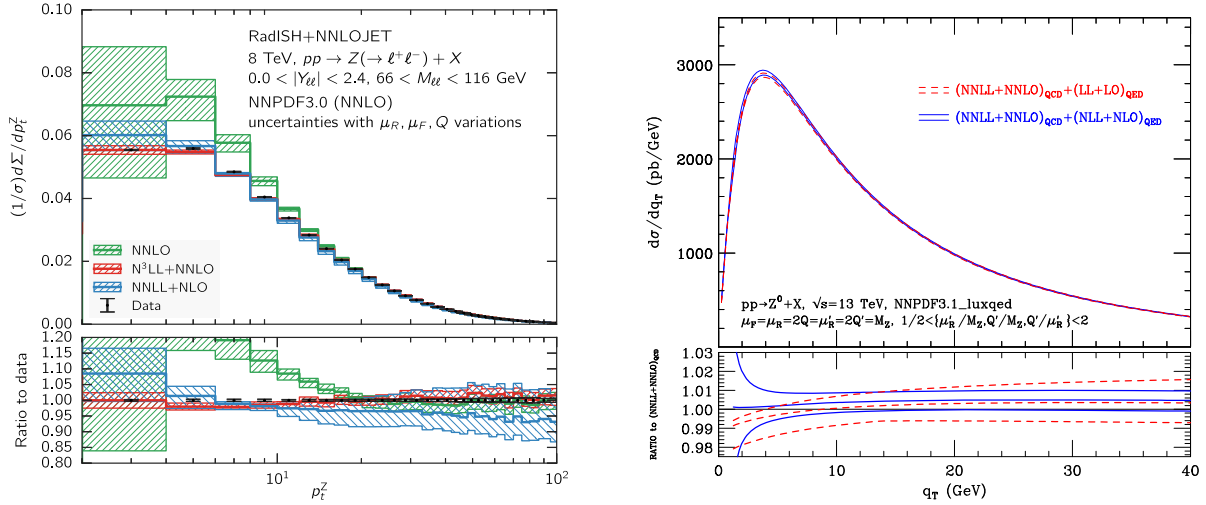
FIG. 9. Left panels: transverse momentum of the charged-lepton pair in the inclusive production of two charged leptons at NNLO, NNLL + NLO, and N^{3}LL + NNLO QCD, showing the QCD scale uncertainties. From Bizoń et al., 2018. Right panels: transverse momentum of the charged-lepton pair in the inclusive production of two charged leptons at NNLL + NNLO QCD plus LL + LO and NLL + NLO QED, showing the QED-related uncertainties only. From Cieri, Ferrera, and Sborlini, 2018.

convergence is mandated. As the functional form of these convergence-impairing terms is dependent of the phase-space region probed by the respective observable, all resummation formulations are observable specific. In the literature, several approaches to identify and resum the relevant logarithms have been formulated; see Collins, Soper, and Sterman (1985), Ladinsky and Yuan (1994), Balazs and Yuan (1997), Becher and Neubert (2011), Bozzi et al. (2011), Mantry and Petriello (2011), Catani et al. (2014), Monni, Re, and Torrielli (2016), Ebert and Tackmann (2017), Bizoń et al. (2018), Bermudez Martinez et al. (2019), Coradeschi and Cridge (2019), and Bacchetta et al. (2020). This is particularly relevant for electroweak precision measurements like the W mass, or for probing so-called intrinsic transverse momentum of the partons inside the proton.

For the production of vector bosons associated with light-flavor jets, the transverse momentum of the vector boson is of particular interest. In this observable, resummation is required to accurately describe the small-p_T region, whereas the large-p_T region suffers no such effects and is most accurately described by fixed-order perturbation theory. Thus, to achieve the best predictions for the spectrum, the resummed calculation at small p_T has to be matched to the fixed-order calculation at large p_T. Several solutions fitting the various resummation procedures are available. Figure 9 displays two examples. On the left, the state-of-the-art next-to-next-to-next-to-leading logarithmic (N^{3}LL) resummation matched to the NNLO fixed-order prediction in QCD is shown (Bizoń et al., 2018). The effect of resumming large logarithms in the expansion of the cross section in the strong coupling α_s, as well as the large logarithms appearing in the simultaneous expansion in the electroweak coupling α, is shown in the right panels of Fig. 9 (Cieri, Ferrera, and Sborlini, 2018; de Florian, Der, and Fabre, 2018). Although the effects are somewhat small in this case, they will be needed for a meaningful interpretation of the high-precision data to be taken in future LHC runs.

Other resummed calculations are available for related observables, such as the ϕ^* distribution (Banfi, Dasgupta, and Marzani, 2011), which can be measured with superior experimental precision (Vesterinen and Wyatt, 2009; Banfi et al., 2011), or the jet veto efficiency (Stewart, Tackmann, and Waalewijn, 2011; Banfi et al., 2012; Tackmann, Walsh, and Zuberi, 2012).

3. Monte Carlo event generators

The previously discussed high-precision calculations suffer from one important shortcoming: they are parton-level calculations and do not fully account for parton evolution or nonperturbative effects. Thus, to arrive either at particle-level[3] predictions that can be directly compared to detector-corrected experimental data or at simulated detector readouts to derive the detector corrections in the first place, these high-precision calculations need to be interfaced with parton-shower calculations and multiparton interaction and hadronization models, as well as hadron decays. This is implemented in so-called Monte Carlo event generators such as HERWIG (Bellm et al., 2016), PYTHIA (Sjöstrand et al., 2015), and SHERPA (Bothmann et al., 2019). They can produce fully differential calculations, i.e., results that explicitly provide the flavor and four-momentum of every particle that is produced in a high-energy collision. This allows the predictions to be projected onto arbitrary observables a posteriori.

Within the Monte Carlo event generators, the parton showers (PSs) provide a fully differential resummation of the parton splitting process in terms of their respective evolution variables, albeit at a lower theoretical accuracy than the inclusive observable-specific resummations discussed in

---

[3]Particles with a lifetime of $c\tau > 10$ mm are considered stable in the typical collider experiments. The stage of event evolution where all remaining particles are stable on this scale is referred to as particle level.
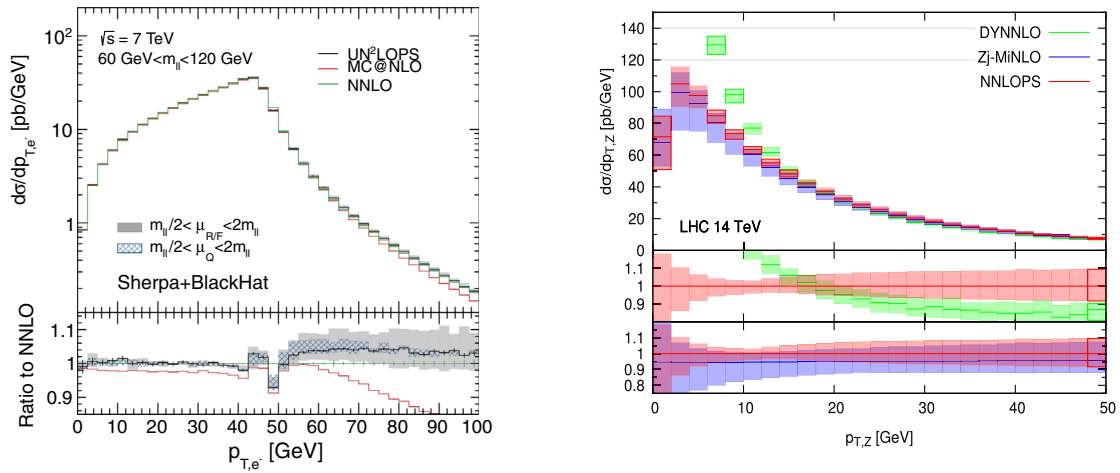
FIG. 10.   Left panels: lepton transverse momentum in the inclusive production of a charged-lepton pair calculated at NNLO QCD accuracy matched to the parton shower using the UN^{2}LOPS method as implemented in SHERPA compared to MC@NLO and NNLO calculations. From Höche, Li, and Prestel, 2015. Right panels: reconstructed Z-boson transverse momentum in the production of a charged-lepton pair calculated at NNLO QCD accuracy matched to the parton shower using the MINLO method as implemented in POWHEG interfaced to PYTHIA8 compared to DYNNLO and NNLOPS calculations. From Karlberg, Re, and Zanderighi, 2014.

Sec. II.A.2. They are matched to fixed-order expressions for the hard scattering at the leading, next-to-leading, and next-to-next-to-leading orders to improve the precision of the calculation outside the strongly hierarchical regime. While the matching to LO matrix elements is trivial, there are two general variants of matching strategies for the combination with next-to-leading order matrix-elements, POWHEG (Nason, 2004; Frixione, Nason, and Oleari, 2007; Höche *et al.*, 2011a) and MC@NLO (Alwall *et al.*, 2014; Frixione and Webber, 2002; Höche *et al.*, 2012). Both are formulated in a generic way and especially the MC@NLO method can be applied in an automated way to arbitrary processes. These methods have been applied to inclusive vector boson production (Frixione and Webber, 2004; Alioli *et al.*, 2008; Hamilton, Richardson, and Tully, 2008; Höche *et al.*, 2011a) as well as vector boson production associated with up to three jets (Alioli *et al.*, 2011; Frederix *et al.*, 2012; Höche *et al.*, 2012, 2013b; Re, 2012; Campbell *et al.*, 2013; Ježo, Klasen, and König, 2016; Siegert, 2017). In addition, at least in the POWHEG approach for the inclusive Drell-Yan production, next-to-leading-order electroweak corrections have been matched to coevolving QCD + QED parton showers (Barzè *et al.*, 2012; Bernaciak and Wackeroth, 2012; Barzè *et al.*, 2013; Mück and Oymanns, 2017). They constitute state-of-the-art tools for calculating standard model predictions for electroweak precision measurements, such as the W mass and the angular coefficients and charged-lepton asymmetry in lepton-pair production.

The current logarithmic accuracy of parton showers, however, allows them to be matched only to matrix elements at NNLO accuracy with the most trivial color structure. Thus, results are available only for inclusive W- and Z-boson production, not for their production associated with a jet. Here again two different schemes exist: for NNLOPS-matched calculations, MINLO (Hamilton *et al.*, 2013; Hamilton, Nason, and Zanderighi, 2012) simulations reweighted to inclusive NNLO distributions (Karlberg, Re, and Zanderighi, 2014; Monni *et al.*, 2020), and q_T slicing

combined with MC@NLO predictions in the UN^{2}LOPS scheme (Höche, Li, and Prestel, 2015). Figure 10 details the results of both approaches, including their uncertainties, and compares them to the fixed-order results with the same accuracy. In both approaches, the advantages of combining the resummation properties of the parton shower with the fixed-order matrix element become apparent throughout the respective spectrum. The otherwise unphysical description of the low transverse-momentum region of the weak boson is now described in a reliable way. For prompt-photon production, as it is always accompanied by a jet at leading order, no NNLOPS description is available.

Beyond the description of a fixed multiplicity at the highest possible accuracy, the inclusive production of a vector boson with any number of jets is of prime interest in the experiments. Thus, multijet-merged calculations aim to combine the advantages of both high-precision descriptions of hard and wide-angle radiation through fixed-order matrix elements with the description of the soft-collinear intrajet dynamics offered by the parton shower. Prescriptions to merge multiple LO-accurate parton-shower (LOPS) calculations of successive jet multiplicities into inclusive calculations were derived about 20 years ago. They can be grouped with the CKKW-like methods (Catani *et al.*, 2001; Lönnblad, 2002; Lavesson and Lönnblad, 2008b; Hamilton, Richardson, and Tully, 2009; Höche *et al.*, 2009, 2011b; Hamilton and Nason, 2010; Lönnblad and Prestel, 2012, 2013b) on the one hand, and the MLM-like approaches (Mangano, Moretti, and Pittau, 2002; Alwall *et al.*, 2008), on the other hand.

The CKKW-like approaches split the emission phase space of a lower-order process into a matrix-element region and a parton-shower region using the merging scale Q_{cut} as a separator. While the soft and collinear phase space is populated by the parton shower acting on lower-multiplicity matrix elements, radiation into the matrix-element region is vetoed. This veto, as it is determined from the parton-shower emission
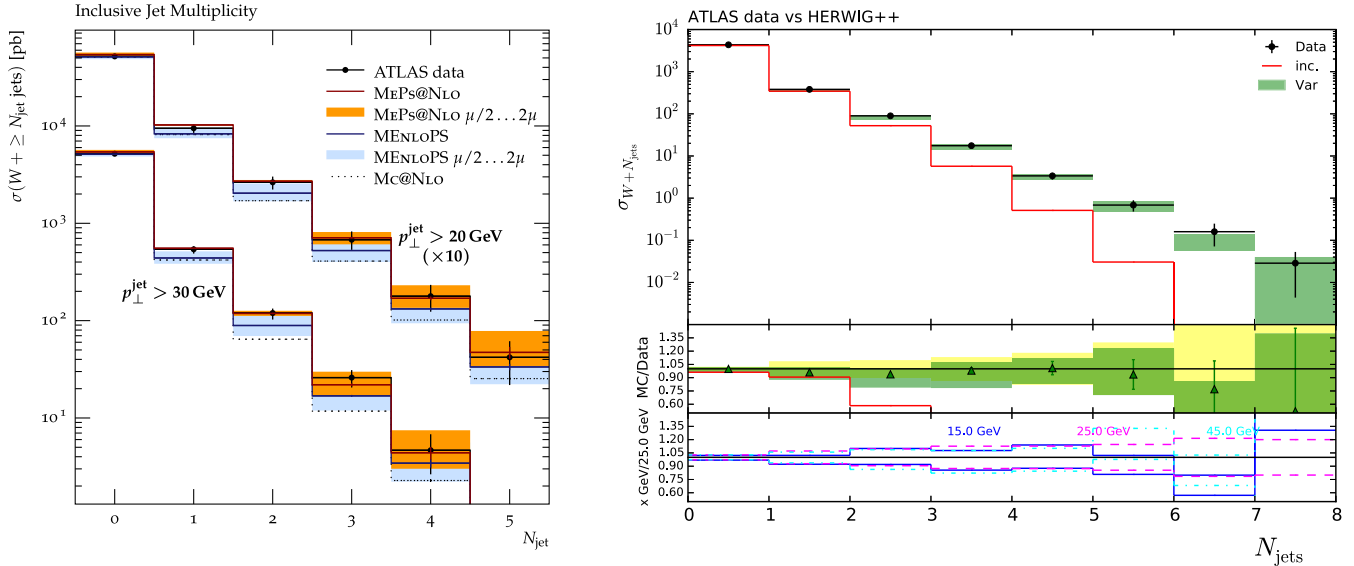
FIG. 11. Left panel: inclusive jet multiplicity in the production of a charged lepton and a neutrino associated with jets using the MEPS@NLO method and merging up to two jets at NLO and four jets at LO accuracy as implemented in SHERPA, compared to MENLOPS predictions and ATLAS data. From Höche *et al.*, 2013a. Right panels: exclusive jet multiplicity in the production of a charged lepton and a neutrino associated with jets using the FXFX method and merging up to two jets at NLO accuracy as implemented in MadGraph5 AMC@NLO and HERWIG++. From Frederix *et al.*, 2016.

probability, now provides the correct Sudakov weight for the higher-multiplicity matrix element to correctly include the respective resummation properties in this region.

Conversely, the MLM-like prescriptions attach an unconstrained parton shower to the matrix-element configuration of each jet multiplicity, letting it run its course without any awareness of the merging scale that was used to define the matrix-element region initially. However, at this point of the generation jets are reconstructed using a given jet algorithm and matched, in both direction and transverse momentum, to their counterparts in the originating matrix element. If nonmatching jets are found in either configuration, the event is discarded, in this way providing the needed Sudakov weights. Although the two methods yield comparable results (Alwall *et al.*, 2008), it should be noted that a formal proof of the mathematical correctness exists only for the CKKW-like approaches (Höche *et al.*, 2009).

These methods have then subsequently been promoted to merging NLOPS-matched calculations, both in the CKKW-like approach [see Lavesson and Lönnblad (2008a), Gehrmann *et al.* (2013), and Höche *et al.* (2014, 2013a) for the MEPS@NLO variant; see Lönnblad and Prestel (2013a), Plätzer (2013), and Bellm, Gieseke, and Plätzer (2018) for the UNLOPS variant; and see Alioli *et al.* (2015) for the GENEVA variant] and in the MLM-like prescription (FXFX) (Frederix and Frixione, 2012). In the former, possibilities to complement the NLOPS-accurate prescriptions of the lowest few multiplicities with LOPS-accurate higher multiplicities have been formulated (Hamilton and Nason, 2010; Höche *et al.*, 2011b, 2014; Gehrmann *et al.*, 2013). Figure 11 displays the results of these state-of-the art computations compared to data taken by the ATLAS experiment at the LHC at 7 TeV. When contrasted, the NLO-accurate predictions prove to be superior in both their central values and their uncertainties.

As discussed in Sec. II.A.1, electroweak corrections are important not only for precision measurements but also in observables probing regions of large momentum transfers. Thus far, however, no solution to incorporate the exact NLO electroweak corrections in the TeV regime has been formulated. Nonetheless, there are two methods to incorporate the dominant electroweak correction in this region in an approximate way. The first method (Chiesa *et al.*, 2013) supplements the leading-order matrix elements used in a LO-accurate multijet-merged prediction with multiplicative EW Sudakov form factors (Denner and Pozzorini, 2001a, 2001b). Conversely, the second method (Kallweit *et al.*, 2016) completes the NLO QCD components of NLO-accurate multijet-merged calculations with exact NLO EW virtual corrections and approximate NLO EW real emission corrections integrated over the single-emission phase space. The latter can, where needed, be supplemented with subleading LO corrections to account for further relevant contributions. Results for both methods are shown in Fig. 12, and the general feature of a logarithmic suppression of the production cross section, the so-called EW Sudakov correction, can be observed, reaching several tens of percent for the transverse momentum of the vector boson.

Electroweak effects also become relevant through the radiation of either massive weak bosons (again, mostly relevant for TeV scale objects) (Christiansen and Sjöstrand, 2014; Krauss *et al.*, 2014) or photon bremsstrahlung (Bloch and Nordsieck, 1937; Yennie, Frautschi, and Suura, 1961; Barberio, Eijk, and Wąs, 1991; Seymour, 1992; Hamilton and Richardson, 2006; Schönherr and Krauss, 2008). The latter mainly affects observables that depend on the charged-lepton kinematics, ranging from a few percent on charged-lepton p_T spectra to $\mathcal{O}(1)$ effects on invariant mass distributions below resonance peaks or threshold-induced shoulders. In particular,
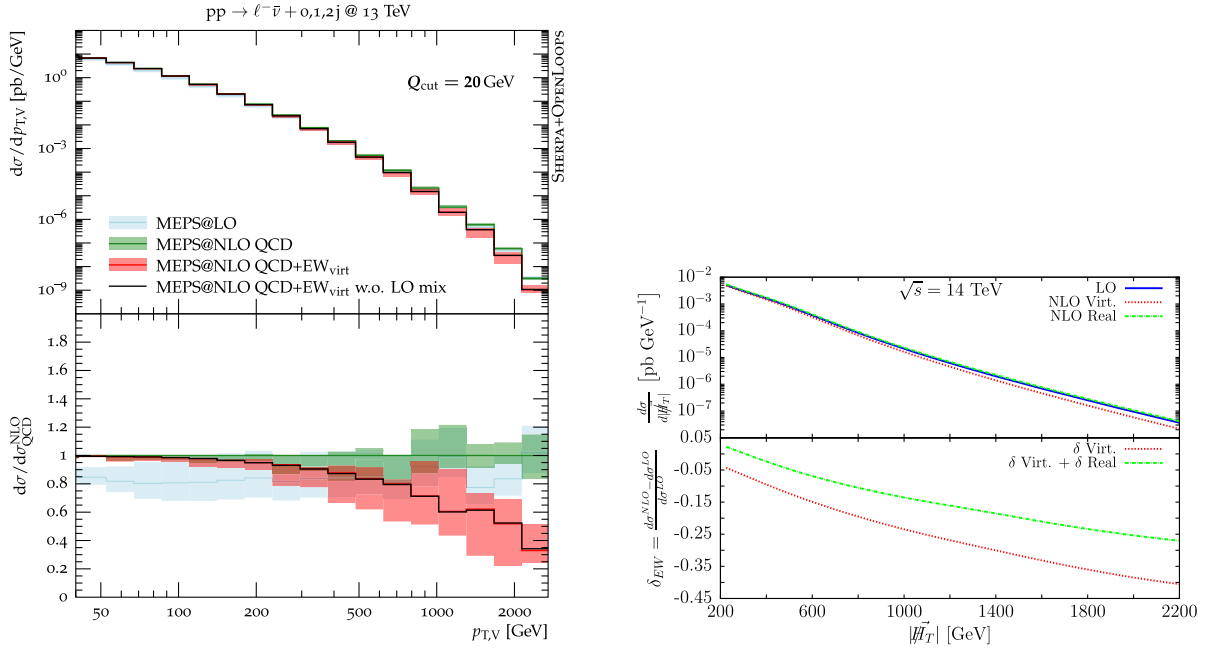
FIG. 12.   Left panels: reconstructed W boson transverse momentum in the production of a charged lepton and a neutrino associated with jets calculated using the MEPS@NLO method, including approximate electroweak corrections as implemented in SHERPA. From Kallweit *et al.*, 2016. Missing transverse momentum in neutrino-pair production associated with jets at leading order in QCD, including EW corrections in the Sudakov approximation as implemented in ALPGEN and HERWIG. From Chiesa *et al.*, 2013.
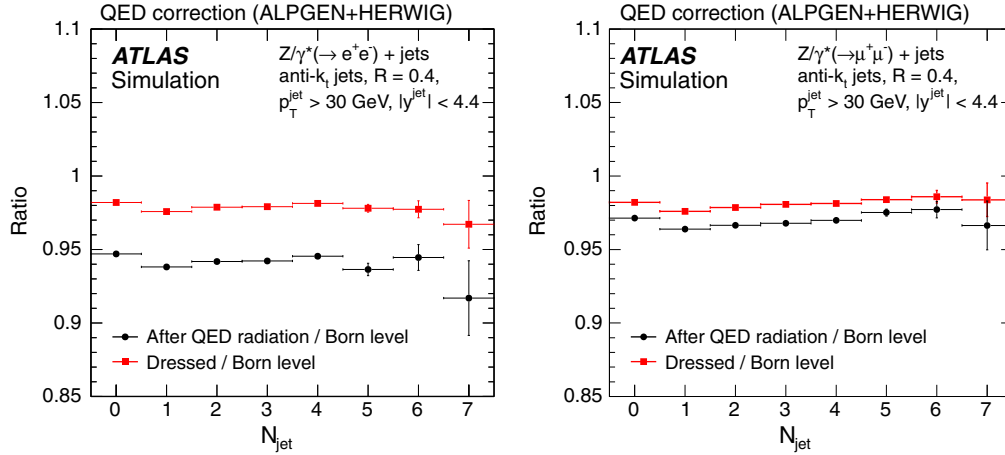

FIG. 13.   QED final-state correction factors from Born level to the infrared-safe bare and dressed charged-lepton definitions calculated using PHOTOS (Davidson, Przedzinski, and Wąs, 2016) for (left panel) electrons and (right panel) muons as a function of the number of accompanying jets. From ATLAS Collaboration, 2013e.

since QED is an infrared-free theory, various different charged-lepton definitions can be and are used in measurements at various colliders: bare charged leptons take the final-state charged lepton at face value, and dressed charged leptons recombine all photonic energy in a cone of size ΔR with the bare charged lepton. While the bare charged-lepton definition demands a charged-lepton mass carried through at least some parts of the calculation (Dittmaier, Kabelschacht, and Kasprzik, 2008), the dressed charged-lepton definition is suitable also for calculations with massless leptons through its insensitivity to collinear radiation. The historic and occasionally still used Born charged-lepton definition relies on

event record documentation entries[4] and is not infrared safe at any higher order. It thus should be abandoned, particularly for precision measurements. Figure 13 details the corrections

---

[4]In event generators, before NLO EW parton-shower-matched calculations were available and, in fact, in most cases still now, the charged-lepton kinematics are generated first at LO accuracy before dressing the interaction by photon radiation. The Born charged-lepton definition then relates the physical bare or dressed charged lepton to its Born-level counterpart by using the recorded technical details of how the previous calculation was carried out.
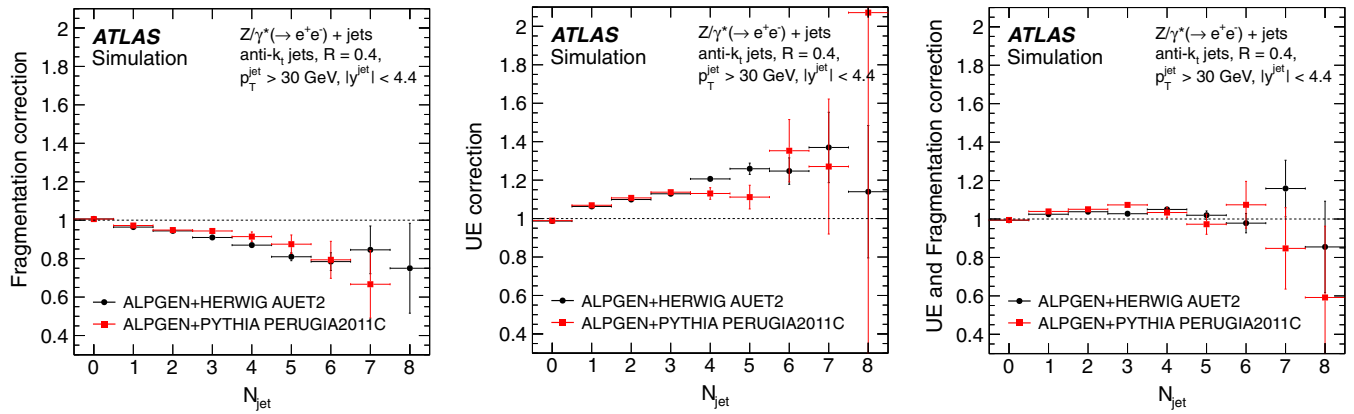
FIG. 14. Nonperturbative correction factors calculated using HERWIG and PYTHIA for the ATLAS Z + jet measurement in the electron-pair decay channel as a function of the number of accompanying jets: (left panel) fragmentation, (middle panel) underlying event, and (right panel) the result of the two. From ATLAS Collaboration, 2013e.

effected through photon bremsstrahlung, where the dominant effect originates in the changes of the charged-lepton transverse momentum and invariant mass distributions, which influence the efficiency of the kinematic selection.

Besides providing a fully exclusive event description at parton level, event generators comprise tools to calculate nonperturbative effects like multiparton interactions (Sjöstrand and Zijl, 1987; Butterworth, Forshaw, and Seymour, 1996; Sjöstrand and Skands, 2004; Bähr, Gieseke, and Seymour, 2008; Corke and Sjostrand, 2010; Gieseke, Loshaj, and Kirchgäßer, 2017), parton-to-hadron transitions (Field and Feynman, 1977; Andersson *et al.*, 1983; Field and Wolfram, 1983; Webber, 1984; Winter, Krauss, and Soff, 2004), and hadron decays to arrive at a fully differential event description at particle level. Since methods to calculate these effects on timescales of $\mathcal{O}(1\,\mathrm{CPU\,s})$ per event are not currently available, phenomenological models with tunable, *a priori* unknown, parameters are used. These parameters, believed to be universal, have to be determined by a finite set of measurements in dedicated phase-space regions, to be used in all other calculations. The size of these nonperturbative corrections is typically estimated by using HERWIG and PYTHIA, and Fig. 14 shows an example of these corrections for an ATLAS Z + jet study at the LHC. These corrections are usually applied to partonic calculations, such as the fixed-order NNLO QCD calculations described in Sec. II.A.1, to be compared to data.

B. Experimental results

The extensive program for measurements of V + jet processes at the Tevatron has provided critical incentive for the development of sophisticated higher-order calculations and MC generators. In the first years of the LHC data taking, LHC experiments benefited from the availability of accurate calculations and MC generators tuned to Tevatron data; however, the production of V + jet events at the LHC is not a simple rescaling of Tevatron scattering. Therefore, a new program for extensive measurements of V + jet processes was set up early on in the LHC physics program and V + jet papers were

among the first published by the LHC collaborations (ATLAS Collaboration, 2011b, 2011c; CMS Collaboration, 2011b, 2012a). While the first LHC measurements of V + jet processes established SM measurements and assessed the validity of theoretical predictions at the LHC energy scales, later measurements considerably improved the experimental precision, reaching the percent level, and were thus able to expose data-prediction discrepancies and shortcomings in calculations. Such precision measurements highlighted the need for the development of more precise higher-order calculations in QCD and electroweak physics at the LHC, as detailed in Sec. II.A.

With the high precision achieved by LHC experiments, accurate definitions of the quantities that are experimentally measured are of great importance, as they must be theoretically sound; i.e., independent of the order of the theoretical approximation used, they must be related to fundamental physical quantities rather than parameters in theoretical models and as close as possible to experimental definitions to minimize model-dependent extrapolations. These general guidelines allow for accurate comparison of experimental results with theoretical predictions and ensure that results can be compared with future predictions without prior knowledge of the experimental apparatus or possibly dated theoretical models. In this spirit, V + jet measurements at the Tevatron and the LHC are primarily reported in fiducial phase spaces. Cross-section measurements for W/Z + jet processes at the LHC are reported with decay charged leptons defined at "dressed-level," and corrections to a Born-level definition are often provided; see Sec. II.A.3. The cross sections measured in different decay channels of the W or Z bosons can be combined when the charged leptons are defined at Born level. However, a channel combination with charged leptons defined at dressed level is also done with a per-mille accuracy, i.e., below the experimental precision of the measurements. For a discussion of phase space and particle definitions at the LHC, see ATLAS Collaboration (2015c). For the measurements of the γ + jet production cross sections, isolation requirements are imposed on the photon to improve the identification at detector level and to suppress the contribution of photons from the fragmentation of quarks and gluons at particle level; see Sec. II.A.
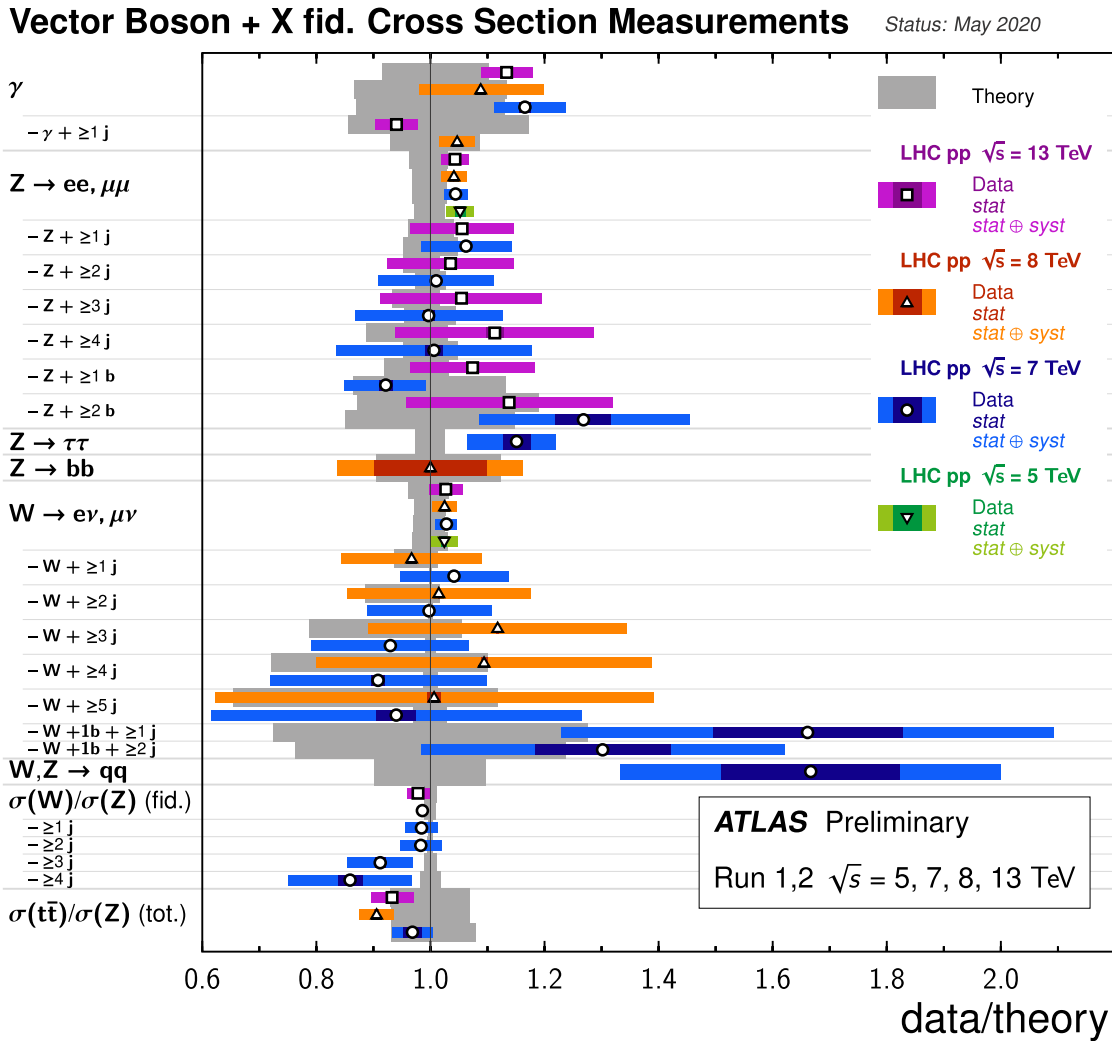
Vector Boson + X fid. Cross Section Measurements

Status: May 2020

FIG. 15.   Summary of ratios of vector boson $+X$ cross-section measurements and predictions at 5, 7, 8, and 13 TeV center-of-mass energies in pp collisions at the LHC. From ATLAS Collaboration, 2019e.

Experimental measurements include absolute or normalized differential cross sections in a fiducial phase space. The differential cross sections are measured as a function of several observables, i.e., event-based observables (jet multiplicity N_{jets}, boson transverse momentum p_T, H_T that is the scalar sum of the p_T of clustered jets, event shapes, etc.) and jet-based observables (nth-jet p_T or rapidity y). Measurements also include angular correlations between final-state objects (jet-jet, lepton-jet, Z-jet, γ-jet objects, etc.), such as the azimuthal difference $\Delta\phi$, the rapidity difference $\Delta y, \Delta R = \sqrt{\Delta\phi^2 + \Delta\eta^2}$, and the invariant mass of the two leading jets m_{jj}.

Particle-level measurements are finally compared to theoretical predictions from MC simulations or to fixed-order calculations. While MC simulations provide particle-level final states, fixed-order calculations [such as those using BlackHat (Berger *et al.*, 2008, 2009, 2010, 2011; Ita *et al.*, 2012; Bern *et al.*, 2013), MCFM (Campbell and Ellis, 2010) or JETPHOX (Catani *et al.*, 2002; Aurenche *et al.*, 2006)] are at parton level and are often corrected for nonperturbative effects, such as underlying event and hadronizations (3% to 4% corrections), as discussed in Sec. II.A.3. Uncertainties in

fixed-order NLO calculations in perturbative QCD (pQCD) due to missing higher-order terms are conventionally estimated by variations of the scales (renormalization and factorization) and are typically found in the 4%–20% range. These are followed by uncertainties on parton densities in the 1%–4% range, and on α_s in the 1%–3% range.

Figure 15 shows the breadth of V + jet measurements at different center-of-mass energies at the LHC and gives an overview of the level of agreement between measurements and state-of-the-art theoretical predictions. It is impressive to see such a level of agreement overall; however, in the most precise experimental measurements, such as the ratios of W + jets and Z + jets, discrepancies are visible. These discrepancies become more significant, up to 2 standard deviations or greater, in some regions of phase space in differential cross-section measurements. These measurements and comparisons with theoretical predictions are presented in greater detail later.

1. Experimental event reconstruction

In experimental analyses, V + jet events are reconstructed by identifying particles, such as photons, leptons, and clusters of particles such as jets, and applying selection requirements

to purify the data samples. After background subtraction and corrections for the detector efficiency and resolution (*unfolding*), the production cross sections are measured inclusively or differentially in a fiducial phase space at particle level that is defined as close as possible to the detector-level kinematic selection. The unfolding of experimental results is an important part of the process of extraction of experimental measurements, as it allows for the direct comparison with theoretical predictions with no prior knowledge of the detector layout, efficiency, or resolution.

a. Particle reconstruction: Photons, electrons, muons, missing transverse momentum, and jets

The selection of photons is based on energy clusters reconstructed in the electromagnetic calorimeter, and depending on the number of matching tracks in the tracker they can be classified as unconverted or converted photons. Photons are reconstructed within the tracker acceptance, typically of $|\eta| < 1.0$ at the Tevatron and $|\eta| < 2.37$–2.5 in the ATLAS and CMS detectors at the LHC. See CMS Collaboration (2015g) and ATLAS Collaboration (2019a) and references therein for a representative selection of recent articles on photon reconstruction, calibration, and identification strategies and performance at ATLAS and CMS. Since the reconstruction of the photon momentum relies on measurements of energy deposits in cells in the calorimeter system, the transverse momentum of the photon is often reported as transverse energy (E_T). Measurements of prompt-photon production require an isolation of photons to avoid a large contribution from neutral-hadron decays into photons. While a smooth cone isolation criterion (see Sec. II.A) is used for photon isolation in theoretical calculations, experimentally a cone-base isolation technique is most suitable for finite-granularity detectors: the photon is required to be isolated based on the amount of transverse energy in a cone of typical size $\Delta R = 0.4$ around the photon.

An electron is reconstructed as a charged-particle track geometrically associated with energy clusters in the electromagnetic calorimeter, while a muon is identified as a track segment in the muon system consistent with a track in the inner tracker and can be associated with a minimum ionization signature in the calorimeters. Both electrons and muons are reconstructed within the inner tracker acceptance and are required to be isolated to further suppress background from misidentified objects, such as hadrons and semileptonic heavy-flavor decays. The isolation requirements are tuned so that the electron or muon isolation efficiencies are high for the signal, typically greater than 90%. See CMS Collaboration (2015f, 2020d), LHCb Collaboration (2015c, 2019c), ATLAS Collaboration (2016d, 2019a), and Aaij *et al.* (2019) and references therein for details on electron and muon reconstruction, calibration, and identification, as well as their performance at the LHC. Small correction factors, typically within 1%, are applied to correct differences in the photon, muon, and electron efficiencies between data and simulation.

Jets are clustered from energy deposits in the calorimeters in the ATLAS detector (ATLAS Collaboration, 2016g, 2020a) and from particle candidates reconstructed by a particle flow algorithm in the CMS detector (CMS Collaboration, 2017d,

2017i, 2020e). Different jet algorithms are used at the Tevatron and the LHC. At the Tevatron, iterative cone algorithms (such as the midpoint algorithm) with split-merge prescriptions to resolve cases of overlapping stable cones are used with a typical cone radius of $R = 0.4$–0.7. The experiments at the LHC migrated to the anti-k_t infrared and collinear-safe jet algorithm, which also produces cone-shaped clustered jets. Jets are calibrated based on the jet p_T response in MC simulations, and the pileup (the particle production from multiple interactions per bunch crossing) contribution to the jet energy is subtracted on an event-by-event basis in the calibration process using data-driven techniques. *In situ* measurements of the momentum balance in the dijet γ + jet, Z + jet and multijet events are used to correct for any residual difference in the jet energy scale between data and simulation.

In W + jet analyses with the W decaying leptonically, the event selection purity can be improved by imposing a requirement on the presence of missing transverse momentum in the event since the neutrino escapes direct detection. The missing transverse momentum is calculated as the negative vectorial sum of the transverse momenta of the final-state particles. In the CMS experiment particles are reconstructed by a particle flow algorithm and are used as inputs to the computation of the missing transverse momentum, while in the ATLAS experiment the selected final-state particles (such as electrons, muons, photons, and jets) are used together with soft particles that are not associated with any other selected object, i.e., low-energy deposits in the calorimeter or low-momentum tracks associated with the primary vertex (LHCb Collaboration, 2015c; ATLAS Collaboration, 2018e; CMS Collaboration, 2019e).

b. Event reconstruction: Photon + jets

Events with a photon and jets reconstructed in the final states are recorded using highly efficient (close to 100% efficiency) single-photon triggers; see CMS Collaboration (2017j) and ATLAS Collaboration (2020b) and references therein for a representative selection of articles on photon trigger architecture and performance at the LHC. Despite the application of the tight identification and isolation requirements on the photon, a non-negligible background originating from hadrons misidentified as photons contaminates the selected sample. The signal purity is typically higher for a photon reconstructed centrally in the detector, increases as the photon E_T or jet p_T increases, and can reach values in the 70%–90% range at high photon E_T. The background is subtracted using data-driven methods based on signal-suppressed control regions. The photon reconstruction and selection efficiencies depend on the photon E_T and η and are in the range of approximately 70%–100%. They decrease with an increasing number of jets in the event, primarily due to the photon isolation requirement.

Photons are selected in a broad range of minimum E_T requirements, approximately 20–200 GeV; similarly, the minimum jet p_T requirement varies and ranges from about 15 to 100 GeV.

The γ + jet cross-section measurements are dominated by experimental systematic uncertainties, such as photon calibration and identification and jet energy scale, at the level of a

few percent over a broad range of jet or photon transverse momenta. However, at around the TeV energy scale statistical uncertainty in the data becomes the leading contribution at the LHC.

c. Event reconstruction: W/Z + jets

Events with a W or Z boson provide clean experimental signatures in the leptonic decay channels that can be triggered by single high-p_T electron or muon, or low-p_T dilepton (electron and muon) triggers (CMS Collaboration, 2017j; Aaij *et al.*, 2019; LHCb Collaboration, 2019a; ATLAS Collaboration, 2020b). The two leptonic channels with one (in W events) or two (in Z events) electrons or muons provide useful cross-checks of the results and can provide additional information to constrain experimental uncertainties in the combination of the cross sections. In addition to requirements for the charged-lepton and jet transverse momenta and (pseudo)rapidity acceptance, in W + jet events further requirements for the missing transverse momentum or the transverse invariant mass are applied, while for Z + jet event reconstruction a requirement on the dilepton invariant mass is imposed in a window around the nominal Z-boson mass. Typical selection requirements for W/Z + jet events include electrons or muons with a minimum p_T in the range 20–30 GeV within the tracker acceptance, jets with a distance parameter in the range $R = 0.4$–0.7, with a p_T requirement in the range 20–50 GeV, and in rapidity ranges that vary from about two to five units, with a minimal separation between the lepton and jets of ΔR (lepton, jet) > 0.4–0.7. In the LHCb experiment the weak boson decay charged leptons are reconstructed in the forward pseudorapidity region, in the range $2.0 < \eta < 4.5$, while jets are reconstructed in the pseudorapidity range $2.2 < \eta_{jet} < 4.2$. W + jet and Z + jet events have different levels of background contamination. While at high jet multiplicity the background from $t\bar{t}$ production is dominant for both processes, W + jet events have a larger background contribution from multijet production in which hadronic particles are misidentified as an electron or a muon. The multijet background is estimated using data-driven techniques and contributes to $\approx$ 5%–15% of the W + jet data samples. The background from $t\bar{t}$ events contributes to about 0% (1 jet), 20% (Z + 6 jets), and 80% (W + 6 jets) and is estimated by MC or with data-driven techniques, and it can be suppressed by a b-jet veto. Figure 16 shows the jet multiplicity distributions and the levels of background contamination in W + jet and Z + jet events in the muon decay channels in the CMS detector.

Experimental uncertainties are dominated at low jet p_T or low N_{jets} by systematics associated with the energy scale and resolution of the jets. At high jet p_T or high N_{jets}, unfolding and statistical uncertainties become important. At high N_{jets} the uncertainties on the backgrounds dominate in W + jet analyses. Figure 17 shows the level of experimental uncertainties in the Z + jet production cross-section measurement as a function of the jet multiplicity, and the level of jet energy calibration uncertainty in $W+ \geq 1$ jet events as a function of the leading-jet rapidity. The levels of experimental uncertainties in W/Z + jets are similar in analyses at 7, 8, and 13 TeV
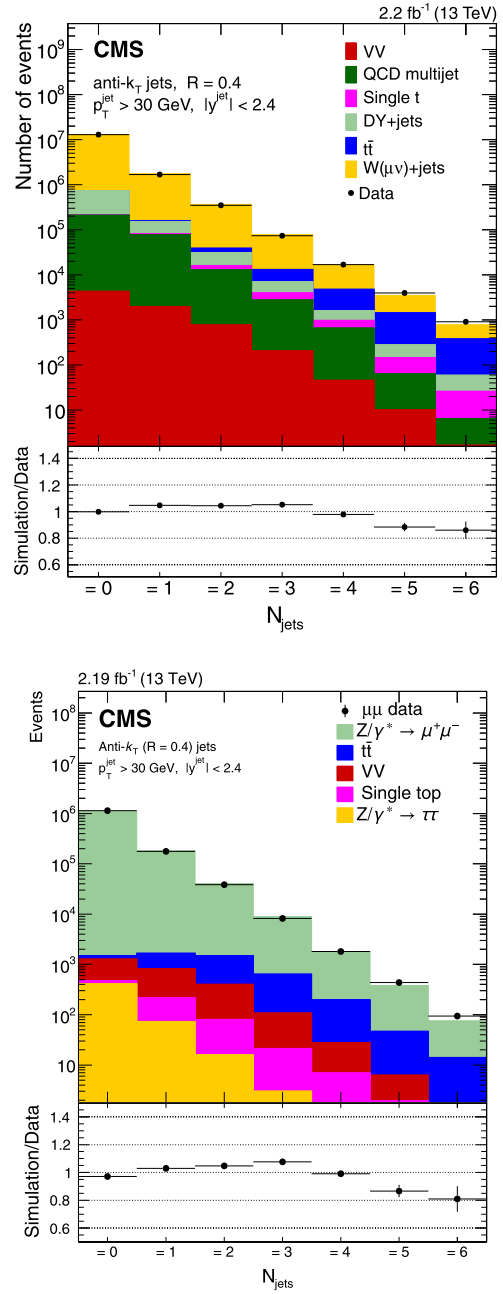

FIG. 16. Top panels: reconstructed data, simulated signal, and background events in the jet multiplicity distributions in pp collisions at 13 TeV center-of-mass energy at the LHC for W + jet events in the muon decay channel of the W boson. From CMS Collaboration, 2017e. Bottom panels: similar reconstructed data, simulated signal, and background events for Z + jet events in the muon decay channel of the Z boson. From CMS Collaboration, 2018d.

center-of mass energies at the LHC and comparable with Tevatron experiments.

Measurements of ratios of differential cross sections allow for partial cancellations of uncertainties (both experimental and theoretical). The comparison of the experimental uncertainties in Fig. 17 (bottom-right panel) for W + jets and in Fig. 18 for the ratio of W + jet to Z + jet differential cross sections, known as R_{jets}, shows that in R_{jets} the experimental

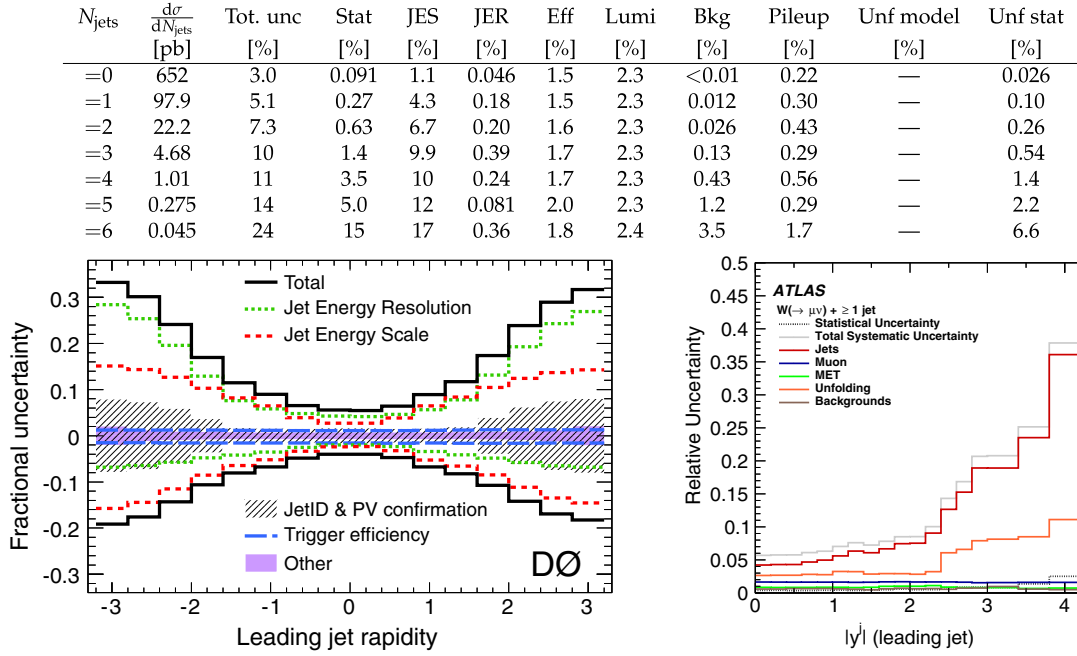| N_{jets}	$\frac{d\sigma}{dN_{\text{jets}}}$ [pb]	Tot. unc [%]	Stat [%]	JES [%]	JER [%]	Eff [%]	Lumi [%]	Bkg [%]	Pileup [%]	Unf model [%]	Unf stat [%]
=0	652	3.0	0.091	1.1	0.046	1.5	2.3	<0.01	0.22	—	0.026
=1	97.9	5.1	0.27	4.3	0.18	1.5	2.3	0.012	0.30	—	0.10
=2	22.2	7.3	0.63	6.7	0.20	1.6	2.3	0.026	0.43	—	0.26
=3	4.68	10	1.4	9.9	0.39	1.7	2.3	0.13	0.29	—	0.54
=4	1.01	11	3.5	10	0.24	1.7	2.3	0.43	0.56	—	1.4
=5	0.275	14	5.0	12	0.081	2.0	2.3	1.2	0.29	—	2.2
=6	0.045	24	15	17	0.36	1.8	2.4	3.5	1.7	—	6.6

FIG. 17. Table: cross section in exclusive jet multiplicity in $Z +$ jets with 13 TeV pp collisions at the LHC for the combination of the decay channels and the breakdown of uncertainties. From CMS Collaboration, 2018d. Bottom-left panel: fractional experimental uncertainties in $W + 1$ jet analysis in 1.96 TeV $p\bar{p}$ collisions at the Tevatron as a function of the leading-jet rapidity. From D0 Collaboration, 2013d. Bottom-right panel: similar analysis in 7 TeV pp collisions at the LHC. From ATLAS Collaboration, 2015a.

systematics, and especially those associated with jets, cancel from about 40% to about 5% at high jet rapidity. This large cancellation of uncertainties allows for an accurate test of SM predictions at the percent level in a wide region of phase space.

2. Cross sections and jet rates

Measurements of $V +$ light-jet production cross sections as functions of the jet multiplicity, jet transverse momenta, and jet rates are carried out at hadron colliders, as they provide
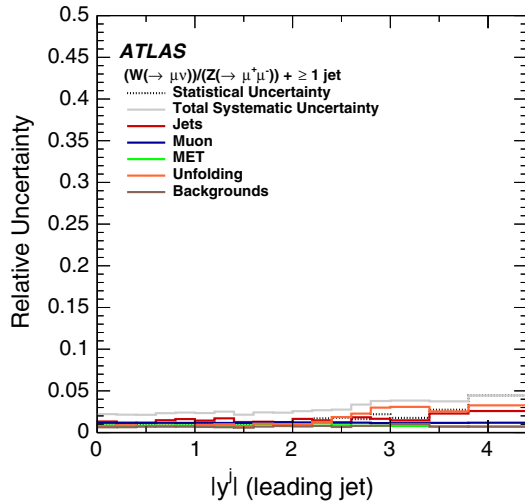

FIG. 18. Relative experimental uncertainties on the inclusive ratio $W + 1$ jet to $Z + 1$ jet cross section as a function of the leading-jet rapidity in 7 TeV pp collisions at the LHC. From ATLAS Collaboration, 2014a.

benchmarks for an understanding of the underlying QCD dynamics and its modeling in MC generators. This section starts with a presentation of the measurements of the associated production of jets and a photon and concludes with a discussion of the measurements of the associated productions of jets and a massive vector boson, i.e., W or Z.

a. Photon + jets cross-section measurements

The processes of $\gamma +$ jet production have the largest cross sections of all $V +$ jet processes and they approach the $W/Z +$ jet cross sections at high photon transverse momentum, i.e., in the regime where weak boson mass effects play a lesser role. Figure 19 presents the triple differential cross section as a function of the photon transverse momentum, and the γ and jet pseudorapidities, at the Tevatron in $p\bar{p}$ collisions at 1.96 TeV center-of-mass energy and at the LHC in pp collisions at 7 TeV center-of-mass energy. The D0 measurement is carried out in two regions of the jet rapidity and in event configurations in which the jet and photon have either the same or opposing signs in rapidity, while the CMS analysis is in two regions of the jet pseudorapidity and in four regions of the photon pseudorapidity. In both cases the measurements span several orders of magnitude in the production cross sections. The predictions include the NLO pQCD calculation implemented in JETPHOX and, in the CMS analysis, the tree-level matrix elements with up to three parton jets matched to parton showering in the SHERPA generator. The predictions are overall consistent with the data but unable to describe the cross-section variations across the entire measured range of phase space. Tevatron results are an important benchmark for theoretical calculations and have served as a stepping-stone for more accurate modeling of such processes
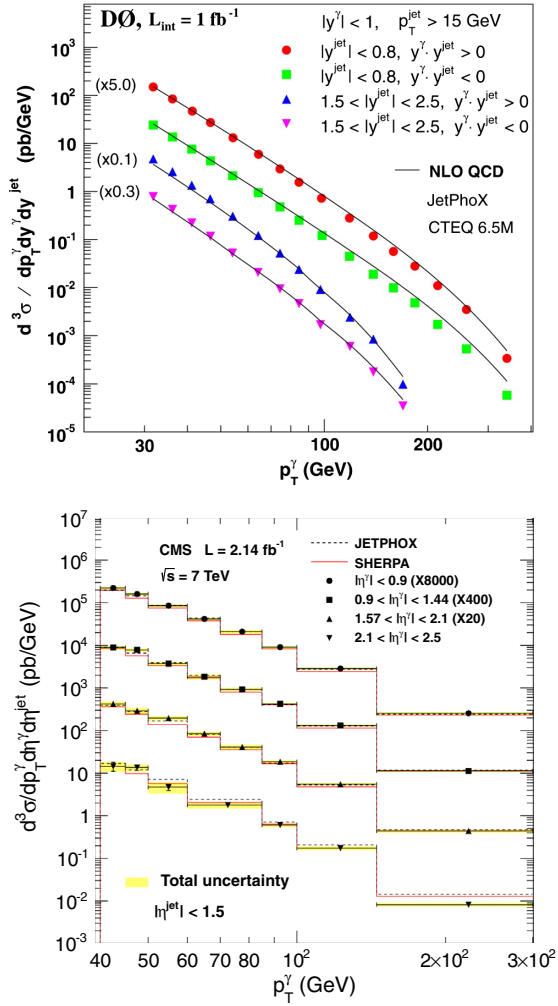
FIG. 19. Top panel: triple differential cross sections as a function of p_T^γ in four photon rapidity intervals in $p\bar{p}$ collisions at 1.96 TeV center-of-mass energy at the Tevatron. From D0 Collaboration, 2008b. Bottom panel: similar triple differential cross sections in four different ranges of η^γ for $p_T^{jet} > 30$ GeV and $|\eta^{jet}| < 1.5$ in pp collisions with 7 TeV center-of-mass energy at the LHC. From CMS Collaboration, 2014e. The measured cross sections are compared with the NLO pQCD calculation generated by JETPHOX and with the LO MC SHERPA simulation (bottom panel).

for the LHC. However, despite this progress in theoretical predictions some data-theory discrepancies are observed at the LHC in specific kinematic regions of γ + jets. For example, in regions with large photon η and p_T in γ + 1-jet events, the ratios between the data and the NLO pQCD predictions generated by JETPHOX and SHERPA are in the range of 50%–70% (CMS Collaboration, 2014e), and in the photon p_T region greater than 750 GeV in γ + 2-jet events (ATLAS Collaboration, 2017b) the discrepancy between the data and the NLO calculation reaches about 2σ.

In addition to testing QCD calculations and MC predictions, the measurements of photon + jet production can be used to constrain the parton density functions (PDFs). The results in Fig. 20 are shown as an example of ratios between theory and LHC data for the measurement of the differential
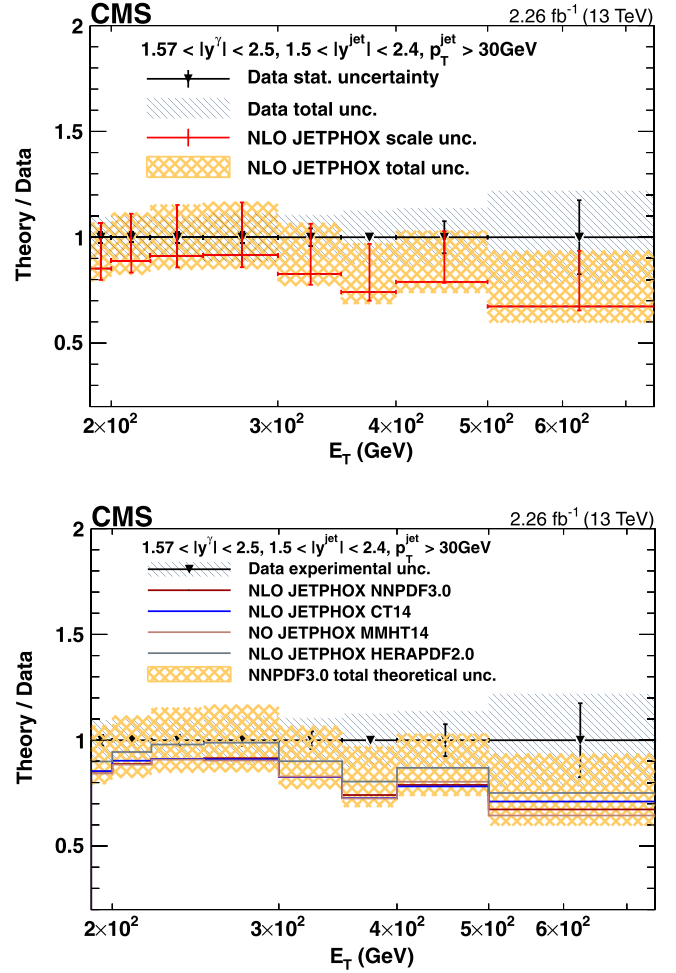

FIG. 20. Ratios of NLO (JETPHOX) predictions to data as a function of the photon transverse energy in γ + jet events in the forward photon and jet rapidity regions in pp collisions at the LHC with 13 TeV center-of-mass energy. Top panel: contribution of the scale uncertainty to the total theoretical uncertainty in the NLO JETPHOX calculation compared to the experimental uncertainties. Bottom panel: NLO JETPHOX calculation with various NLO PDF sets compared to the experimental uncertainties. From CMS Collaboration, 2019c.

cross section for γ + jet production as a function of the photon E_T. The measurement is carried out in two photon and two jet rapidity regions, while the figure shows the results in the forward photon and forward jet bin. The measurement shows good agreement between the LHC data and NLO predictions in pQCD from JETPHOX. As Fig. 20 (top panel) shows, the experimental and theoretical uncertainties are comparable, and the theoretical jet scale uncertainty dominates the theoretical uncertainties in the NLO pQCD approximation. Figure 20 (bottom panel) shows the NLO prediction generated by JETPHOX using various NLO PDF sets. Although the differences between the studied PDF sets are small and subleading with respect to the scale uncertainty estimated in the NLO pQCD approximation, new calculations at higher orders in QCD with smaller scale uncertainties, i.e., next-to-next-to-leading order, are available (Campbell, Ellis, and Williams, 2017a, 2017b; Chen
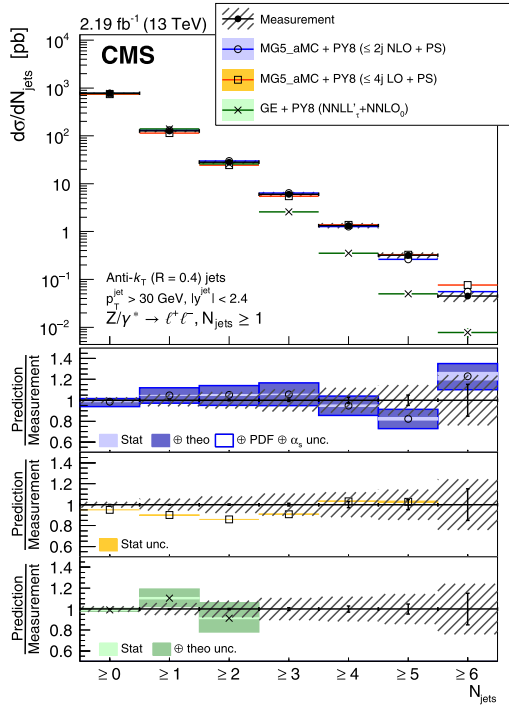
FIG. 21. Cross section as a function of the inclusive jet multiplicity for $Z+$ jet events at 13 TeV center-of-mass energy in pp collisions at the LHC. From CMS Collaboration, 2018d.

et al., 2020) and provide motivation for the use of such measurements at the LHC to improve the gluon and other PDFs (Campbell *et al.*, 2018), especially in the kinematic regions where the experimental uncertainties are smaller or comparable to theoretical uncertainties, such as in the low to middle range of photon E_T.

For other inclusive photon and photon + light-jet measurements carried out at the Tevatron and at the LHC, see the analyses given by D0 Collaboration (2010a, 2011b), ATLAS Collaboration (2011a, 2011b, 2012g, 2013a, 2014b, 2016e, 2017d, 2019d, 2019f, 2020c), CMS Collaboration (2011a, 2011b, 2013f, 2019d).

b. $W/Z+$ jets cross-section measurements

A typical measurement of $W/Z+$ jet processes is the production cross section (multiplied by the leptonic branching ratio) as a function of jet multiplicity, as shown in Fig. 21 for $Z+$ jet production. Such a measurement is important for assessing the accuracy of SM predictions that are used to estimate the $W/Z+$ jet yield in searches of new physics signatures.

The production of $W/Z+$ jets is a multiscale process and various observables can be used to define the scale of the process, depending on the kinematic configuration. A common variable used to set the scale in $W/Z+$ jet processes is H_T, which is also used to discriminate the new physics from the SM background, as in supersymmetry searches. This variable has, however, different definitions: in ATLAS it is defined as the scalar sum of the transverse momenta of leptons (including neutrinos) and jets in the event, while in CMS it is defined as the scalar p_T sum of the jets only. Figure 22 shows two examples of the differential cross section for $W+ \geq 1$ jet production as a function of H_T by the CMS and ATLAS experiments. The measurements in Figs. 21 and 22 show excellent agreement with theoretical predictions over 4 orders of magnitude in the cross section. The multitude of models that are compared to data show the variety of theoretical approaches that can be validated with such measurements. These results show that MC simulations with multiparton
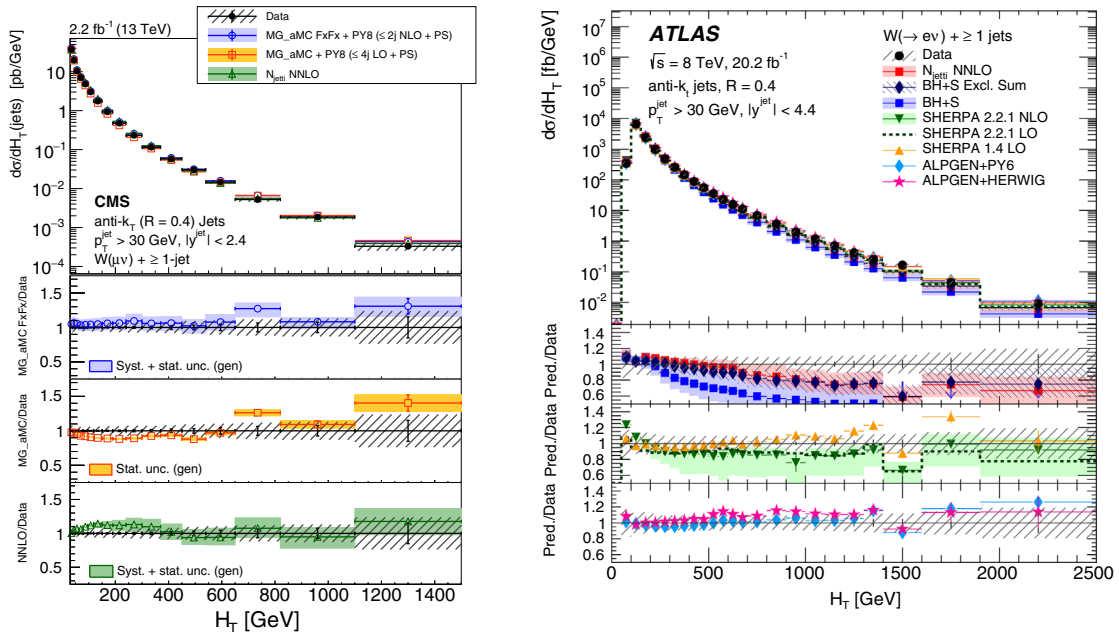

FIG. 22. Left panels: differential cross section for the production of a W boson with at least one jet as a function of H_T at 13 TeV in pp collisions at the LHC. From CMS Collaboration, 2017e. Right panels: similar differential cross section at 8 TeV. From ATLAS Collaboration, 2018b.
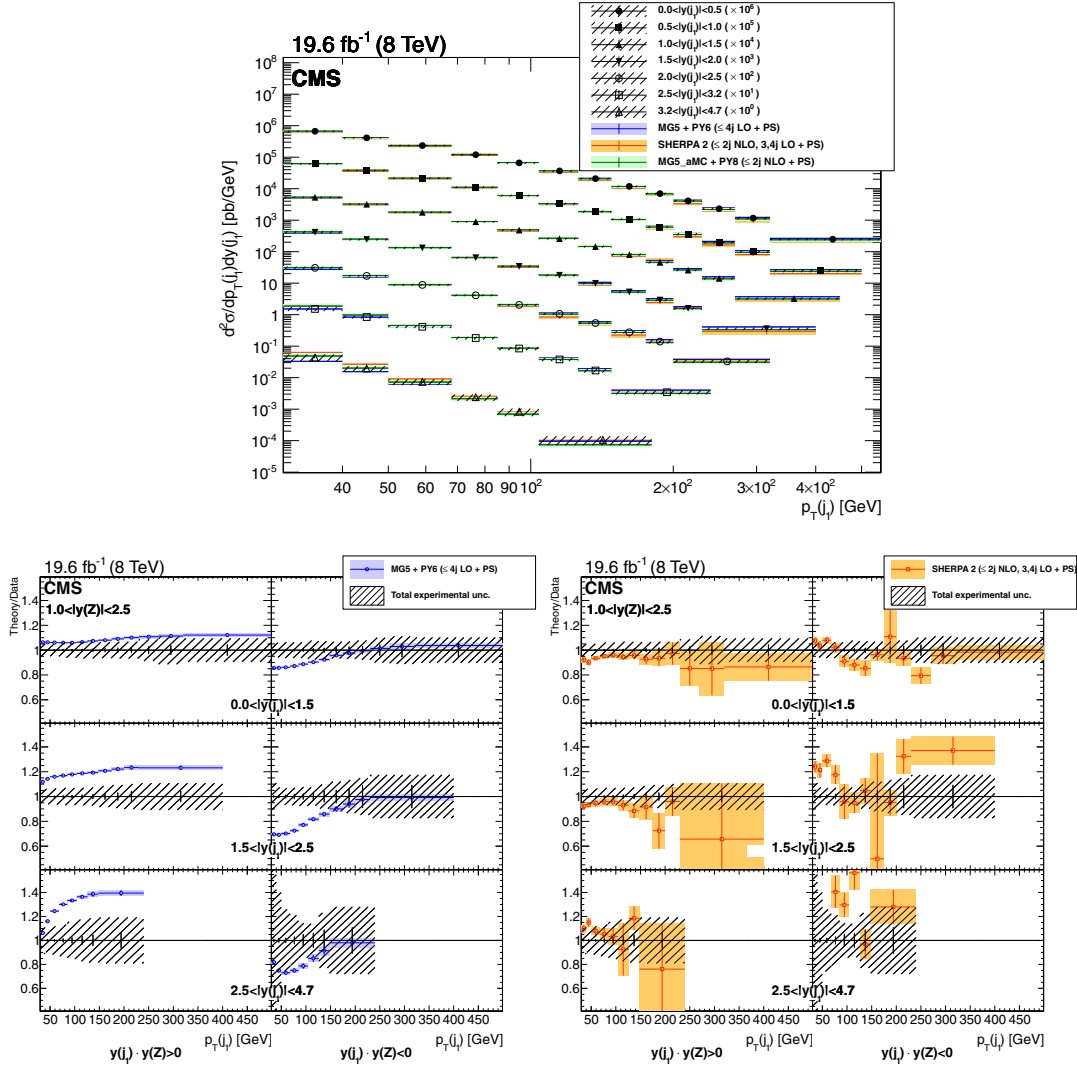
FIG. 23. Differential cross section (top panel) and theory-to-data ratio (bottom panels) for $Z +$ jet production as a function of the leading-jet transverse momentum and rapidity in 8 TeV pp collisions at the LHC. From CMS Collaboration, 2017a.

calculations in the matrix element matched to the parton shower are in agreement with the data up to high jet multiplicity and in a broad energy scale range. The high experimental precision also exposes discrepancies between measurements and predictions. In Fig. 22 (right panels) discrepancies with pQCD NLO calculations (BlackHat) are visible at large H_T values, when the jets are measured in a broad rapidity region ($|y^{jet}| < 4.4$). The accuracy of the calculation improves when higher-order pQCD corrections are included, i.e., in N_{jetti} NNLO (Boughezal, Focke, Liu, and Petriello, 2015; Gehrmann-De Ridder et al., 2016b) or with the exclusive sum approach (Alcaraz Maestre et al., 2012) in BlackHat (Berger et al., 2010, 2011; Bern et al., 2013), in which NLO information from higher-multiplicity processes are included with the standard fixed-order prediction; see Sec. II.A.

The large statistics of $W/Z +$ jet events allows one to carry out double differential measurements, as is typically done in inclusive jet or $\gamma +$ jet measurements; see the two examples given in experiments by CMS Collaboration (2017g) and

ATLAS Collaboration (2019b). Figure 23 shows an example of a double differential cross section as a function of the leading-jet p_T and rapidity that is performed in a broad region of phase space up to jet $p_T = 500$ GeV and $|y| = 4.7$. Such measurements are expected to provide valuable input for our understanding of parton density functions in addition to QCD dynamics. However, in several regions of phase space the precision of experimental results is higher than current prediction-to-prediction differences, and discrepancies between the data and theoretical predictions can be up to 40%, i.e., larger than the effects from PDFs, and thus the potential PDF sensitivity of the data cannot be exploited. The MC simulation that includes NLO QCD corrections provides a more accurate normalization and better modeling of the shapes of the distributions than LO QCD predictions. Similar conclusions can be reached from several other results on $Z +$ jet and $W +$ jet processes: the inclusion of higher-order QCD corrections in fixed-order calculations and MC simulations generally provides predictions that more accurately describe the data and are also more precise. Figures 24
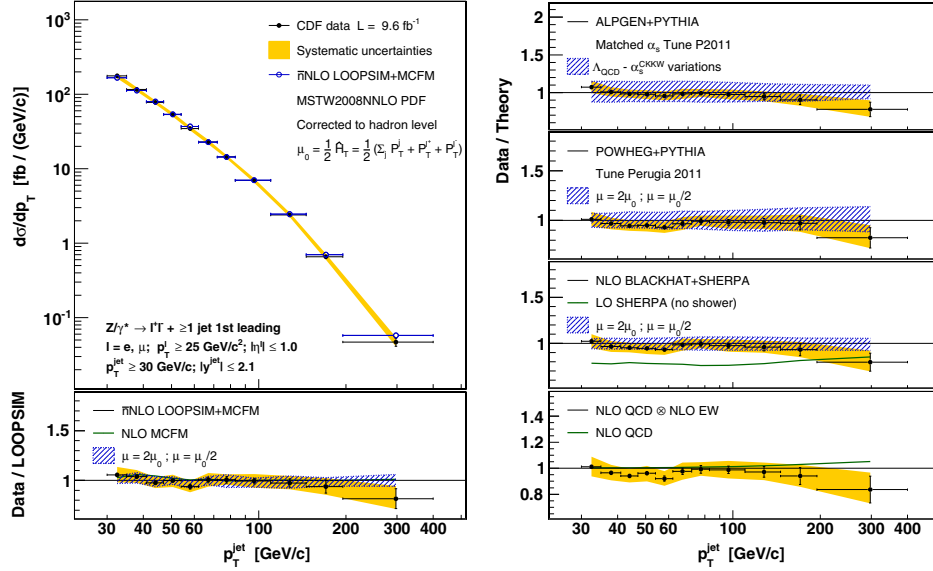
FIG. 24. Differential cross section and data-to-theory ratios as a function of the leading jet p_T for $Z+ \geq 1$-jet events in 1.96 TeV $p\bar{p}$ collisions at the Tevatron. From CDF Collaboration, 2015.

and 25 show examples of such an effect. Better agreement with the data and smaller uncertainties are found in predictions that include higher-order corrections, such as in the NLO MadGraph5_aMC@NLO MC prediction with respect to the LO MadGraph, the ñNLO approximation with LOOPSIM + MCFM (Rubin, Salam, and Sapeta, 2010) and the NNLO N_{jetti} calculation, for the distribution of the leading-jet p_T at the Tevatron up to 400 GeV, and at the LHC up to 1 TeV. Such an effect was corroborated by other studies, such as those of CMS Collaboration (2017e, 2018d) and ATLAS Collaboration (2019b), where data are compared to NNLO predictions. These experimental results also

show that such processes can test theoretical calculations in a broad region of phase space with great precision, i.e., with an uncertainty as low as a few percent in the $W+ \geq 1$-jet events.

The jet multiplicity in $W/Z +$ jet events is correlated to the energy scale of the process. Figure 26 shows the correlation between the average jet multiplicity ($\langle N_{jet} \rangle$) and H_T in $W +$ jet and $Z +$ jet events at the Tevatron and at the LHC, and a similar correlation is demonstrated between $\langle N_{jet} \rangle$ and the Z boson p_T in $Z +$ jets events in Fig. 27. At $H_T \approx 300$ GeV in W events or $p_T^Z \approx 300$ GeV in Z events, the average jet multiplicity is about 2, while at $H_T = 1000$ GeV the average jet multiplicity reaches 3. In the Tevatron study in Fig. 26 (left panels) a fixed-order NLO calculation is used to compute the mean number of jets in an inclusive $W + n$-jet sample by using the following prescription to improve the description beyond the NLO approximation: $\langle N_{jets} \rangle = n + (d\sigma_{n+1}^{NLO} + d\sigma_{n+2}^{LO})/d\sigma^{NLO}$ (Alcaraz Maestre et al., 2012). Such a calculation describes this effect well, while the MC simulations underestimate the effect of the correlation. At the LHC good agreement between data and simulation is found.

Multidifferential cross-section measurements of the vector boson production allow detailed studies of QCD dynamics. In the absence of QED corrections, the five-dimensional differential cross section $d\sigma/(dp_T^Z dy^Z dm^Z d\cos\theta \, d\phi)$ that describes the kinematics of the two leptons from the Z-boson decay can be decomposed into a sum of nine harmonic polynomials $P_i(\cos\theta, \phi)$ and eight dimensionless angular coefficients $A_i = A_i(p_T^Z, y^Z, m^Z)$ $(i = 0 - 7)$, which represent the ratios of helicity cross sections with respect to the unpolarized one (σ^{U+L}) (Mirkes, 1992; Mirkes and Ohnemus, 1994),[5]

FIG. 25. Differential cross section as a function of the leading-jet p_T in $W+ \geq 1$-jet events with 8 TeV pp collisions at the LHC. From CMS Collaboration, 2017g.

[5]In the presence of QED corrections, the expansion in terms of spherical harmonics does not terminate after $l = 2$ but instead turns into an infinite sum.
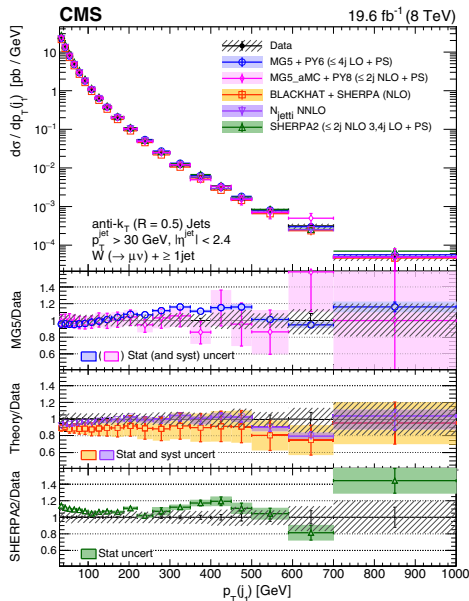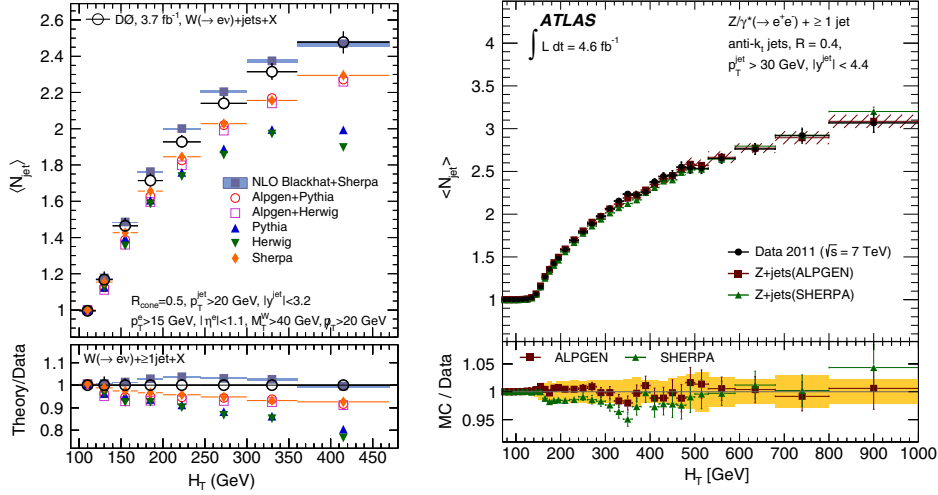
FIG. 26.   Left panels: average number of jets $\langle N_{\text{jet}} \rangle$ as a function of H_{T} in W + jet events in 1.96 TeV $p\bar{p}$ collisions at the Tevatron. From D0 Collaboration, 2013d. Right panels: similar measurements for Z + jet events with 7 TeV pp collisions at the LHC. From ATLAS Collaboration, 2013e.
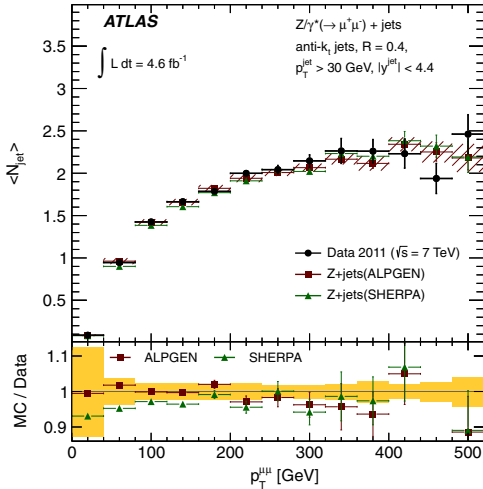

FIG. 27.   Average number of jets $\langle N_{\text{jet}} \rangle$ as a function of the Z-boson p_{T} in Z + jet events with 7 TeV pp collisions at the LHC. From ATLAS Collaboration, 2013e.

$$d\sigma / (dp_{\text{T}}^Z dy^Z dm^Z d\cos\theta\, d\phi)$$
$$= 3 d\sigma^{U+L} / (16\pi\, dp_{\text{T}}^Z dy^Z dm^Z) \{ (1 + \cos^2\theta)$$
$$+ \tfrac{1}{2} A_0 (1 - 3\cos^2\theta) + A_1 \sin 2\theta \cos\phi + \tfrac{1}{2} A_2 \sin^2\theta \cos 2\phi$$
$$+ A_3 \sin\theta \cos\phi + A_4 \cos\theta + A_5 \sin^2\theta \sin 2\phi$$
$$+ A_6 \sin 2\theta \sin\phi + A_7 \sin\theta \sin\phi \}. \tag{1}$$

In this formulation the dependence on the QCD dynamics from the Z-boson production mechanism, i.e., p_{T}^Z, y^Z, and m^Z, is entirely provided by the A_i coefficients and σ^{U+L}. However, to access all eight coefficients, the full dependence on θ and ϕ has to be analyzed. In particular, for Z production at LO in QCD, i.e., $\mathcal{O}(\alpha_s^0)$, only A_4 is nonzero, while at NLO, i.e., $\mathcal{O}(\alpha_s)$, A_{0-3} also receive nonzero contributions due to the spin-1 nature of the additional gluon. The final coefficients A_{5-7} receive contributions starting at NNLO QCD,

i.e., $\mathcal{O}(\alpha_s^2)$, arising through the effective ggZ interaction (Hagiwara, Kuruma, and Yamada, 1992), and they are thus comparatively small.

The CDF Collaboration at the Tevatron carried out a measurement of some of the A_i angular coefficients in $p\bar{p}$ collision data at a center-of-mass energy of 1.96 TeV (CDF Collaboration, 2011), and the average value of the A_4 coefficient was used to indirectly measure the weak mixing angle $\sin^2\theta_W$ (CDF Collaboration, 2013a). The ATLAS and CMS collaborations at the LHC measured the angular coefficients for W-boson polarization at 7 TeV (CMS Collaboration, 2011c; ATLAS Collaboration, 2012e), and more recently for the Z boson at 8 TeV (CMS Collaboration, 2015b; ATLAS Collaboration, 2016b). From the Z-boson angular coefficient A_4 measured at the LHC, the $\sin^2\theta_W$ parameter is also extracted (ATLAS Collaboration, 2018d). Other measurements of $\sin^2\theta_W$ at the LHC are included in CMS Collaboration (2011d, 2018e), ATLAS Collaboration (2015b), and LHCb Collaboration (2015a), while CDF and D0 Collaborations (2018) provided a legacy combination of Tevatron measurements (see references therein for individual Tevatron measurements). As illustrated in Fig. 27, for high values of the Z-boson p_{T} the measurements become sensitive to the production of the Z boson associated with jets. Although NLO and NNLO are in general agreement with the A_i distributions as functions of the Z-boson p_{T} in the data, the A_2 coefficient, which is among the most sensitive coefficients to higher-order corrections, increases less steeply in the data than in the calculations as the Z-boson p_{T} increases; see Fig. 28. The difference between the A_0 and A_2 coefficients, i.e., $A_0 - A_2$, is particularly interesting since it is zero if calculated at NLO in pQCD, the so-called Lam-Tung relation (Lam and Tung, 1978, 1980), and becomes positive at NNLO in pQCD. As Fig. 29 (top panel) shows, the measured values of $A_0 - A_2$ increase for increasing values of p_{T}^Z, up to about 0.15, while significant deviations are observed in the comparison with MC predictions that include NLO pQCD calculations matched to the parton shower. While ATLAS and CMS experimental measurements
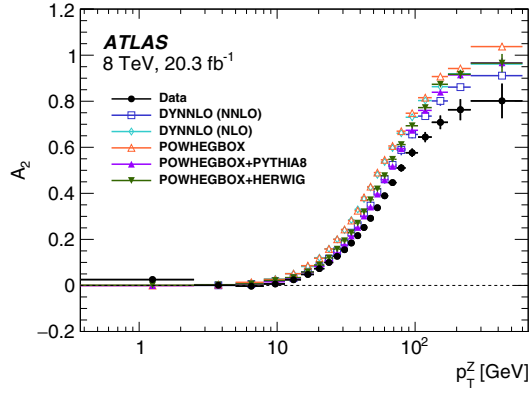
FIG. 28. Distribution of the angular coefficient A_2 as a function of p_T^Z, integrated over y^Z, in data, measured in 8 TeV pp collisions at the LHC, compared to the predictions at NLO, i.e., $\mathcal{O}(\alpha_s)$, and NNLO, i.e., $\mathcal{O}(\alpha_s^2)$, in pQCD, as well as to those from NLO calculations with two different parton-shower models. From ATLAS Collaboration, 2016b.

FIG. 29. Top panel: distribution of the angular coefficient $A_0 - A_2$ as a function of p_T^Z, integrated over y^Z, in data, measured in 8 TeV pp collisions at the LHC, compared to the predictions at NLO, i.e., $\mathcal{O}(\alpha_s)$, and NNLO, i.e., $\mathcal{O}(\alpha_s^2)$, in pQCD, as well as to those from NLO calculations with two different parton-shower mod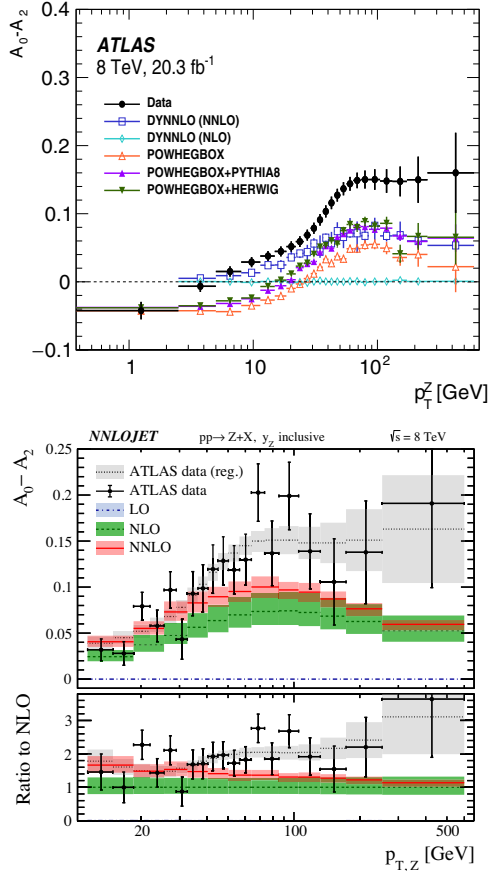els. From ATLAS Collaboration, 2016b. Bottom panels: theoretical predictions with associated uncertainties at $\mathcal{O}(\alpha_s)$ (denoted here as LO), $\mathcal{O}(\alpha_s^2)$ (denoted here as NLO), and $\mathcal{O}(\alpha_s^3)$ (denoted here as NNLO) are compared to the data. From Gauld et al., 2017.

are consistent, the CMS measurement is not sufficiently precise to show significant disagreement between data and predictions. These measurements prompted a dedicated study (Gauld et al., 2017) of the A_i coefficients in Z-boson events that calculated $\mathcal{O}(\alpha_s^3)$ pQCD corrections and their uncertainties on $A_0 - A_2$. As seen in Fig. 29 (bottom panels), the $\mathcal{O}(\alpha_s^3)$ corrections are large and lead to a significant improvement in the agreement with the data; however, a tendency of underestimating the data is visible at high Z-boson p_T. Note that in Fig. 29 (bottom panels), unlike in the results shown in Figs. 28 and 29 (top
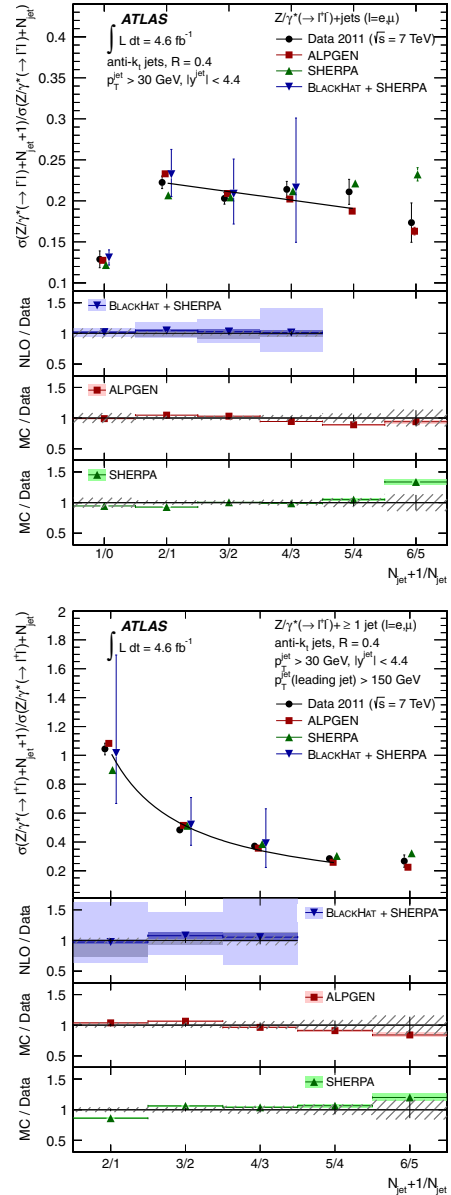
FIG. 30. Ratio of Z + jet cross sections for successive exclusive jet multiplicities N_{jet} in events chosen with symmetric jet selection, i.e., $p_T > 30$ GeV for all jets in the event (top panels) and in events with at least one jet with $p_T > 150$ GeV (bottom panels), with 7 TeV pp collisions at the LHC. Comparisons with fixed-order calculation and MC simulations are included, together with a linear fit (top panels) and a Poisson fit (bottom panels) to the data. From ATLAS Collaboration, 2013e.

FIG. 31.   Cross section for the production of $W+ \geq 2$ jets as a function of the difference in (left panels) the rapidity and (right panels) the dijet invariant mass between the two leading jets for 1.96 TeV $p\bar{p}$ collisions at the Tevatron. Comparisons with a fixed-order calculation and MC simulations are included. From D0 Collaboration, 2013d.

panel), the $\mathcal{O}(\alpha_s^2)$ and $\mathcal{O}(\alpha_s^3)$ calculations are denoted as NLO and NNLO, respectively.

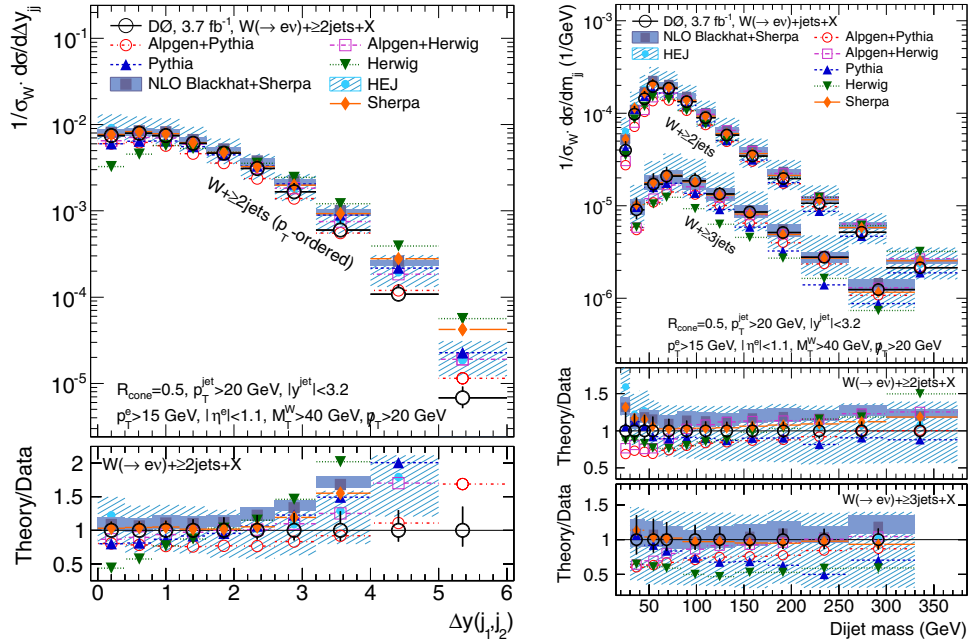The studies of QCD scaling properties are useful for a better understanding of QCD dynamics and in analyses that employ jet vetoes to separate signal processes from $W/Z +$ jet backgrounds (Berends *et al.*, 1989; Gerwick *et al.*, 2012). Figure 30 from ATLAS Collaboration (2013e) reports a study of two different types of scaling in $Z +$ jets in the exclusive jet multiplicity ratios $R_{(n+1)/n} = N_{Z+(n+1)}/N_{Z+n}$. When a symmetric selection of the jet transverse momenta is applied, i.e., $p_T > 30$ GeV for all jets, the so-called staircase scaling is seen, whereas when an asymmetric selection of the jet transverse momenta is applied, i.e., $p_T(\text{leading}) > 150$ GeV and $p_T > 30$ GeV for all other jets, a falling distribution is seen, i.e., the so-called Poisson scaling. The scaling properties measured in the data are well reproduced by the theory. The staircase scaling is a property of non-Abelian theories with $R_{(n+1)/n} = R = e^{-b}$, as $\sigma_n = \sigma_0 e^{-bn}$, and occurs in events with democratic jet selection and no major scale separations. The first bin of the distribution in Fig. 30 (top panels), i.e., $R_{1/0}$, is suppressed by PDF effects by about 60%. The Poisson scaling (already known from final-state-radiation QED at e^+e^- colliders) occurs in events that feature large differences between the scale Q of the process and the radiation cutoff scale Q_0. For $Q \gg Q_0$ each emission is independent from the previous one (the primary emission is typically off the hard parton leg), while for $Q \approx Q_0$ the emissions are correlated (for secondary emissions from secondary quark lines). In this configuration the ratio $R_{(n+1)/n} = \langle n \rangle / n + 1$ follows a Poissonian distribution with $P_n = (1/n!)\langle n \rangle^n e^{-\langle n \rangle}$ and occurs in Abelian theories too. Asymptotically the staircase approximation dominates for large N_{jets}, as can be seen in Fig. 30 (bottom panels).

For other cross-section measurements of $W/Z +$ jet processes at the Tevatron run 2 and at the LHC, see CDF Collaboration (2008b, 2008c), D0 Collaboration (2008a, 2009d, 2011c), ATLAS Collaboration (2011c, 2012f, 2012h, 2017h, 2019b), CMS Collaboration (2012a, 2015c, 2015e, 2017e, 2018d), and LHCb Collaboration (2016, 2019b).

3. Event properties

The measurements of angular distributions provide important tests of the modeling of QCD in the theory, as these measurements are sensitive to the parton emission at small and large angles. Hard emissions at large angles are typically calculated by matrix elements, while unresolved soft or collinear radiation is typically modeled in MC generators by the parton shower. Measurements of the angular $[\Delta\phi(j_1, j_2)]$ or rapidity $[\Delta y(j_1, j_2)]$ separation between the two associated leading jets or their invariant mass (m_{jj}) distribution are important for studies of vector boson fusion or scattering to disentangle the electroweak from the QCD production mechanism; see Sec. III. Figures 31 and 32 show selected measurements of $\Delta y(j_1, j_2)$ and m_{jj} at the Tevatron and the LHC, respectively, in events with a W boson produced associated with at least two jets selected in a broad kinematic region, i.e., jet $p_T > 30\,(20)$ GeV and $|y| < 4.4\,(3.2)$ at the LHC (Tevatron). The fixed-order NLO calculation (BlackHat) is in good agreement with data on $\Delta y(j_1, j_2)$, especially at the LHC. A similar level of discrepancy is seen at the Tevatron and the LHC for SHERPA, while ALPGEN and HEJ [based on Balitsky-Fadin-Kuraev-Lipatov (BFKL)-like resummation] MC generators are in better agreement with the data. The fixed-order NLO calculation (BlackHat) is in good agreement with the data in the m_{jj} distribution in the range accessible by the Tevatron, i.e., up to about 300 GeV.
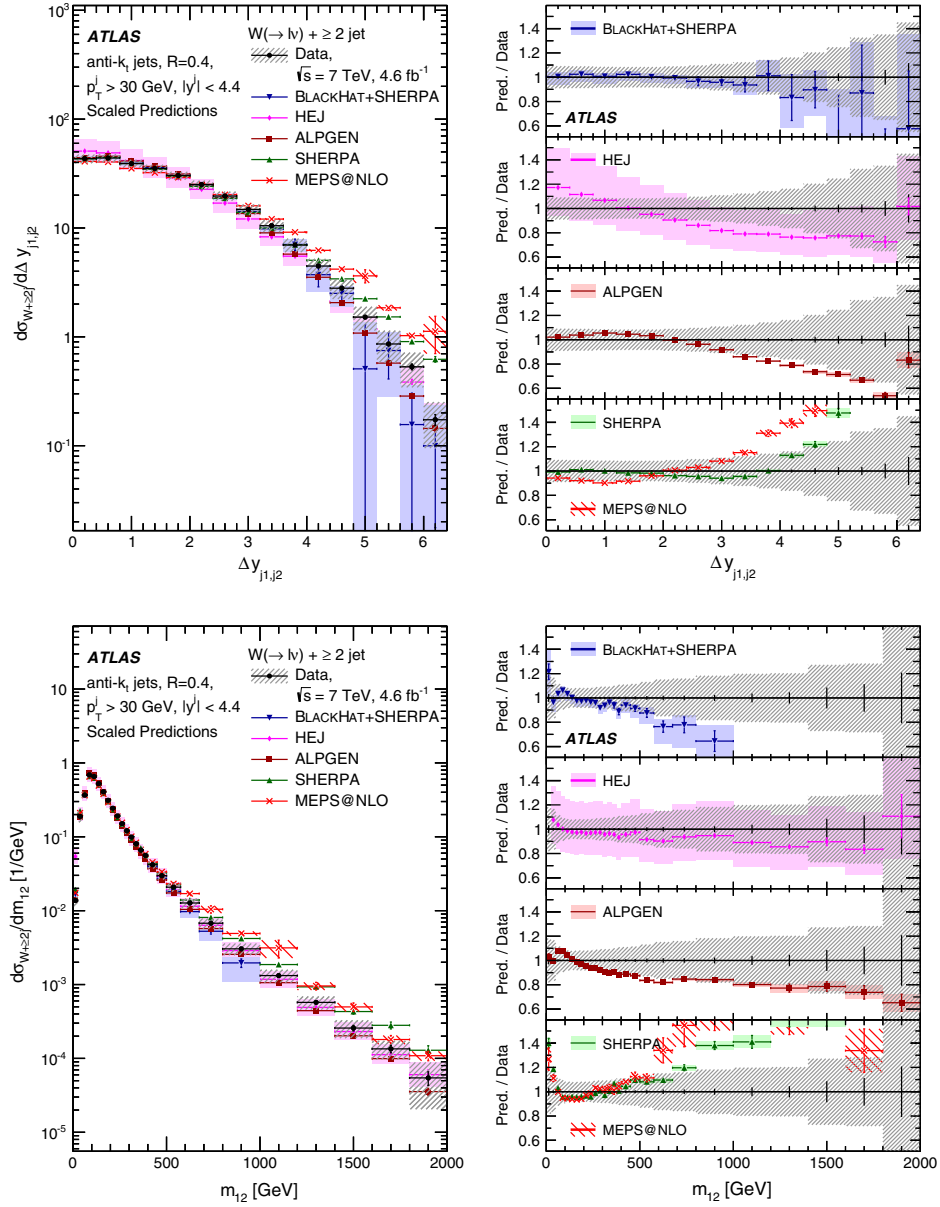
FIG. 32. Cross section for the production of $W+ \geq 2$ jets as a function of the difference in (top panels) the rapidity and (bottom panels) the dijet invariant mass between the two leading jets for 7 TeV pp collisions at the LHC. Comparisons with a fixed-order calculation and MC simulations are included. From ATLAS Collaboration, 2015a.

The LHC measurement of the m_{jj} distribution extends to 2 TeV, and the fixed-order NLO calculation is compared to LHC data up to 1 TeV, showing good agreement up to approximately 500 GeV. The HEJ simulation is in agreement with data over the entire m_{jj} range at the Tevatron and the LHC, but its associated uncertainties are large. Significant discrepancies in the high-m_{jj} region at the LHC are visible in LO and NLO multileg MC predictions in the SHERPA and MEPS@NLO calculations. In such a kinematic region important contributions are expected from the modeling of the beam remnant, underlying event, multiparton interactions, and parton shower. Similar measurements at the LHC (ATLAS Collaboration, 2017h; CMS Collaboration, 2017a, 2017g) in a restricted phase space, i.e., jet $|y| < 2.4$ and m_{jj} up to 700 GeV–1 TeV, are compatible with those presented

previously but in such a kinematic region do not show significant data-theory discrepancies. In an updated analysis of $W+ \geq 2$-jet events at the LHC in the same broad phase space of jet $p_T > 30$ GeV and $|y| < 4.4$, which extends the reach of the m_{jj} distribution to 3 TeV (ATLAS Collaboration, 2018b), good agreement is found between the data and updated theoretical calculations, while the same level of discrepancy is observed with the older LO SHERPA version (1.4). These measurements show that the extension of the kinematic reach of the LHC can expose theoretical mismodeling and can be used to improve the theoretical predictions.

D0 Collaboration (2013d) studied the probability of emission of a third jet in events with a W and at least two associated jets, as a function of the rapidity separation between the two tagged jets, under various definitions of jet tagging (two
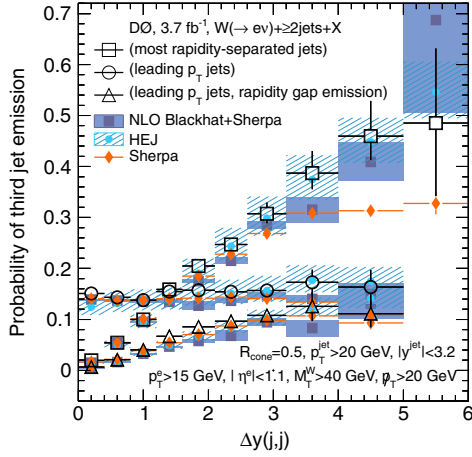
FIG. 33. Measurement of the probability for the emission of a third jet in events with $W+ \geq 2$ jets as a function of the dijet rapidity separation of the two tagging jets for 1.96 TeV $p\bar{p}$ collisions at the Tevatron, and comparisons with theoretical predictions. The definitions of jet tagging are the two most-rapidity-separated jets, the two highest-p_T jets, and the two highest-p_T jets with a third jet produced in the rapidity gap between them. From D0 Collaboration, 2013d.

most-rapidity-separated jets, the two highest-p_T jets, or the two highest-p_T jets with a third jet produced in the rapidity gap between them); see Fig. 33. Such a measurement provides a laboratory for studies of rapidity gaps, central jet veto, and vector boson fusion jet dynamics. They can test the high-p_T and the wide-angle jet production, in a manner complementary to studies of dijet events. The results show that in such configurations there are competing effects of increasing phase space for high-p_T jet emission between jets and decreasing PDFs at large x. The BFKL-based resummation calculation in the HEJ generator best describes the data.

The study of events with a photon and jets is used for searches of new physics signatures, such as heavy resonance states decaying into a photon and a jet. Such new physics processes can produce distinct features in the $\gamma + jet$ final state, such as deviation in the invariant mass of the photon and the jet ($m^{\gamma-\text{jet}}$) or angular correlations between the photon and the jet with respect to SM expectations. Figure 34 presents measurements of differential cross sections as a function of $m^{\gamma-\text{jet}}$ in $\gamma + jet$ events at the LHC at 13 TeV center-of-mass energy, and as a function of azimuthal angular separation between the photon and the third leading jet in events with a photon and at least three jets in pp collisions at 8 TeV center-of-mass energy. The differential cross section of $d\sigma/dm^{\gamma-\text{jet}}$ shown in Fig. 34 (top panels) is monotonically decreasing by more than 4 orders of magnitude up to the highest measured value of $m^{\gamma-\text{jet}} = 3.25$ TeV. Both NLO QCD predictions (fixed-order JETPHOX and SHERPA MC generator that includes the matching of the NLO matrix element with parton showering) describe the data within the experimental and theoretical uncertainties. However, in the highest $m^{\gamma-\text{jet}}$ range a trend of the simulation to overestimate the data is seen. Figure 34 (bottom panel) shows that the cross section $d\sigma/\Delta\phi^{\gamma-\text{jet}\,3}$ increases as $\Delta\phi^{\gamma-\text{jet}\,3}$ increases, indicating the preference for back-to-back configuration between the photon
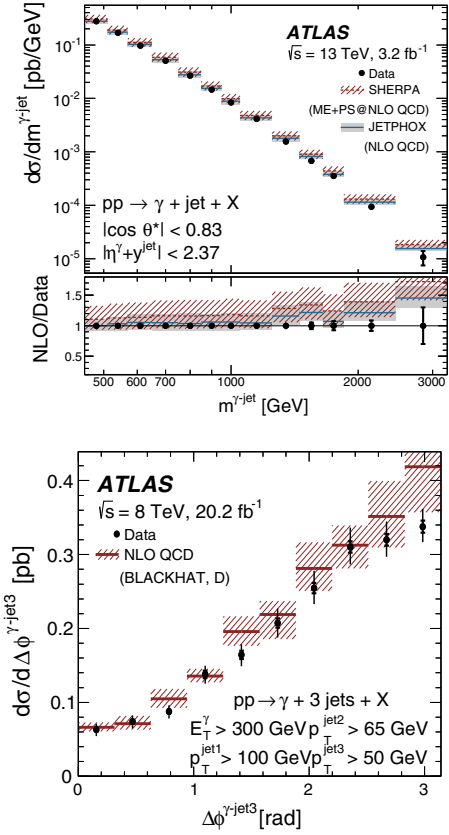

FIG. 34. Top panels: differential cross sections measured at the LHC for isolated-photon plus jet production as a function of $m^{\gamma-\text{jet}}$ at 13 TeV center-of-mass energy. From ATLAS Collaboration, 2018c. Bottom panel: similar differential cross sections for isolated-photon plus three-jet production as a function of $\Delta\phi^{\gamma-\text{jet}\,3}$ for $E_T^\gamma > 300$ GeV at 8 TeV center-of-mass energy. From ATLAS Collaboration, 2017b. Comparisons with theoretical predictions from fixed-order calculations and a MC generator at NLO in pQCD are also made.

and the third leading jet in $\gamma + jet$ events. The fixed-order NLO pQCD prediction by BlackHat gives an adequate description of the angular correlations and their evolution with the energy scale that, however, shows a tendency to systematically overestimate the data.

A recent analysis of $\gamma + 2$ jets $+ X$ production at 13 TeV at the LHC with 36.1 fb^{-1} of integrated luminosity is carried out in two distinct regions of phase space: one enriched with direct photon production and one with photon fragmentation processes. Experimental cross sections are measured as a function of several observables, including $m^{\text{jet+jet}}$, $m^{\gamma+\text{jet+jet}}$ as well as azimuthal and rapidity differences between the photon and the leading jet and between the two jets. Good agreement between data and MC predictions with tree-level multijet matrix element merged to parton shower or with NLO accuracy in QCD are observed in the sample enriched with direct photon production, whereas discrepancies are observed in the sample enriched with fragmentation processes. The precision of the measurement is significantly better than the differences between the predictions, indicating that theoretical uncertainties are much larger than those of an experimental nature (ATLAS Collaboration, 2020c).
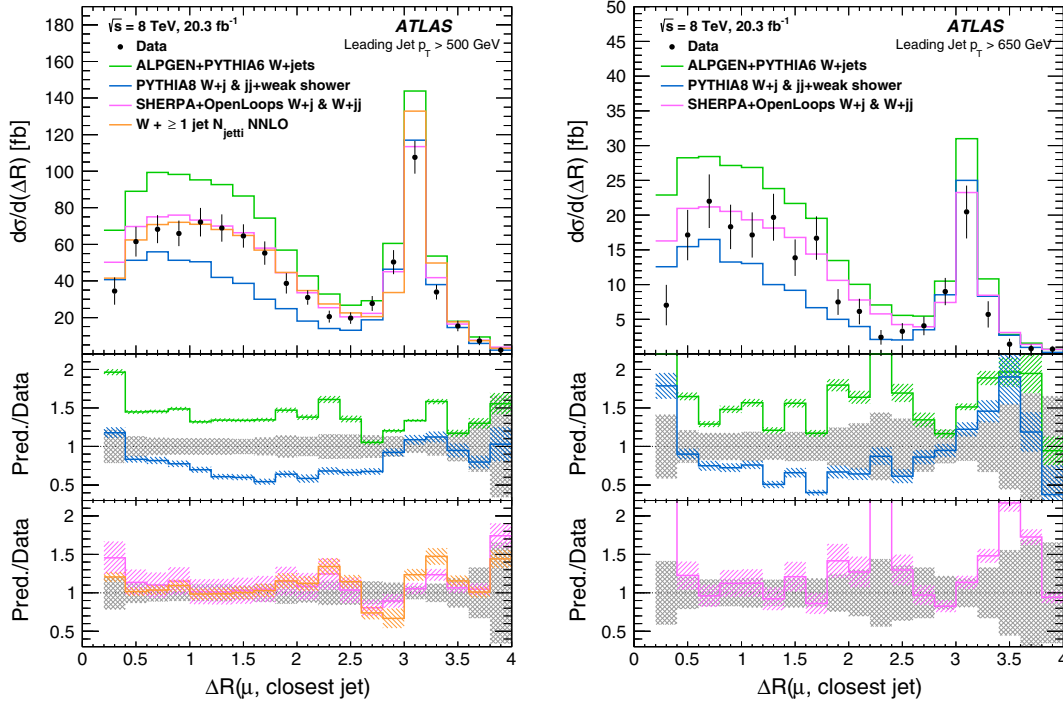
FIG. 35.   Differential $W + $ jet cross section as a function of the angular separation ΔR between the W decay muon and the closest jet for events with p_T (leading jet) > 500 GeV (left panels) and p_T (leading jet) > 650 GeV (right panels), with 8 TeV pp collisions at the LHC. Several different theoretical predictions from MC generators are compared to experimental data. From ATLAS Collaboration, 2017e.

The real emission of a vector boson from an initial- or final-state quark has a collinear divergence in the limit of a massless boson. This may be detected as a collinear enhancement in the distribution of the angular separation between the vector boson and the closest jet. Parton-shower algorithms are implemented in MC generators to account for QCD and QED emissions in the soft and collinear approximation, and an analogous mechanism occurs for the emission of real weak bosons. At high energies the real emission of weak bosons in dijet events can significantly contribute to the inclusive $W + $ jet measurement. Measurements of $W + $ jet production at the LHC are often insensitive to such an effect, as they require large separation between the decay charged lepton and any of the jets. ATLAS Collaboration (2017e) analyzed event configurations in which a muon from a W decay was produced close to a high-transverse-momentum jet. Figure 35 shows the differential cross section for $W + $ jet events with at least one jet with $p_T > 500$ GeV or higher, and any additional jets with $p_T > 100$ GeV, as a function of the ΔR distance between the W decay muon and the closest jet. An enhancement of the collinear event fraction is expected for increasing values of the leading-jet p_T, as the W emission from the jet is enhanced. This effect is illustrated in Fig. 35: as the value of leading-jet p_T increases from $p_T > 500$ GeV to $p_T > 650$ GeV, the fraction of events in the collinear region at low ΔR increases with respect to the fraction of events in the back-to-back configuration. The ALPGEN MC simulation for $W + $ jet production overestimates the data, especially in the collinear region. The prediction by PYTHIA8, which is modified to explicitly include the process of W-boson emission as electroweak final-state radiation in the parton shower of a

dijet event, underestimates the data in the collinear region. The best agreement over the entire distribution is provided by SHERPA + OpenLoops $W + 1$-jet and $W + 2$-jet calculations that incorporate NLO QCD and NLO EW corrections. In the high-p_T regime the NLO EW corrections have a significant effect, up to about 20%. The "$W + \geq 1$ jet N_jetti NNLO" prediction, which uses a technique based on N jettiness to split the phase space for the real emission corrections, provides a description similar to SHERPA + OpenLoops. Such a topology will be more accessible and important with run 2 data at 13 TeV center-of-mass energy and with larger datasets at the LHC, as well as at higher proton collision energies, for example, at future higher-energy proton colliders.

Other studies of correlations between the vector boson and the jets have been undertaken, as they provide important benchmarks for calculations and for the tuning of MC simulations. One example is the study of the Z-boson production in a boosted regime of the Z boson that is important for modeling the background from a Z boson decaying into neutrinos in searches of new physics with missing transverse energy in the final state. Figure 36 shows different levels of azimuthal correlations between the Z boson and the three leading jets [$\Delta\phi(Z, j_i)$] in $Z + \geq 3$-jet events in two different event configurations, i.e., with $p_T^Z > 0$ GeV or $p_T^Z > 150$ GeV. Large correlations are visible between the Z boson and the leading jet, whereas smaller correlations are present between the Z boson and the subleading jets. In events with a boosted Z the correlation between the Z boson and the leading jet is enhanced. Good modeling is provided by LO multileg (SHERPA, MadGraph) and NLO $Z + 1$-jet (POWHEG) generators. The PYTHIA6 prediction, which relies on the
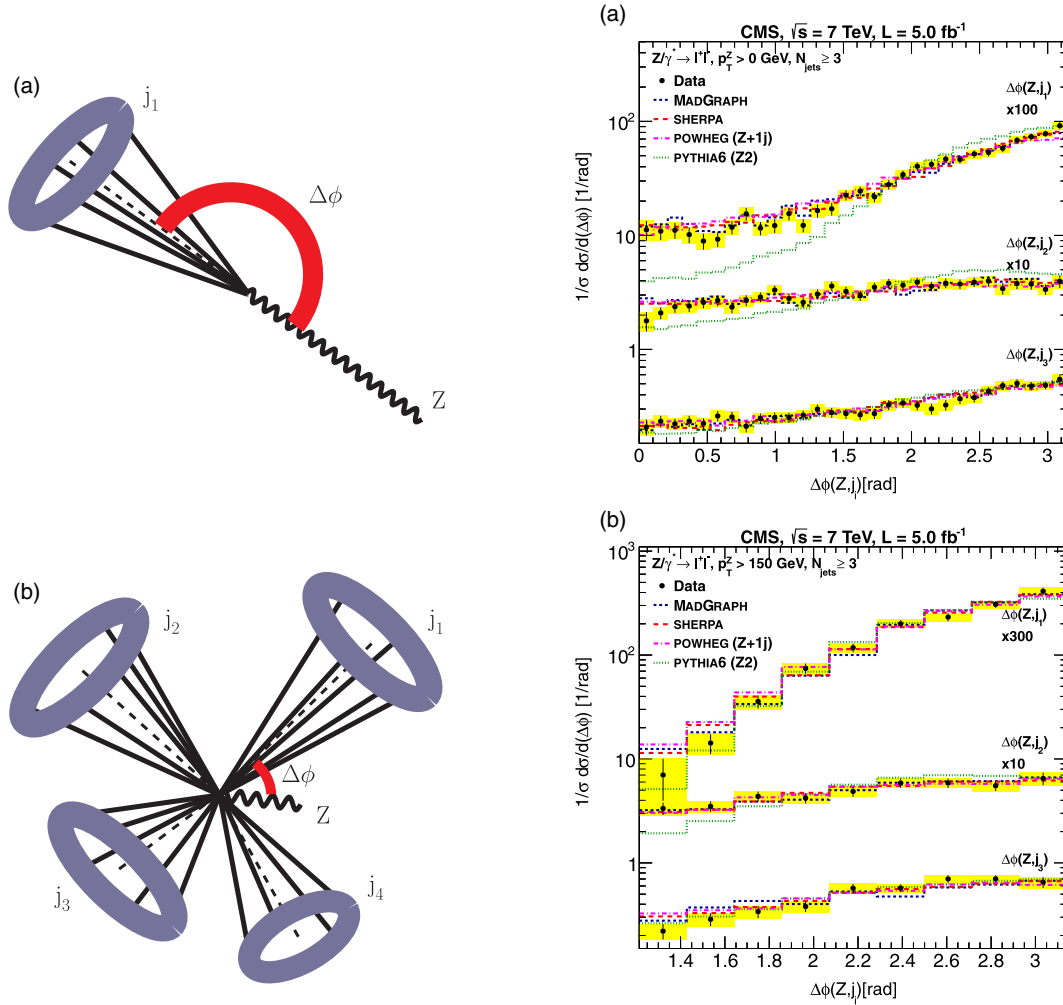
FIG. 36.   Topology of Z + jet events for (top-left panel) $\Delta\phi(Z, j_1) \to \pi$ and (bottom-left panel) $\Delta\phi(Z, j_1) \ll \pi$. Normalized $\Delta\phi(Z, j_i)$ $(i = 1, 2, 3)$ distributions for the inclusive $N_{\mathrm{jets}} \geq 3$ for (top-right panel) $p_{\mathrm{T}}^Z > 0$ GeV and (bottom-right panel) $p_{\mathrm{T}}^Z > 150$ GeV, with 8 TeV pp collisions at the LHC, compared to theoretical predictions from MC generators. From CMS Collaboration, 2013c.

parton-shower simulation for parton emission, shows better modeling in the small-$\Delta\phi$ region in the high-Z p_{T} regime, where the soft and collinear approximation of the parton shower is most applicable.

Multiparton interations (MPIs) are a necessary ingredient of simulations for the description of particle multiplicities and energy flow, and they may contaminate event samples for precision measurements (such as those for Higgs boson properties) and new physics searches. The greater the $\sqrt{s}$ (and thus the lower the parton momentum fraction x), the bigger the impact of MPIs at high p_{T}. Therefore, the MPI contribution is generally more significant at the LHC than at the Tevatron. The impact of MPIs in physics processes is difficult to measure, as it coexists with initial- and final-state radiation, beam remnants, and the hard interaction. Experimentally the MPI contribution must also be disentangled from pileup interactions. Double parton scattering (DPS) is a specific case of MPIs and its production cross section is typically parametrized as $\sigma_{\mathrm{DPS}} = \sigma_A \sigma_B / \sigma_{\mathrm{eff}}$, where σ_A and σ_B are the parton-level cross sections of the two underlying processes (assumed to be independent), while σ_{eff} is an effective area parameter and is assumed to be independent of phase space and process. These

assumptions are tested by measuring σ_{eff} in several processes and at different energy scales. The DPS contribution to the inclusive W production was studied in $W + 2$-jet events by ATLAS Collaboration (2013b) and CMS Collaboration (2014f). Figure 37 (top panels) shows examples of the two contributions to the $W + 2 - $jet event sample: DPS (top-left panel) and single parton scattering (SPS) (top-right panel). The fraction of DPS events in $W + 2 - $jet data and σ_{eff} are extracted from a fit of DPS and SPS templates to the normalized transverse-momentum balance $\Delta_{p_{\mathrm{T}}}^{\mathrm{rel}} = (|\vec{p}_{\mathrm{T}}^{j1} + \vec{p}_{\mathrm{T}}^{j2}|)/(|\vec{p}_{\mathrm{T}}^{j1}| + |\vec{p}_{\mathrm{T}}^{j2}|)$. Figure 37 shows the template fit results compared to the data. The values of σ_{eff} measured at 7 TeV by the ATLAS and CMS experiments are $15 \pm 3(\mathrm{stat})_{-3}^{+5}(\mathrm{syst})$ and $20.7 \pm 0.8(\mathrm{stat}) \pm 6.6(\mathrm{syst})$ mb, respectively. To test the energy dependence of σ_{eff}, it is important to repeat such measurements at experiments with greater center-of-mass energies. Moreover, higher $\sqrt{s}$ in future measurements implies a larger phase space available for DPS, and thus a greater need for more precise DPS measurements.

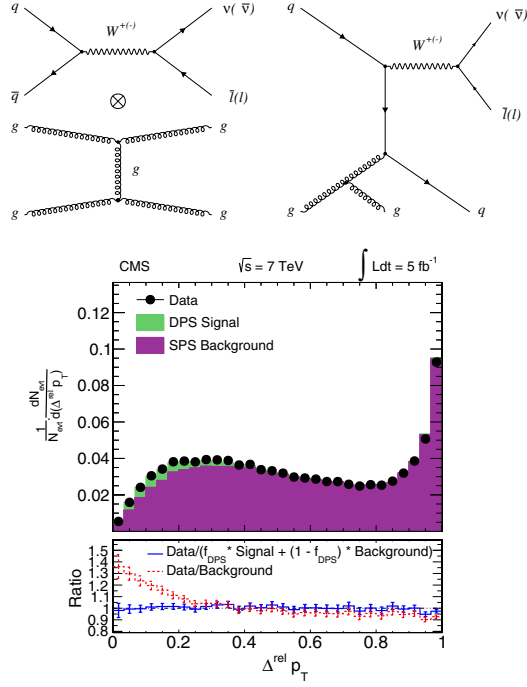For other measurements of $V +$ jet properties, see D0 Collaboration (2010b), CMS Collaboration (2011c),

FIG. 37. Feynman diagrams for $W + 2$-jet production from (top-left panel) DPS and (top-right panel) SPS. Bottom panels: fit results for the DPS-sensitive observable $\Delta_{p_T}^{rel}$ at 7 TeV pp collisions at the LHC. From CMS Collaboration, 2014f.

ATLAS Collaboration (2013c, 2013e, 2017f, 2017h), and LHCb Collaboration (2014b).

4. Cross-section ratios

Measurements of production cross sections of individual $V +$ jet processes are limited in high-statistics regions of phase space by systematic uncertainties that are common between processes, while measurements of ratios of different $V +$ jet processes exploit partial cancellations of experimental uncertainties as well as theoretical effects that are common between the two processes in the ratio. Such ratios can provide high-precision tests of the standard model, as they are sensitive to nonuniversal corrections in QCD and electroweak calculations as well as PDFs. In this section several ratios are presented. In the ratio of W^+ to W^- productions, pQCD and electroweak effects cancel to a large extent, making this measurement particularly sensitive to PDFs, and specifically to the ratio of up quark to down quark at high Bjorken x. In the W-to-Z-boson ratio, effects from nonperturbative QCD processes largely cancel at high energy scales, whereas other effects do not cancel, such as boson mass effects at low energy scales, quark-gluon and quark-antiquark contributions to $V +$ jet productions, and nonuniversal electroweak corrections. Such a ratio is therefore useful for validating theoretical predictions used to estimate $W +$ jet or $Z +$ jet backgrounds in searches for new physics. Similarly, in the ratio of Z to γ bosons, mass effects cancel at high energy scales, whereas higher-order QCD and electroweak corrections can have large contributions, thus making such a ratio a precise test of higher-order effects in perturbative calculations.
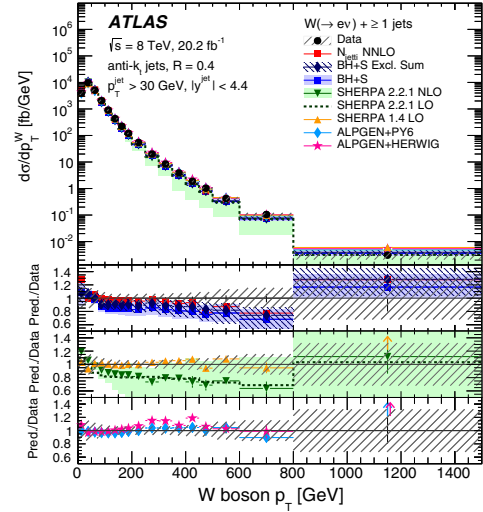

FIG. 38. Differential cross section for the production of a W boson as a function of the W p_T for events with $N_{jets} \geq 1$ in pp collisions at 8 TeV center-of-mass energy at the LHC. The experimental results are compared with several theoretical predictions calculated at different orders and with different approximations in pQCD, and with different parton-shower implementations. From ATLAS Collaboration, 2018b.

In the analysis presented by ATLAS Collaboration (2018b) measurements are carried out for $W^{\pm}$ production, as well as for W^+ and W^- production and the cross-section ratio of W^+/W^- in events with the W boson produced with associated jets, as a function of a number of variables that are sensitive to higher-order terms and the PDFs. In the W^+/W^- ratio in W events with at least one associated jet, many of the experimental and theoretical uncertainties cancel out, making it a more precise test of the theoretical predictions, especially in a kinematic regime with x values higher (approximately up to $x = 0.1$–0.3) than what is typically accessible in measurements of inclusive W production at ATLAS and CMS ($10^{-4} < x < 10^{-1}$). Figure 38 shows the differential cross section as a function of the p_T of the W boson for events with $W^{\pm} + \geq 1$ jet production. Good overall agreement is found between the data and most of the LO, NLO, and NNLO calculations. Variations in the modeling of different SHERPA generator versions are seen, whereas different parton-shower models interfaced to the ALPGEN generator show little impact, with PYTHIA providing a slightly better description of the data. In the W^+/W^- cross-section ratio in Fig. 39, differences due to QCD and electroweak higher-order effects cancel out to a large extent. In the ratio, the experimental precision is greatly improved and most predictions show a trend to overestimate the data. The data are also compared with different PDF sets with a common calculation using the MCFM program. Sensitivity to PDFs is visible in the variation of agreement between the data and the different PDF sets, especially in the region of $p_T \approx 200$–400 GeV, where experimental uncertainties are in the 2%–6% range. In this region the predictions from different PDF sets may differ by about 2% to 5% and, in some cases, differ from the data up to 2 to 3 standard deviations.

The production mechanisms of $W +$ jets and $Z +$ jets are similar once the kinematic effect of the different boson masses
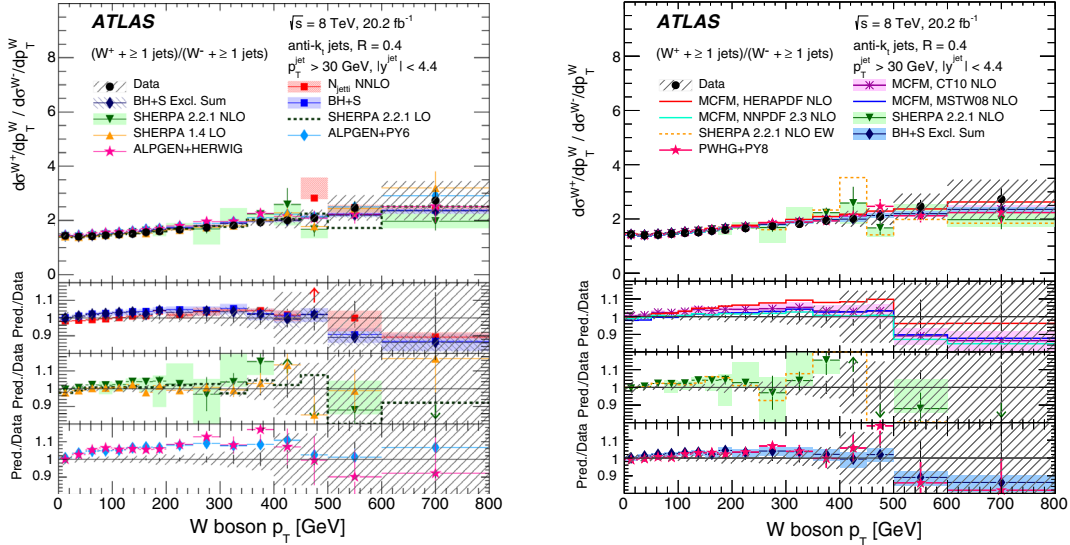
FIG. 39. Differential cross section for the W^+/W^- ratio as a function of the W p_T for events with $N_{jets} \geq 1$ in pp collisions at 8 TeV center-of-mass energy at the LHC. The experimental results are compared with several theoretical predictions calculated at different orders, with different approximations in pQCD and different parton-shower implementations, and with NLO MCFM predictions for four different PDF sets. From ATLAS Collaboration, 2018b.

and the leptonic branching ratios are taken into account. In ratios of differential cross sections in W + jet and Z + jet events (R_{jets}), the experimental uncertainty cancels significantly, as seen in Fig. 18. Theoretical uncertainties, if treated as correlated between the two types of processes, can be significantly reduced too: QCD scale variations, estimated at NLO in pQCD, and PDF uncertainties overall account for a

2%–4%-level uncertainty in R_{jets} with at least one jet in the final state with jet $p_T \simeq 800$ GeV, compared to the 20% level of uncertainty in events with a W boson with at least one associated jet. Such a reduction in theoretical uncertainty is also visible in the phenomenological study presented in Fig. 7 in Sec. II.A.1. Figure 40 shows that the level of mismodeling of the MC simulations that is seen in the cross-section
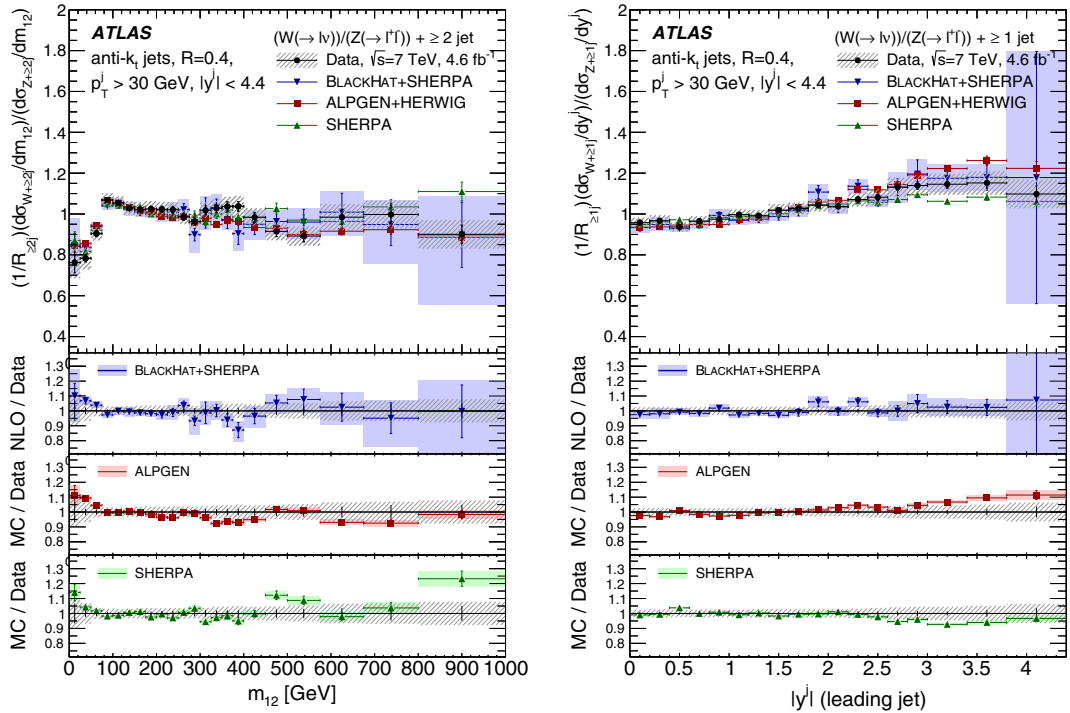
FIG. 40. The normalized ratio of W + jet and Z + jet production cross sections R_{jets}, as a function of the dijet invariant mass m_{12}, for $N_{jets} \geq 2$ (left panels), and the leading-jet absolute rapidity $|y^j|$ for $N_{jets} \geq 1$ (right panels) with 7 TeV pp collisions at the LHC. The experimental results are compared with NLO calculations in pQCD using BlackHat as well as with MC generators. From ATLAS Collaboration, 2014a.
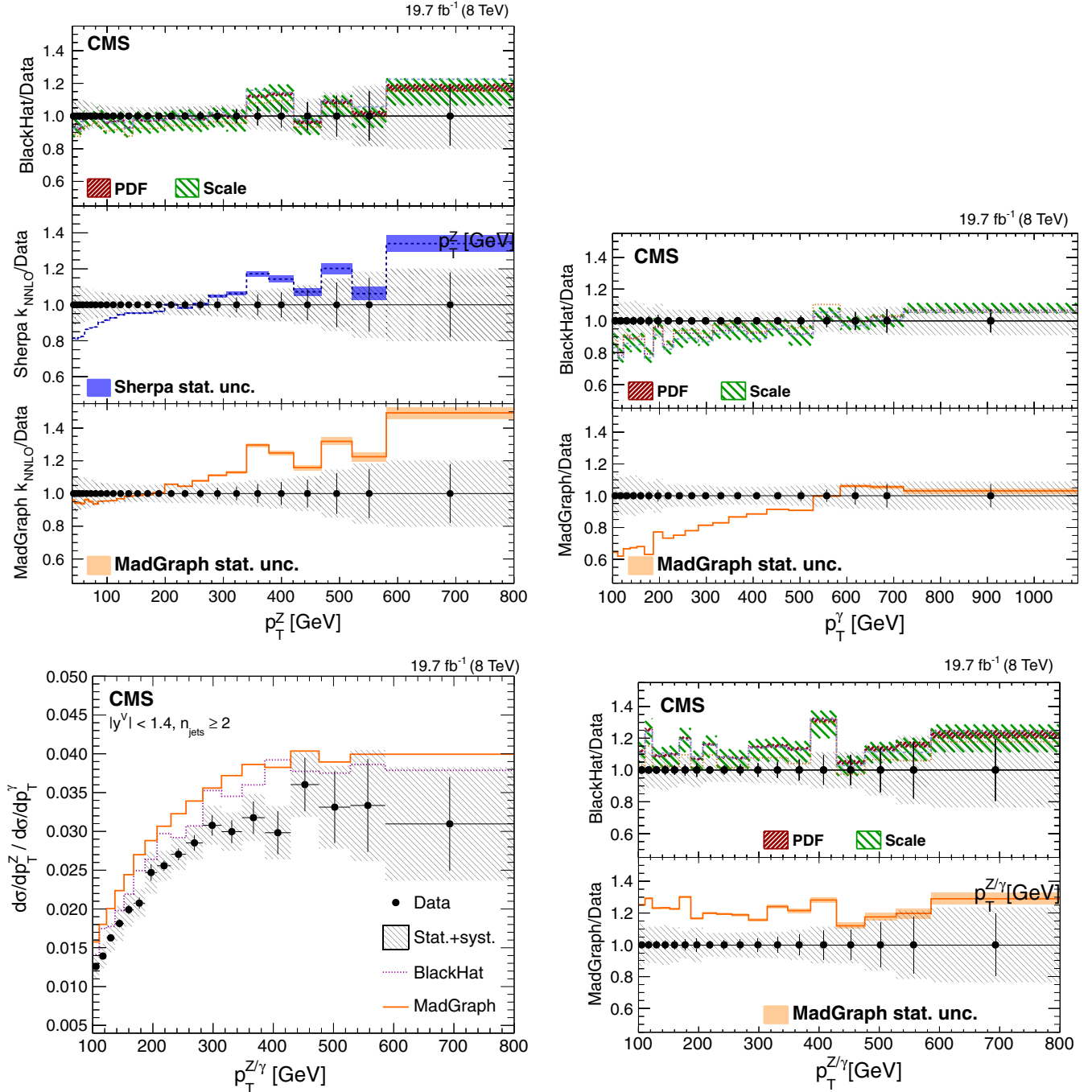
FIG. 41. Top panels: prediction-to-data ratios of differential cross sections for Z and central ($|y^\gamma| < 1.4$) γ productions as a function of the boson p_T for inclusive Z + jet and γ + jet processes with a $N_{jets} \geq 2$ selection, with 8 TeV pp collisions at the LHC. Bottom panels: differential cross section ratio of Z + jets over γ + jets and its prediction-to-data ratios as a function of the boson transverse momentum for central bosons ($|y^V| < 1.4$) in the $N_{jets} \geq 2$ sample. Experimental results are compared with the NLO pQCD calculation using BlackHat and with the MadGraph MC generator. From CMS Collaboration, 2015a.

measurement as a function of m_{jj} for W + jets in Fig. 32 is largely reduced in R_{jets}. This effect points toward an underlying cause for the mismodeling in MC generators that has the same effect in both processes. The low part of the m_{jj} distribution in W + jet or Z + jet events has sensitivity to jet kinematics and nonperturbative effects in soft QCD radiation that differ between W and Z events and do not cancel in the R_{jets} ratio, as seen in the R_{jets} values lower than 1

for $m_{jj} < 100$ GeV in Fig. 40 (left panels). The agreement between predictions and data in the region of high rapidity of the p_T-leading jet [see Fig. 40 (right panels)] can be affected by the modeling of the parton shower and PDF. Such a ratio measurement is important not only for a better understanding of the theoretical modeling of W/Z + jet processes but also for the estimation of backgrounds on searches for new physics. For example, the calculation of such a ratio is used
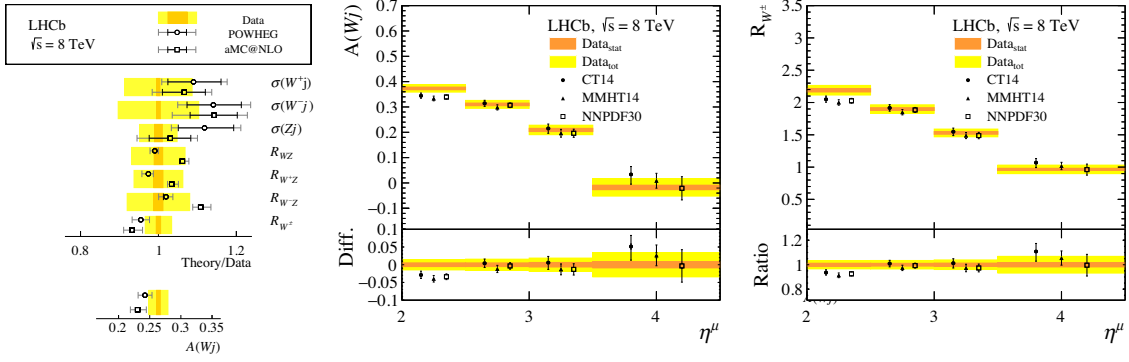
FIG. 42.   Summary of the $W/Z +$ jet measurements performed in a fiducial region with the LHCb experiment at 8 TeV pp collisions at the LHC (left panel) compared with predictions from two MC generators. The cross sections for $W^+ + \geq 1$ jet, $W^- + \geq 1$ jet, and $Z+ \geq 1$ jet are denoted as $\sigma(W^+ j)$, $\sigma(W^- j)$, and $\sigma(Zj)$, respectively, while the ratios $\sigma(Wj)/\sigma(Zj)$, $\sigma(W^+ j)/\sigma(Zj)$, $\sigma(W^- j)/\sigma(Zj)$, and $\sigma(W^+ j)/\sigma(W^- j)$ are denoted as R_{WZ}, $R_{W^+ Z}$, $R_{W^- Z}$, and $R_{W^\pm}$, respectively. The asymmetry of $\sigma(W^+ j)$ and $\sigma(W^- j)$ is denoted as $A(Wj)$. The asymmetry $A(Wj)$ (middle panel) and the ratio $R_{W^\pm}$ (right panel) as a function of the muon pseudorapidity η^μ compared with NLO calculations performed with the FEWZ calculation and three different PDF sets. From LHCb Collaboration, 2016.

as a *transfer factor* to estimate the $Z(\to \nu\nu) +$ jet background yield in a search signal region by extrapolating the measurement of the $W(\to l\nu) +$ jet yield from a data control region; see the examples given by CMS Collaboration (2012c, 2017c, 2019f) and ATLAS Collaboration (2014d, 2014h, 2016i).

The ratio of $\gamma +$ jets and $Z +$ jets is also of great interest, especially in the high-p_T region of the vector bosons, where the Z-boson mass effects play a less significant role than in the low-p_T region. This ratio can test the impact of QCD and electroweak higher-order corrections with greater experimental accuracy, thanks to cancellation of experimental systematic uncertainties such as jet energy calibration and luminosity; see Fig. 41. The NLO pQCD calculation with BlackHat describes the Z-boson p_T spectrum well, but it tends to underestimate the low part of the photon p_T spectrum in events with at least two associated jets. In the LO multileg MC generators (MadGraph + PYTHIA6 and SHERPA) a similar systematic trend of mismodeling the Z p_T in $Z+ \geq 2$ jets is seen, as is a significant bias at modeling the shape of the photon p_T distribution; see the MadGraph + PYTHIA6 prediction. The p_T distribution of the Z/γ ratio flattens at high boson p_T values, i.e., those greater than 350 GeV. The boson p_T shape mismodeling observed in the individual Z and γ production events largely cancels out in the Z/γ ratio and a residual overestimation of the ratio by a flat 20% is observed in QCD LO multileg MC generators; see the MadGraph + PYTHIA6 prediction. A less significant systematic mismodeling is also visible in the NLO fixed-order calculation by BlackHat.

The production of W and Z bosons associated with jets is studied in the forward region of proton-proton collisions with the LHCb experiment. Such measurements provide additional tests of the SM in a region of phase space not directly accessible by ATLAS and CMS at the LHC and provide additional constraints on PDFs in a different range of Bjorken x. As shown in Fig. 42, in the LHCb experiment the charged leptons from the weak boson decay are reconstructed in the forward pseudorapidity region of $2.0 < \eta^l < 4.5$, while jets are in the region $2.2 < \eta^{jet} < 4.2$ with the anti-k_t algorithm with distance parameter $R = 0.5$ and $p_T^{jet} > 20$ GeV (LHCb

Collaboration, 2016). Cross sections and their respective ratios are measured for $W^+ + \geq 1$ jet, $W^- + \geq 1$ jet, and $Z+ \geq 1$ jet. In addition, the asymmetry of $W^+ + \geq 1$ jet and $W^- + \geq 1$ jet production and the asymmetry as a function of the charged lepton η are measured. Owing to the cancellation of the scale uncertainties, the ratios as a function of the charged lepton η are expected to provide sensitivity to the PDFs. Figure 42 shows the broad range of measurements that are carried out in this analysis and the extensive comparisons with predictions from different MC generators and PDFs. Overall good agreement is seen between data and predictions; however, slightly larger values of the asymmetry and the ratio of $W^+ + \geq 1$ jet to $W^- + \geq 1$ jet cross sections are seen in the data than in the NLO QCD predictions in the first bin of the charged lepton η.

III. ELECTROWEAK PRODUCTION OF A VECTOR BOSON AND TWO JETS

A. Theoretical predictions

The production of a single vector boson in vector boson fusion (VBF) constitutes an experimental signature of special interest because of its sensitivity to the self-interactions of the electroweak gauge bosons. It presents a prime test bed for searches for new physics signals that are connected to the electroweak symmetry breaking.

The electroweak production of a single vector boson proceeds at $\mathcal{O}(\alpha^4)$ at leading order and contains multiple distinct topologies. Of particular interest are (a) the classic vector boson fusion topologies, (b) the closely related multiperipheral topologies, (c) bremsstrahlung-like electroweak boson emission off electroweak quark scattering topologies, and (d) semileptonic diboson production topologies (s-channel). They are depicted in Fig. 43. Although not all topologies exist for all external flavor configurations, the different diagrams of Fig. 43 interfere and cannot be separated. Nonetheless, in different regions of the phase space different topologies will dominate and suitable approximations can be constructed. In addition to the diboson region, in which both
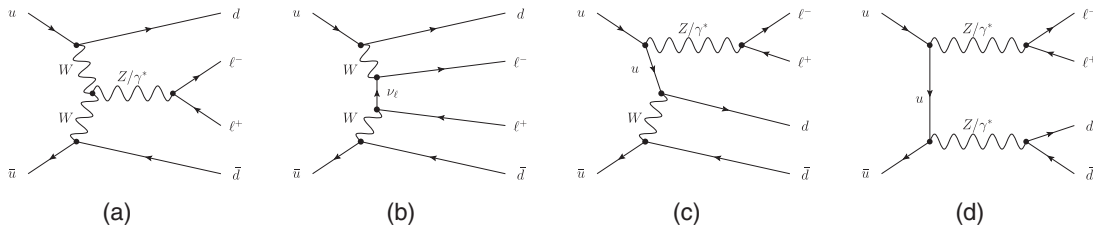
FIG. 43.   Representative Feynman diagrams for the production of two charged leptons associated with two jets at $\mathcal{O}(\alpha^4)$: (a) vector boson fusion and (b) multiperipheral, (c) bremsstrahlung-like, and (d) semileptonic diboson production.

the invariant mass of the lepton pair and the invariant mass of the two final-state jets are close to the nominal W and Z boson masses, the vector boson fusion region is of particular interest. This region is characterized by a large invariant mass of the two final-state jets and their large separation in rapidity, typically $m_{jj} > 600$ GeV and $\Delta y > 4.5$. Here a subclass of the diagrams in Fig. 43(a) dominate the cross section.[6]

The main irreducible background in experimental measurements of the electroweak production of a single vector boson associated with at least two jets is its QCD production channel, proceeding at $\mathcal{O}(\alpha_s^2 \alpha^2)$ at LO.[7] As the electroweak production mode is characterized by a color-neutral t-channel exchange, it exhibits reduced hadronic activity in the central region between the leading jets. Such a suppression does not exist in its QCD production mode, and a veto on central or, in fact, any additional jet activity can further enhance the sought-after signal. Such jet vetoes, however, are typically poorly described by fixed-order perturbation theory due to the emergence of logarithms of the ratio of the hard scale and the jet veto scale, and the best available description for this observable is offered by conventional parton showers.

1. Higher-order computations

All higher-order calculations to date have been performed in the previously introduced vector boson fusion approximation wherein not only are s-channel contributions neglected but also t- and u-channel interferences are not taken into account. This simplifies the calculation immensely in two ways. First, it separates the two quark lines in color space, thus effectively rendering the calculation a "double–deep-inelastic scattering" one. Second, it facilitates the calculation of its NLO QCD correction by removing all components at $\mathcal{O}(\alpha_s \alpha^4)$ that possess EW divergences with respect to the $\mathcal{O}(\alpha_s \alpha^3)$ Born process. The production processes of all EW vector bosons, W, Z, and γ, in this approximation are implemented in the VBFNLO library (Oleari and Zeppenfeld, 2004; Jäger, 2010; Baglio *et al.*, 2014). Figure 44 displays the results for W and photon production in vector boson fusion, respectively. As can be seen, the NLO QCD corrections are generally small.

---

[6]Typically, to maximize the data statistics, experimental measurements apply much looser cuts. The suitability of the VBF approximation in such a phase space must be confirmed if theory predictions calculated in this approximation are to be tested against the data.

[7]This distinction between QCD and EW production channels is tied to a leading-order interpretation of the process where their interference is small in the VBF phase-space region. It breaks down in other regions or at higher orders.

Complete EW corrections are not known and will have to be calculated for the full $\mathcal{O}(\alpha^4)$ process.

2. Monte Carlo event generators

The previously mentioned fixed-order NLO QCD calculations have been matched to parton showers. Explicit implementations exist in the POWHEG generator (Jäger, Schneider, and Zanderighi, 2012; Schissler and Zeppenfeld, 2013) but are also available in the automated NLOPS tools. Further, multijet-merged calculations exist at LO accuracy.

One key aspect in the selection of VBF-type events is the aforementioned rapidity gap. Therefore, a good description of the radiation pattern of the third jet, and any further higher-order radiation, is mandatory. Care must be taken to ensure that the initial color and starting scale assignment in the parton showers is correct in order to preserve the unique rapidity gap structure and not spuriously fill it with additional radiation. The supplementation with LO matrix elements in the previously mentioned matching helps in controlling the associated uncertainties on the level of a few percent, but higher accuracy would be desirable.

B. Experimental results

Initial measurements of the electroweak production of a vector boson and two jets were performed by the CMS Collaboration in the final state with two charged leptons and two jets (VBF Z channel) with 7 TeV proton collision data (CMS Collaboration, 2013b). The precision obtained in this first measurement was around 30%, limited mostly by systematic uncertainties on the jet energy scale and the background modeling.

Improved measurements were obtained with 8 TeV data by both ATLAS Collaboration (2014e) and CMS Collaboration (2015d), with precisions of around 20% and signal significances just above 5 standard deviations. Measurements of the VBF Z process with 13 TeV were also performed by ATLAS Collaboration (2017c) with 2015 data, CMS Collaboration (2018a) with 2016 data, and ATLAS Collaboration (2021) with the full run 2 data. These ATLAS and CMS measurements reach overall precisions of 20% and 10%, respectively.

We note that the measurements provided by ATLAS and CMS are significantly different but complementary. Since the first measurement, CMS has defined the VBF Z signal in an inclusive phase space in the four-fermion final state $\ell\ell jj$, with
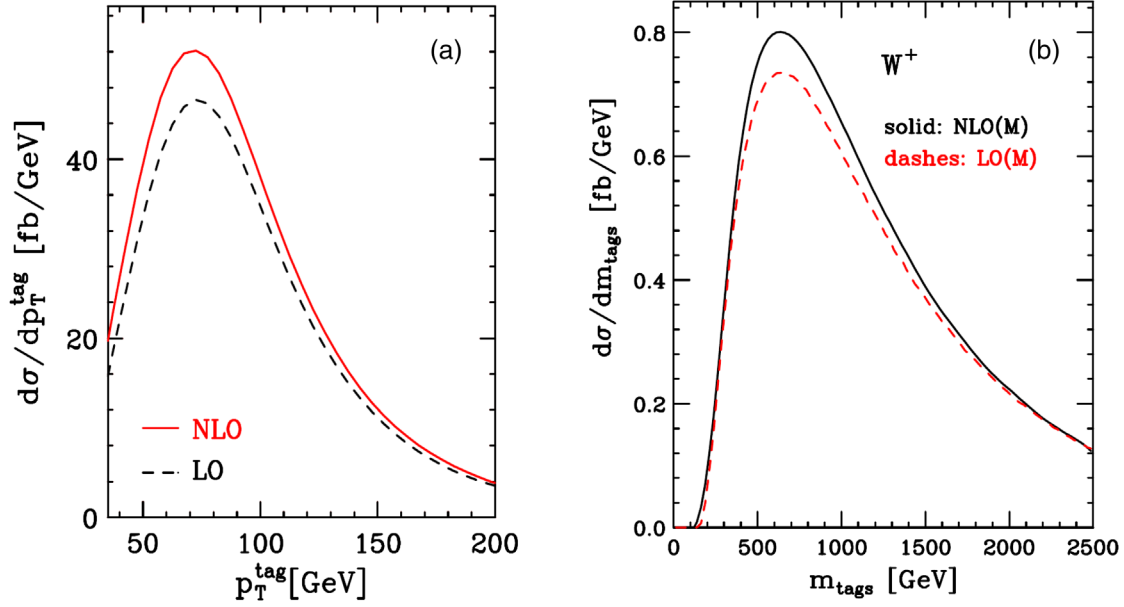
FIG. 44. (a) Leading tagging-jet transverse momentum in prompt-photon production associated with at least two jets through vector boson fusion calculated at LO and NLO QCD accuracy using VBFNLO. From Jäger, 2010. (b) Invariant mass of the tagging-jet pair in the production of a charged lepton and a neutrino associated with at least two jets through vector boson fusion calculated at LO and NLO QCD accuracy using VBFNLO. From Oleari and Zeppenfeld, 2004.

$m_{\ell\ell} > 50$ GeV and $m_{jj} > 120$ GeV, in which all pure EW diagrams of order $\alpha_{\rm EW}^4$ contribute to the signal definition, whereas ATLAS has performed measurements with the signal defined in higher dijet mass fiducial phase-space regions. The ATLAS signal definition is at particle level, where the dijet invariant mass condition is implemented on the two $p_{\rm T}$-leading jets after clustering the final-state particles, and the simulation setup includes NLO QCD corrections, implemented with POWHEG (Jäger, Schneider, and Zanderighi, 2012; Oleari and Zeppenfeld, 2004), and does not include

s-channel diboson contributions. Figure 45 (left panels) shows the dijet invariant mass distribution that is used by ATLAS to extract the signal contribution in the high dijet mass tail with 8 TeV data (ATLAS Collaboration, 2014e). Measurements by CMS are extracted by fitting the dijet invariant mass but also making use of more sophisticated multivariate discriminants with different event observables. Among the CMS multivariate inputs is an internal jet composition discriminator used to separate features of quark- and gluon-initiated jets, applied to the two VBF tagging jets (CMS Collaboration,
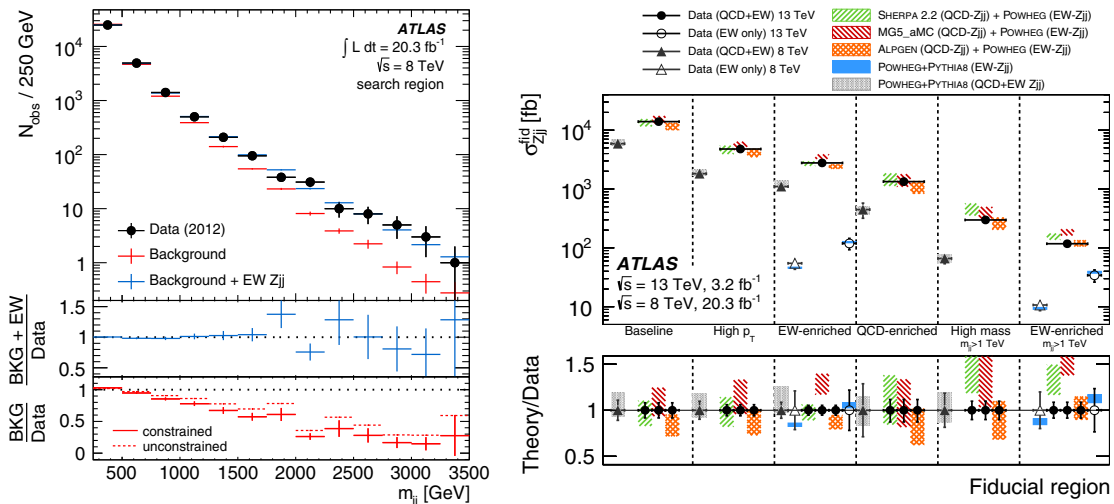
FIG. 45. Left panels: the dijet invariant mass distribution in the search region. The signal and constrained background templates are scaled to match the number of events as a result of a fit to the data. The lowest panel shows the ratio of constrained and unconstrained background templates to the data. From ATLAS Collaboration, 2014e. Right panels: cross-section measurements in different fiducial regions at 8 and 13 TeV compared with theoretical predictions (shaded or hatched bands). The bottom panel shows the ratio of the various theoretical predictions to the data as shaded bands. Relative uncertainties in the measured data are represented by an error bar centered at unity. From ATLAS Collaboration, 2017c.

TABLE I. Summary of VBF Z production cross sections measured at the LHC in the $\ell\ell jj$ final state with different m_{jj} definitions and different proton collision energies. All quoted cross sections are for a single lepton flavor.

m_{jj} cut	$\sqrt{s} = 7$ TeV	$\sqrt{s} = 8$ TeV	$\sqrt{s} = 13$ TeV
120 GeV	154 ± 58 fb (CMS Collaboration, 2013b)	174 ± 43 fb (CMS Collaboration, 2015d)	534 ± 60 fb (CMS Collaboration, 2018a)
250 GeV		54.7 ± 11.2 fb (ATLAS Collaboration, 2014e)	119 ± 26 fb (ATLAS Collaboration, 2017c)
1 TeV		10.7 ± 2.1 fb (ATLAS Collaboration, 2014e)	37.4 ± 6.5 fb (ATLAS Collaboration, 2021)

2013e, 2017b). The ATLAS measurements include several additional fiducial regions where inclusive cross sections are also measured. Figure 45 (right panels) shows a summary of such inclusive measurements with 13 TeV data (ATLAS Collaboration, 2017c). The most recent ATLAS results (ATLAS Collaboration, 2021) focus on differential cross-section measurements, both for the electroweak signal component and, inclusively for the signal and background production, for different observables. Table I shows a summary of inclusive VBF Z cross sections that have been measured to date at the LHC.

Analogous measurements were performed in the single charged-lepton plus dijet final state (VBF W channel) by CMS with 8 TeV collision data (CMS Collaboration, 2016), ATLAS with 7 and 8 TeV collision data (ATLAS Collaboration, 2017g), and CMS with 13 TeV collision data (CMS Collaboration, 2020b). A variety of signal definitions have also been chosen for the VBF W channel. The CMS Collaboration has used four-fermion LO definitions with $m_{jj} > 120$ GeV (as for VBF Z) and with $m_{jj} > 1$ TeV, while the ATLAS Collaboration makes use of NLO signal modeling with $m_{jj} > 0.5$, 1, and 2 TeV cuts defined at particle level after parton showering and jet clustering. Figure 46 shows the multivariate output distribution used to measure the inclusive cross section at 13 TeV in the electron channel, and different

particle-level fiducial cross sections performed at 8 TeV, respectively, by CMS and ATLAS. Table II shows a summary of inclusive VBF W cross sections that have been measured to date at the LHC.

Both of the VBF Z and W measurements by ATLAS at 8 TeV (ATLAS Collaboration, 2014e, 2017g) include a large number of differential distributions unfolded to particle level for both inclusive and signal contributions in different fiducial regions, as shown in Fig. 47.

Interference effects between signal and background sources have been evaluated in the range of 2%–12% of the total signal, depending on the channel and the selected phase space, and are generally positive. Results by CMS include a full simulation of interference contributions that are implemented in the cross-section extraction fits.

The structure of the WWZ and $WW\gamma$ triple gauge couplings (TGCs) can be explored with VBF Z and W measurements, and anomalous contributions to the TGCs were searched for by both ATLAS and CMS in the context of the LEP effective Lagrangian approach (Hagiwara et al., 1987) and effective field theory operators in the Hagiwara-Ishihara-Szalapski-Zeppenfeld basis (Hagiwara et al., 1993). Limits on anomalous coupling parameters were extracted by ATLAS fitting alternatively the dijet invariant mass and the leading-jet p_T in fiducial signal regions (ATLAS
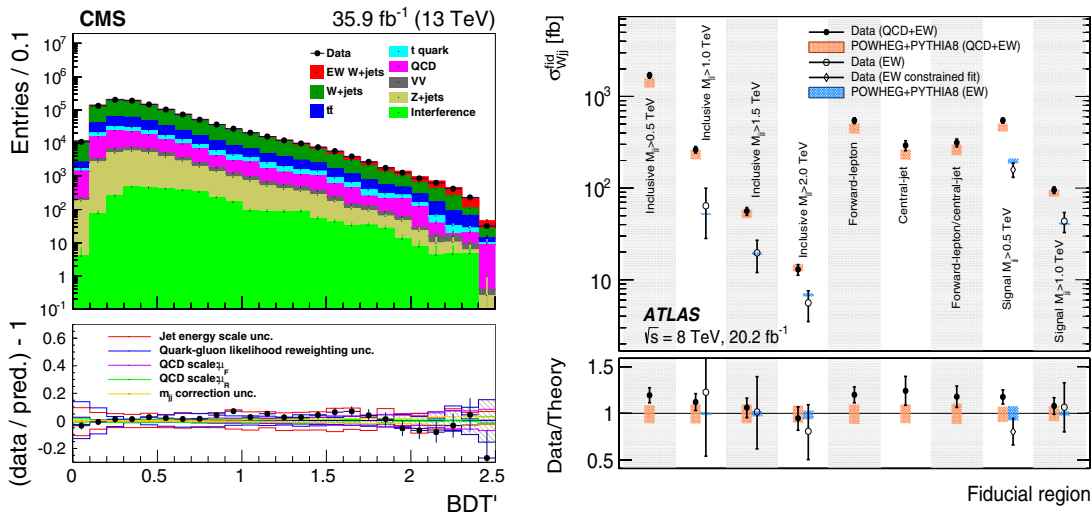

FIG. 46. Left panels: data and prefit MC simulation of the multivariate output distribution used to extract the EW W plus two-jet signal in the electron channel at 13 TeV. From CMS Collaboration, 2020b. Right panels: cross sections for W plus two jets inclusive and EW signal productions in different particle-level fiducial regions at 8 TeV. From ATLAS Collaboration, 2017g.

TABLE II. Summary of VBF W production cross sections measured at the LHC in the $\ell\nu$jj final state with different m_{jj} definitions and different proton collision energies. All cross sections are for a single lepton flavor.

m_{jj} cut	$\sqrt{s} = 7$ TeV	$\sqrt{s} = 8$ TeV	$\sqrt{s} = 13$ TeV
120 GeV			6.23 ± 0.62 pb (CMS Collaboration, 2020b)
500 GeV	2.76 ± 0.67 pb (ATLAS Collaboration, 2017g)	2.89 ± 0.51 pb (ATLAS Collaboration, 2017g)	
1 TeV		0.42 ± 0.10 pb (CMS Collaboration, 2016)	

Collaboration, 2014e, 2017g). Limits were also extracted by the CMS Collaboration, fitting the p_T distributions of the two charged leptons or the single charged lepton in a more inclusive Vjj phase space (CMS Collaboration, 2018a, 2020b), and turned out to be more stringent because of the larger $\sqrt{s}$ of the analyzed dataset, and of a larger acceptance in the high-p_T tails where anomalous TGC effects are generally expected. Examples of kinematic distributions used to fit anomalous TGC contributions are shown in Fig. 48. The reported TGC sensitivities are comparable or even more stringent than some obtained from diboson channels with the same data luminosity, revealing an unexpected high sensitivity in the TGC studies from VBF V measurements.

The full run 2 ATLAS results (ATLAS Collaboration, 2021) focus on extracting limits on the interference between the standard model and dimension-6 scattering amplitudes.

A number of QCD studies of hadronic activity in the selected V plus two jets events have been carried out by CMS and ATLAS using 7 and 8 TeV data (ATLAS

Collaboration, 2014e, 2017g; CMS Collaboration, 2013b, 2015d). Inclusive studies of "radiation patterns" have been performed following the prescriptions and suggestions given by Binoth et al. (2010), where model dependencies were estimated by comparing different generators. CMS Collaboration (2013b) results show good agreement between the data and the predictions by a MadGraph interfaced to PYTHIA parton shower for all chosen observables that are sensitive to hadronic activity. Dedicated studies, restricted to the additional hadronic activity in the expected rapidity gap between the two tagging jets, have also been performed. They are particularly interesting when making use of the larger 13 TeV dataset (CMS Collaboration, 2018a, 2020b). The hadronic activity in the rapidity gap is measured in signal-enriched regions that have similar signal and background yields, using as observables the standard reconstructed jets or jets reconstructed by clustering tracks ("soft track jets") from charged particles. The latter are used, as they can be effectively cleaned from pileup contributions allowing
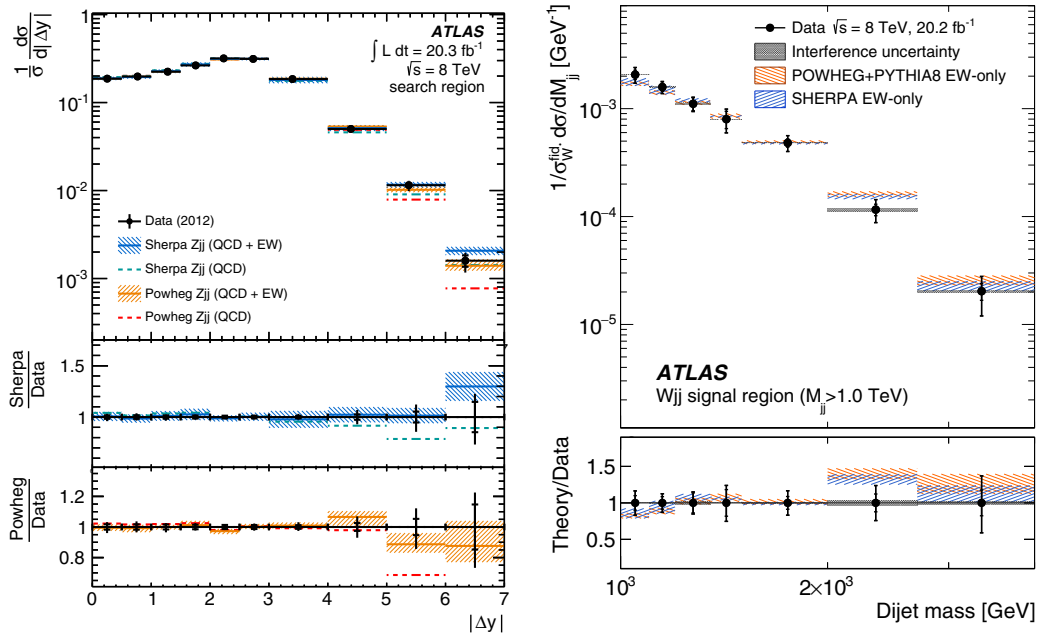
FIG. 47. Left panels: unfolded normalized differential cross-section distribution at 8 TeV as a function of the rapidity separation between the leading jets in the search region. Particle-level predictions are shown for strong and electroweak Zjj production. From ATLAS Collaboration, 2014e. Right panels: unfolded normalized differential EW Wjj production cross sections at 8 TeV as a function of the dijet invariant mass for the signal fiducial region. From ATLAS Collaboration, 2017g. Both statistical (inner bar) and total (outer bar) measurement uncertainties are shown, as are ratios of the theoretical predictions to the data.
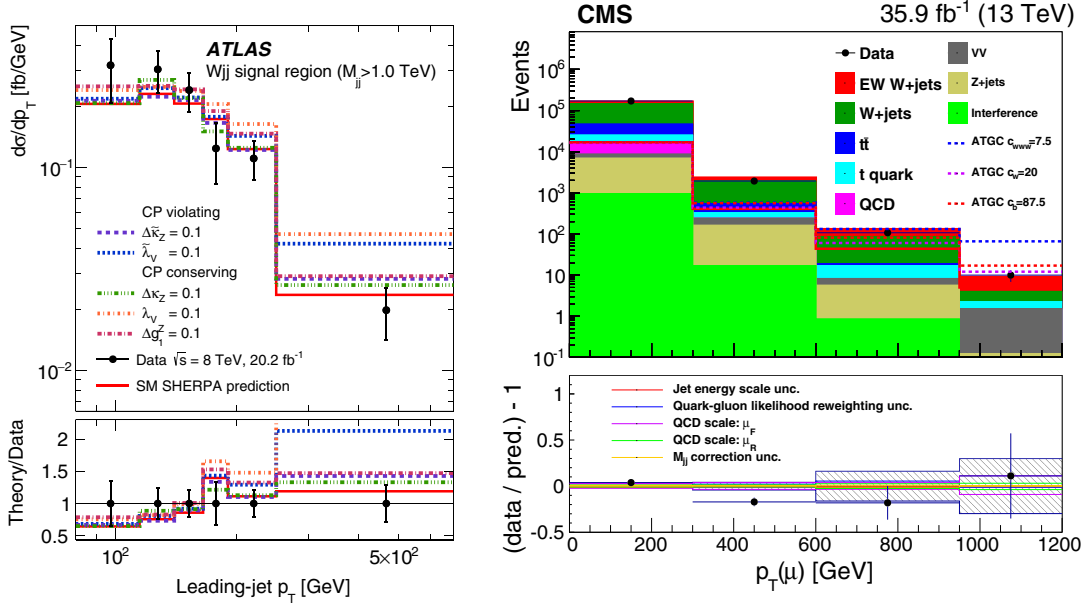
FIG. 48. Left panels: leading-jet p_T for the SM (solid line) and with anomalous TGC parameter deviations of 0.1 from the SM values (dashed lines) compared to an unfolded differential VBF W cross-section distribution measured using 8 TeV data in the $m_{jj} > 1$ TeV signal region. From ATLAS Collaboration, 2017g. Right panels: muon p_T distribution using 13 TeV data and SM backgrounds, and various scenarios for anomalous TGCs. The lower panel shows the ratio between data and prediction minus one with the statistical uncertainty from the simulation (gray hatched band) as well as the leading systematic uncertainties. From CMS Collaboration, 2020b.

precise low-p_T measurements (CMS Collaboration, 2009, 2010). Monte Carlo based studies of the additional jet activity in VBF W and Z channels revealed interesting differences in the prediction of different parton-shower setups (Schissler and Zeppenfeld, 2013).

Figure 49 shows the gap veto efficiency for the "soft" H_T observable, i.e., the scalar sum of track jets p_T in the rapidity gap region, in signal- and background-enriched samples. In the background dominated sample the agreement of the data

with the predictions is good. The data in the signal region disfavor the background-only predictions and are in reasonable agreement with the presence of the signal with the HERWIG++ PS predictions for gap activities above 20 GeV, while the signal with PYTHIA PS seems to generally overestimate the gap activity. In the events with low gap activity, particularly below 10 GeV, as measured with the soft track jets, the data also indicate gap activities below the HERWIG++ PS predictions.
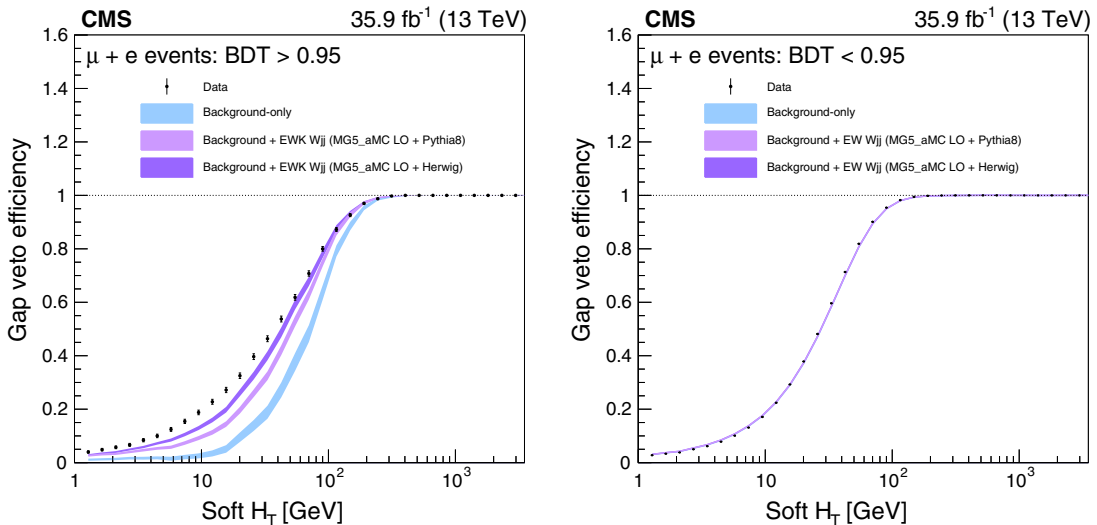

FIG. 49. Veto efficiencies of hadronic gap activity at 13 TeV, evaluated with charged particles in (left panel) signal-enriched and (right panel) background-enriched regions. The data are compared with the background-only prediction as well as background + signal with PYTHIA (Sjöstrand *et al.*, 2015) or HERWIG (Bähr *et al.*, 2008) parton showering. From CMS Collaboration, 2020b.

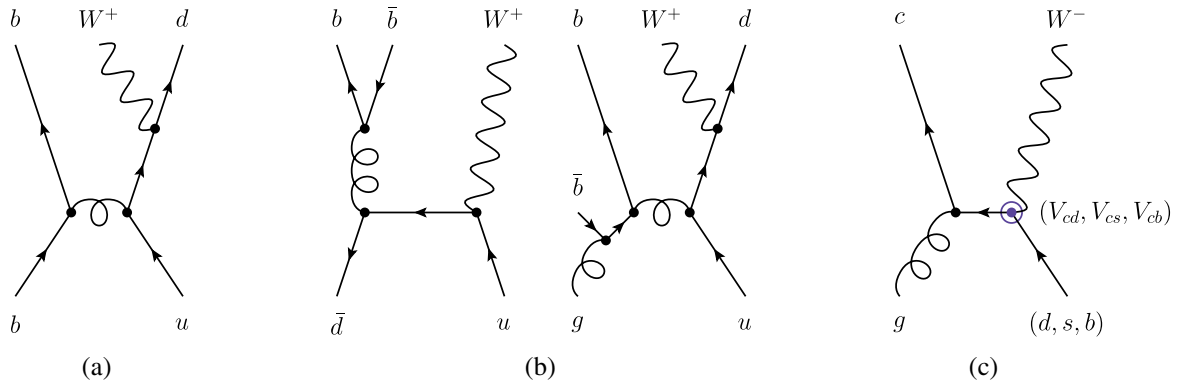FIG. 50. Representative Feynman diagrams for the production of a W boson and at least one b quark at LO in (a) the $n_f = 5$ scheme, (b) the $n_f = 4$ scheme, and (c) additional contributions in the production of at least one c quark associated with the W boson.
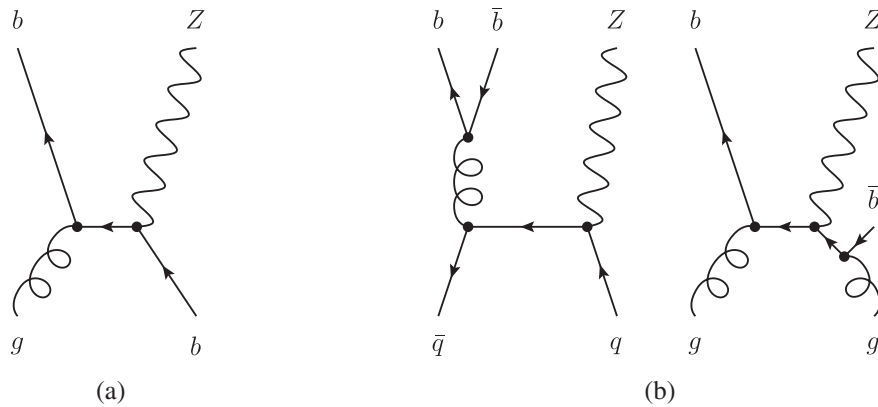

FIG. 51. Representative Feynman diagrams for the production of a Z boson and at least one b quark at LO in (a) the $n_f = 5$ scheme and (b) the $n_f = 4$ scheme.

IV. ASSOCIATED PRODUCTION OF A VECTOR BOSON AND HEAVY-FLAVOR JETS

A. Theoretical predictions

The third important class of vector boson production processes is the production in association with heavy quarks, namely, b and c quarks. The characterizing feature of these quark flavors is their large mass relative to the proton, in combination with a lifetime long enough to form hadrons that decay after macroscopic path lengths. Indeed, this feature, which leads to the presence of differentiable secondary decay vertices, is used in most tagging algorithms that identify the presence of heavy-flavor hadrons. The top-quark associated production features different dynamics and is not discussed in this review.

In Sec. IV.A.1, the features and availability of calculations for this process class are reviewed. A comprehensive review of the calculation techniques was given by Febres Cordero and Reina (2015).

1. Higher-order calculations and flavor schemes

Heavy-quark processes in general can be calculated in at least two different approaches. For definiteness, when b-quark associated production is considered either only the $dusc$ quarks are considered massless and the full mass dependence

of the b quark is retained (the four massless flavor scheme $n_f = 4$, also referred to as 4F) or all five light-quark flavors are considered massless (the five massless flavor scheme, $n_f = 5$, also referred to as 5F). While the former correctly describes all effects that are due to the b mass, the latter allows for the b quark to be extracted directly from the proton, resumming its contribution to the proton's parton density. For consistency, the b quark is thus also only included in the running of the strong coupling in the $n_f = 5$ scheme. The choice of scheme thus has a non-negligible effect on the value of the strong coupling constant on scales beyond the b-quark mass. In particular, the value of $\alpha_s(m_Z)$ differs in both schemes.[8] Thus, ideally one would like to have a calculation with both the finite-mass and the resummation effects accounted for. As a consequence of these considerations, methods have been formulated that combine both *Ansätze*, like the fixed-order plus next-to-leading-logarithm (FONLL) method (Cacciari, Greco, and Nason, 1998; Forte *et al.*, 2010). The diagrams contributing in the respective cases are shown in Figs. 50 and 51 for W and Z associated heavy-flavor production, respectively.

---

[8] A possible remedy was explored by Bertone, Carrazza, and Rojo (2015), who introduced *doped* PDFs, running α_s in $n_f = 5$ and the evolution of the PDFs in $n_f = 4$, which, however, has not seen a widespread use thus far.
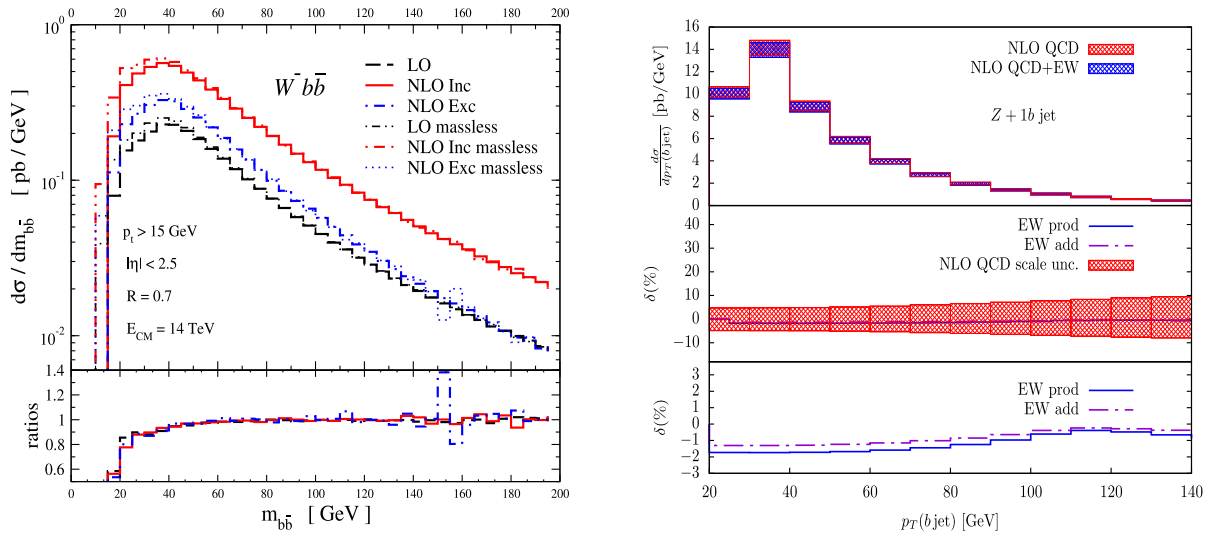
FIG. 52.   Left panels: di-b-jet invariant mass in the pair production of a charged lepton and a neutrino associated with at least two b jets calculated at LO and NLO QCD in both the $n_f = 4$ and $n_f = 5$ massless quark flavor schemes. From Febres Cordero, Reina, and Wackeroth, 2009. Right panels: leading b-jet transverse momentum in the pair production of two charged leptons associated with at least one b jet calculated at NLO QCD with and without NLO EW corrections in the $n_f = 5$ massless quark flavor scheme. From Figueroa *et al.*, 2018.

The generalization for the different mass-dependence treatments of charm quarks is mostly straightforward (Ball *et al.*, 2016). Because the charm quark's isospin partner, the strange quark, is not mass suppressed, in contrast to the bottom's isospin partner, the top quark, and the respective intergenerational mixing matrix elements V_{cd} are sizable in comparison to V_{ub} and V_{cb}, additional topologies contribute in W associated charm production that are strongly suppressed in W associated bottom production; see Fig. 50(c).

One particular aspect of all parton-level calculations that has to be kept in mind is that no flavor-jet-related observable can be defined in complete analogy to the experimental definitions. This is rooted in the fact that the identification of heavy flavors in an experimental setting relies on the properties of heavy-flavor hadrons, in particular, their finite lifetime allowing for a measurable spatial separation of production and decay vertices. A parton-level heavy-flavor tag, on the other hand, can involve only the partonic jet constituents. The requirement for infrared safety then generally necessitates a signed counting of heavy-flavor quanta to guarantee that a collinear $g \to q\bar{q}$ splitting does not alter the jet flavor tag. One useful example here is the flavor-k_T algorithm (Banfi, Salam, and Zanderighi, 2006). Its anti-k_T relative, however, is not infrared safe starting at NNLO, as through its conelike structure soft wide-angle $g \to q\bar{q}$ splittings carry the possibility of losing one heavy quark, thereby again altering the jet flavor tag (Gauld *et al.*, 2020). This is problematic in the limit in which the splitting gluon itself comes from a soft $q \to qg$ splitting, rendering the cancellation of its infrared divergence incomplete (Banfi, Salam, and Zanderighi, 2006).

Four- and five-flavor calculations thus exist for $W/Z/\gamma + b$, $W/Z/\gamma + b\bar{b}$ and $W/Z/\gamma + b\bar{b} +$ jet production at NLO QCD (Campbell *et al.*, 2006, 2007; Febres Cordero, Reina, and Wackeroth, 2009; Stavreva and Owens, 2009; Hartanto and Reina, 2014) and NLO EW (Figueroa *et al.*,

2018) accuracy. Figure 52 shows selected calculations for the $W + b\bar{b}$ and $Z + b$ processes. A $Z/\gamma + b$ calculation at NNLO QCD accuracy in the $n_f = 5$ scheme became available recently (Gauld *et al.*, 2020) that accounted for b-quark mass effects at NLO QCD accuracy with the aforementioned FONLL method and is expected to impact heavy-flavor PDF extractions, in particular. Recently a calculation of $W + c$ production in the $n_f = 5$ scheme at NNLO QCD accuracy also became available (Czakon *et al.*, 2020).

2. Monte Carlo event generators

Along with the automation of matching NLO QCD calculations to parton showers, the availability of precision Monte Carlo event generation has grown for this process class. Thus, the existing NLO QCD matched results produced by the MC@NLO (Frederix *et al.*, 2011) or POWHEG (Oleari and Reina, 2011) generators represent the state of the art for any fixed flavor number scheme. Recently multijet-merged predictions at NLO accuracy became available in the MEPS@NLO method combining the $n_f = 4$ and $n_f = 5$ scheme (Höche, Krause, and Siegert, 2019). Typically, in the multijet merging approach problems arise with double counting of contributions already present in the general $V +$ jets multijet-merged calculations in the massless limit. Therefore, various strategies have been devised to address this issue. Besides a more phenomenological and not theoretically rigorous approach, known as heavy-flavor overlap removal (Mangano, Moretti, and Pittau, 2002), applied thus far to LO-accurate simulations only, more rigorous approaches use schemes equivalent to the FONLL approach (Höche, Krause, and Siegert, 2019). Figure 53 shows the results of both approaches.

B. Experimental results

Processes involving vector bosons associated with bottom or charm quarks provide stringent tests of QCD predictions and are the largest backgrounds in studies of the
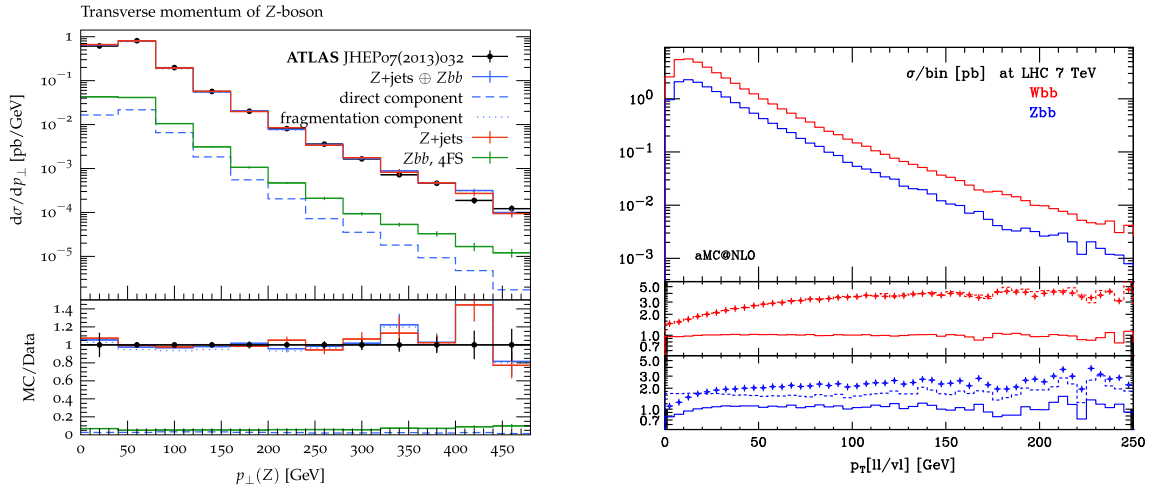
FIG. 53. Left panels: reconstructed Z-boson transverse momentum in the pair production of two charged leptons associated with at least one b jet calculated using the fusing method to combine the $n_f = 4$ and $n_f = 5$ schemes in the MEPS@NLO method in SHERPA. From Höche, Krause, and Siegert, 2019. Right panels: reconstructed vector boson transverse momentum in the production of a pair of charged leptons, and a charged lepton and neutrino associated with a pair of b jets calculated at NLO QCD matched to the parton shower in aMC@NLO. The bottom panels show the ratios of the aMC@NLO result over the corresponding NLO (solid lines), aMC@NLO (dashed lines), and LO (crosses) results. From Frederix et al., 2011.

Higgs boson decaying to two b quarks, in measurements of the properties of the productions of a single top quark or pairs of top quarks, and in numerous searches for physics beyond the SM.

1. Heavy-flavor identification in jets

The identification of jets originating from b or c quarks (heavy-flavor jets) is of primary importance for many measurements and searches with proton collision data. Detectors with precise charged-particle tracking as well as electron and muon identification are well suited for identifying heavy-flavor jets, exploiting mainly the presence of displaced tracks from which a secondary vertex may be reconstructed. Figure 54 shows examples of distributions of combined multivariate algorithms and reconstructed

secondary-vertex mass used to identify and separate heavy-flavor jets associated with vector bosons. The heavy-flavor identifications algorithms and their performances have been described in detail for LHC 7 and 8 TeV proton collision data (CMS Collaboration, 2013d; ATLAS Collaboration, 2016f) and 13 TeV collision data (ATLAS Collaboration, 2018f; CMS Collaboration, 2018b).

In simulated events different procedures can be applied to assign a flavor to a jet. A simple parton-level angular association was used for the most part by Tevatron and LHC run 1 data. A particle-level definition commonly employed for LHC run 2 data makes use of a ghost association (Cacciari and Salam, 2008) of heavy-flavor hadrons to generator-level particle jets. In all definitions, precedence is given first to the b-quark flavor, then to the c-quark flavor.
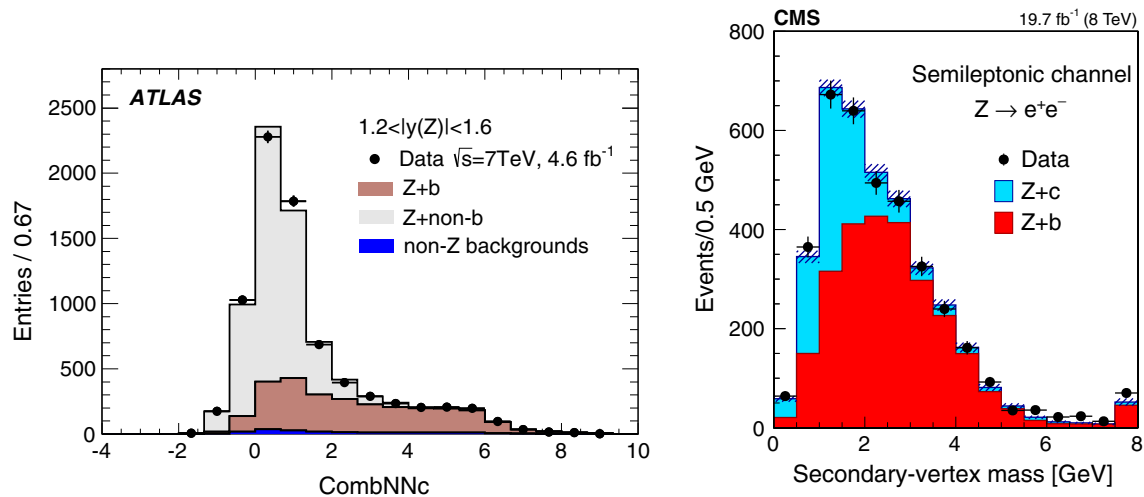

FIG. 54. Left panel: combined neural network output distribution providing separation between jet flavors in Z + jet events at 7 TeV. From ATLAS Collaboration, 2014c. Right panel: secondary-vertex mass distributions for jets associated with a Z boson decaying to electrons, after background subtraction, at 8 TeV. From CMS Collaboration, 2018c.
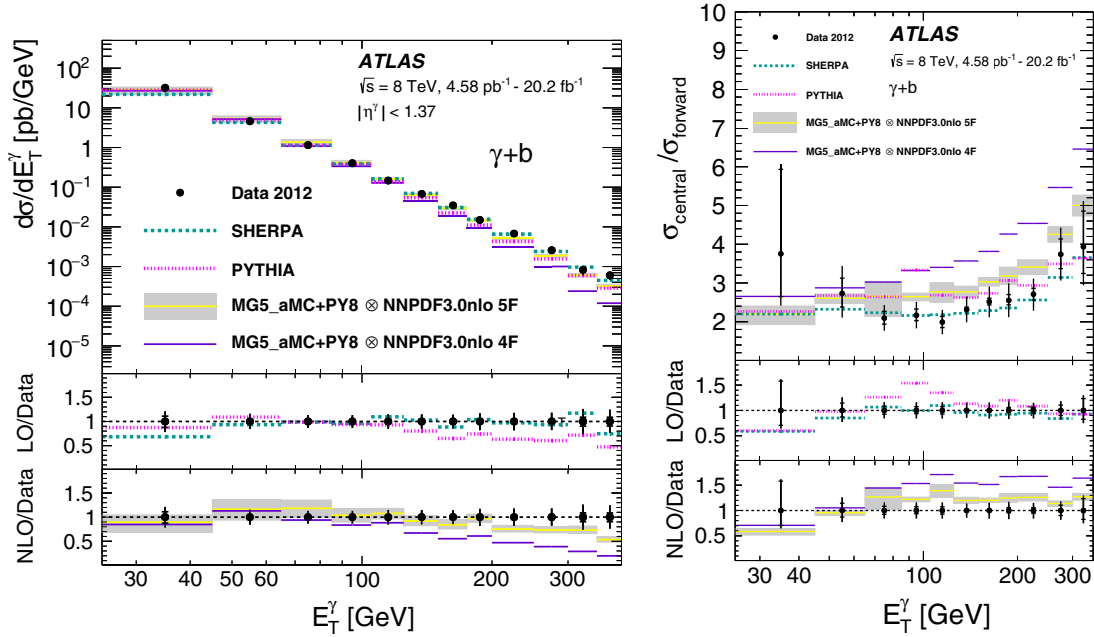
FIG. 55. Left panels: measured $\gamma + b$ cross sections at 8 TeV. Differential cross sections as a function of the photon transverse energy in the central region ($|\eta^\gamma| < 1.37$). Right panels: cross-section ratios of the central region $|\eta^\gamma| < 1.37$ to the forward region $1.56 < |\eta^\gamma| < 2.37$ as a function of the photon transverse energy. From ATLAS Collaboration, 2018a.

Both parton- and particle-based heavy-flavor definitions have been used to define the V plus heavy-flavor-jet measurements described in the following.

2. $V + b$-quark productions

Studies of the production of prompt photons associated with b quarks have been performed with Tevatron data and compared with various QCD predictions. D0 Collaboration (2009c, 2012, 2013a) measurements were performed differentially in the photon p_T, and in the photon and jet rapidity for both the $\gamma + b$ and $\gamma + c$ productions, separating the jet flavors with a combined displaced track jet probability. Similar results were produced by CDF (CDF Collaboration, 2010a, 2013b), alternatively making use of the invariant mass of reconstructed secondary vertices to separate jet flavors. All results showed a need for higher-order perturbative QCD corrections beyond NLO in the larger $p_T > 70$ GeV regions.

The ATLAS Collaboration measured isolated-photon plus heavy-flavor-jet production in 8 TeV proton collisions (ATLAS Collaboration, 2018a). Results were provided differentially in the transverse energy of the photon and in two photon pseudorapidity regions and compared with LO and NLO QCD calculations involving 5F and 4F schemes, as shown in Fig. 55. The NLO predictions underestimate the data in the kinematic region with $E_T^\gamma \geq 125$ GeV using the 4F scheme, and in the kinematic region with $E_T^\gamma \geq 200$ GeV using the 5F scheme. The 4F predictions for the cross-section ratios overestimate the data for $E_T^\gamma \geq 65$ GeV. The best description of the data is provided by SHERPA predictions, which include up to three additional partons and are computed using the 5F scheme. The first measurement of the associated production of a Z boson with a b jet was performed by D0 Collaboration (2005) and indicated a ratio

to light jets of around 2%, which is in agreement with existing NLO QCD predictions. Similar results where derived also by CDF Collaboration (2006) and included a fiducial $Z + b$ cross section with a total uncertainty of around 40%.

A subsequent CDF analysis with a larger data sample reported similar results for the fractions of associated b jets, with improved precision, and differential distributions in jet E_T, jet η, Z-boson transverse-momentum, number of jets, and number of b jets (CDF Collaboration, 2009b). Results were consistent with predictions from LO Monte Carlo generators and NLO QCD calculations within uncertainties. The invariant mass distribution of the tracks forming the secondary vertex was used to extract the b-jet fractions.

More recent measurements by D0 determined the b-jet ratios to light jets with a precision of around 10% using a peculiar technique that combines the properties of the tracks associated with the jet (D0 Collaboration, 2011a). A more recent D0 publication reported the fractions of b-to-light-jet associated production as a function of the Z-boson transverse momentum, the jet transverse momentum, the jet pseudorapidity, and the azimuthal angle between the Z boson and the jet (D0 Collaboration, 2013c). Existing predictions from Monte Carlo event generators did not provide a consistent description of all the examined variables.

In the meantime the first measurements of $Z + b$ productions with LHC data were performed by ATLAS Collaboration (2012b) using 7 TeV proton collision data, reporting both a fiducial cross section and the ratio to the inclusive Z cross section in the same fiducial region, both with a precision of around 30%. Similar measurements were then performed by CMS Collaboration (2012b) with a larger data sample, allowing the precision to improve to better than 20%. The measured cross sections and the kinematic distributions of
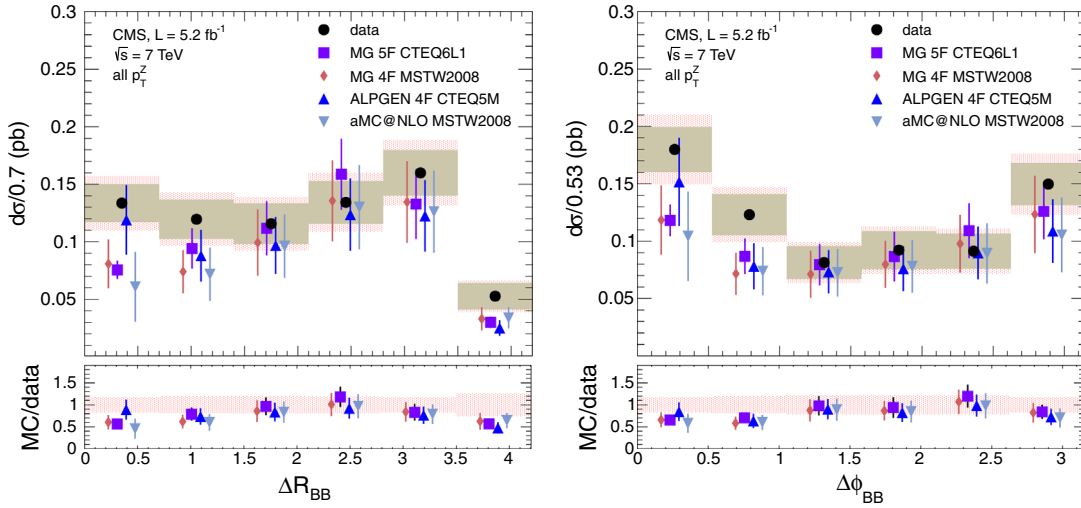
FIG. 56. Measured $Z + BB$ differential cross sections at 7 TeV as a function of (left panels) $\Delta R(BB)$ and (right panels) $\Delta\phi(BB)$. Measurements are compared to the hadron-level predictions made by using MadGraph in the four- and five-flavor schemes. From CMS Collaboration, 2013a.

the b jet and charged leptons were found to be in reasonable agreement with existing predictions.

Dedicated measurements of the production of two b hadrons (B) together with a Z boson were performed with 7 TeV data by CMS with particular focus on the angular correlations between the b hadrons and the Z boson (CMS Collaboration, 2013a). The b hadrons are identified by means of displaced secondary vertices, without the use of reconstructed jets, permitting the study of b-hadron pair production with an angular separation smaller than the jet radius. The results shown in Fig. 56 indicate that the 5F description may not be well suited for describing the collinear production of b hadrons.

Other measurements of total cross sections were carried out separately for a Z boson produced with exactly one b jet and with at least two b jets by CMS Collaboration (2014c). For those results data favor the predictions in the five-flavor scheme, where b quarks are assumed to be massless, while predictions in the four-flavor scheme show a clear disagreement in the $Z + 1b$-jet final state.

The LHCb Collaboration has produced complementary measurements of a $Z + b$-jet cross section in the forward pseudorapidity range $2.0 < \eta < 4.5$ and with jet p_T above 10 or 20 GeV (LHCb Collaboration, 2015b). The results yield 25%–30% precision and are in reasonable agreement with both massless and massive bottom-quark calculations.

Further differential measurements of $Z + b$-jet productions were performed by ATLAS with 7 TeV data (ATLAS Collaboration, 2014c), and CMS with 8 TeV data (CMS Collaboration, 2017h). The ATLAS total cross-section results are generally in good agreement with predictions made using MCFM. Predictions obtained using MadGraph5_aMC@NLO with a 4F scheme underestimate the $Z + 1b$ cross sections, while predictions with the 5F scheme seem to underestimate the $Z + 2b$ yields. Interesting disagreements between predictions and data are also reported in the differential distributions, such as the angular separation between the Z boson and the b jet shown in Fig. 57, where missing

higher-order QCD corrections in the predictions might explain the discrepancies.

The CMS results for $Z + b$ productions with 8 TeV collision data have also been compared with a variety of predictions, yielding fair agreement with the data results. Predictions with 4F scheme seem to underestimate the total $Z + 1b$ cross sections and fail to simultaneously describe both the low- and high-p_T b-jet regions. In the case of a Z boson associated with two b jets, the data distributions are generally well reproduced by predictions, such as the dijet mass shown in Fig. 57.

Measurements of $Z + b$ and $Z + bb$ productions with 13 TeV collision data were performed by ATLAS Collaboration (2020d). A summary of the total measured cross sections and comparisons with different predictions is shown in Fig. 58. The 5F scheme predictions at NLO accuracy show better agreement with the data than 4F scheme ones, and the 4F predictions underestimate the data in events with at least one b jet.

Early measurements of $W + b$ rates by CDF Collaboration (2010b) with Tevatron data revealed some excess over the existing predictions with LO multijet-merged (Mangano, Moretti, and Pittau, 2002) and NLO-accurate calculations (Febres Cordero, Reina, and Wackeroth, 2006; Campbell et al., 2007, 2009) that were not confirmed by subsequent similar D0 measurements (D0 Collaboration, 2013b).

Meanwhile, first measurements of $W + b$ productions with LHC data were performed by ATLAS Collaboration (2012c) with 7 TeV proton collision data. Events are required to have exactly one b-tagged jet reducing significantly the top-quark background. Results are unfolded to a fiducial phase space at particle level, where b jets are defined by the presence of a b hadron associated with the jet and are compared with QCD NLO predictions performed in the five-flavor scheme (Campbell et al., 2012) and other leading-order predictions. Results with a larger dataset were subsequently produced by ATLAS Collaboration (2013d), allowing for improved precision and differential measurements as a function of the b-jet p_T, which are shown in Fig. 59.
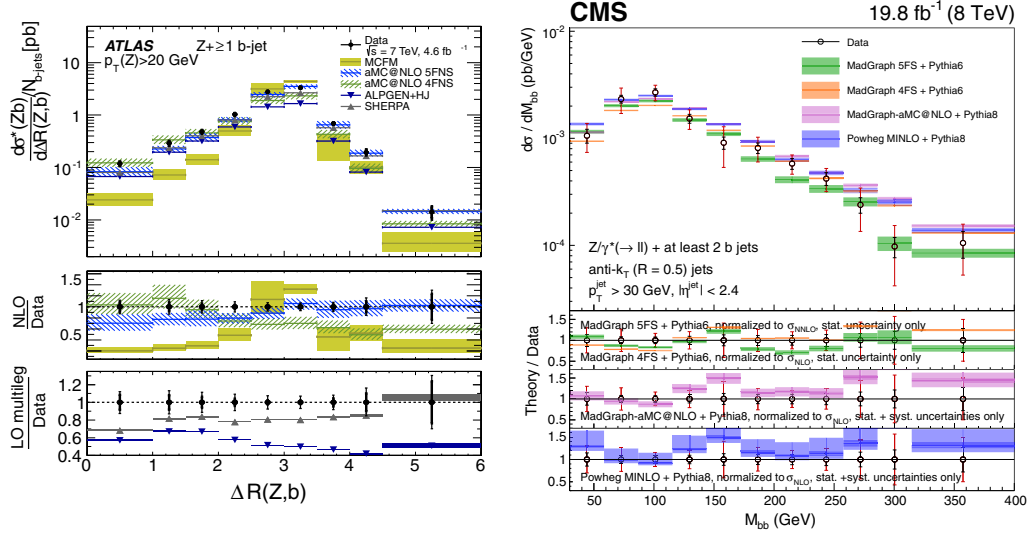
FIG. 57. Measured $Z + b$ differential cross sections at 7 TeV (left panels) and 8 TeV (right panels). Left panels: Z plus b-jet cross section as a function of $\Delta R(Z, b)$. From ATLAS Collaboration, 2014c. Right panels: Z plus 2 b-jets cross section as a function of the invariant mass of the b-jet pair. From CMS Collaboration, 2017h.

Dedicated measurements of the production of a W boson and two b jets were performed by CMS with both 7 TeV (CMS Collaboration, 2014d) and 8 TeV (CMS Collaboration, 2017f) proton collision data. Events are required to have exactly two b-tagged jets and the top-quark background is reduced, requiring no additional jets or isolated electrons or muons. Figure 60 (left panel) shows the data and postfit Monte Carlo distributions for $\Delta R(b, b)$. Results are given in terms of a fiducial $W + bb$ cross section and are in good agreement with several predictions made using MCFM, corrected for DPS and hadronization effects, and using MadGraph + PYTHIA, with different PDF flavor schemes, as shown in Fig. 60 (right panels).

Finally, we remark that, in the context of the measurements of the Higgs boson decays to bottom quarks in the associated VH production mode, the ATLAS and CMS Collaborations

both determined normalization "scale factors" for the $W/Z + b(b)$ background sources, with respect to NLO QCD predictions, and with a precision in the 10%–20% range (ATLAS Collaboration, 2018d; CMS Collaboration, 2018f). In this phase space of the Higgs to bottom-quark measurements, CMS reported significantly large scale factors for $W + b(b)$ productions, up to a factor of 2 with respect to the reference NLO QCD predictions, while ATLAS normalizations are consistent with predictions.

3. $V + c$-quark productions

First measurements of associated production of Z bosons with charm-quark jets were performed by D0 Collaboration (2014), which reported an integrated fraction of c jets of 8% with a 10% relative uncertainty, and a ratio to b-jet production
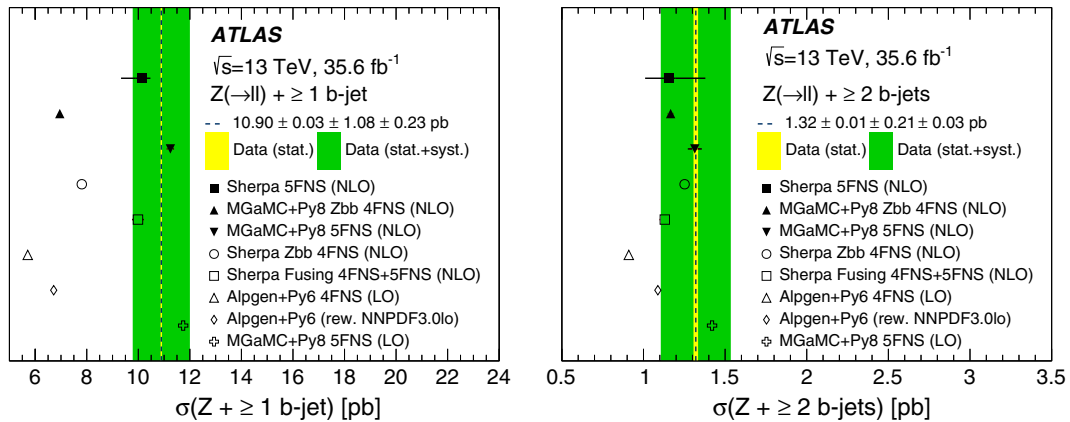
FIG. 58. Measured cross sections for (left panel) a $Z+ \geq 1$ b jet and (right panel) $Z+ \geq 2$ b- jets. The data are compared to different predictions in the 4F and 5F approximations. The yellow band corresponds to the statistical uncertainty of the data, and the green band corresponds to statistical and systematic uncertainties of the data, added in quadrature. The error bars on the SHERPA 5F (NLO) predictions correspond to the statistical and theoretical uncertainties added in quadrature. Only statistical uncertainties are shown for the other predictions. From ATLAS Collaboration, 2020d.
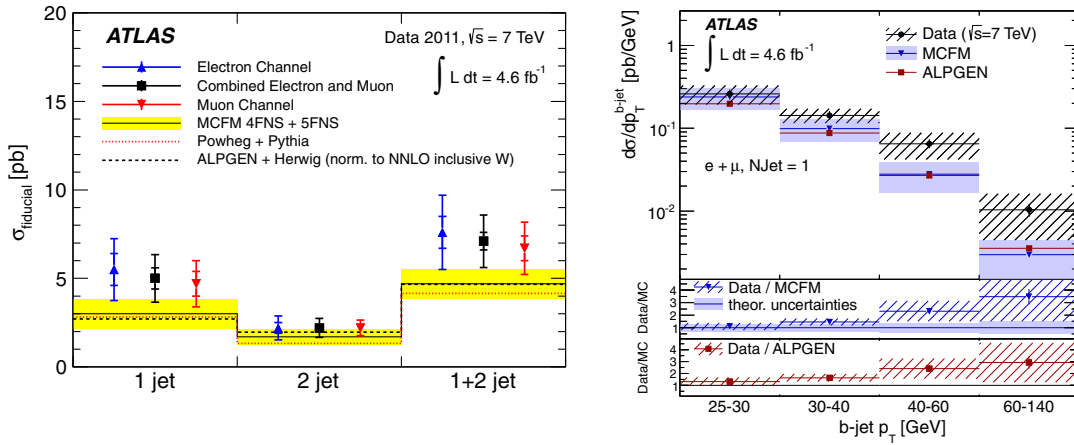
FIG. 59. $W + b(b)$ fiducial and differential cross sections at 7 TeV. Left panel: total cross sections in the 1-, 2-, and $(1 + 2)$-jet exclusive bins with the statistical (inner error bar) and statistical plus systematic (outer error bar) uncertainty in the electron, muon, and combined electron plus muon channel. Right panels: differential $W + b$-jet cross sections with total uncertainties as a function of the b-jet p_T in the 1-jet fiducial region compared to the MCFM and ALPGEN predictions. From ATLAS Collaboration, 2013d.

of about 4 with a 15% relative uncertainty. The cross-section ratios were also measured differentially as a function of jet and Z-boson transverse momenta showing significant deviations from existing perturbative QCD calculations and event generator predictions.

The first observation of $Z + c$ production at LHC was reported by LHCb in the forward region $2 < y < 4$ with data from proton collisions at 7 TeV and made use of fully reconstructed D^0 and $D^\pm$ decays (LHCb Collaboration, 2014a).

The CMS Collaboration has performed a measurement of associated $Z + $ charm production in proton collisions at 8 TeV (CMS Collaboration, 2018c). The selection of event candidates relies on the identification of semileptonic decays of c or b hadrons with a muon in the final state and through the reconstruction of exclusive decay channels of $D^\pm$ and $D^{*\pm}$ (2010) mesons. The total $Z + c$ cross section is measured with a precision of 10%, while the cross-section ratio $(Z + c)/(Z + b)$ is determined to be 2.0 ± 0.3. Differential cross sections are measured as a function of the transverse

momentum of the Z boson and the heavy-flavor jet. The measurements are in agreement with NLO QCD predictions, including parton-shower development and nonperturbative effects. Results in the highest transverse-momentum regions are compatible with predictions using PDF sets with no intrinsic charm component. Results with 13 TeV collision data were released recently that made use of jet secondary-vertex mass distributions to separate light, charm, and bottom flavor components (CMS Collaboration, 2020a, 2020c). Results are given in terms of $b/$light, $c/$light, and c/b production ratios, both inclusively and differentially with respect to the Z-boson p_T and the jet p_T. The experimental results are in reasonable agreement with current theoretical predictions that, however, carry a larger uncertainty. Figure 61 shows $Z + c$ cross-section measurements at 8 TeV and c/b cross-section ratio measurements at 13 TeV, both as a function of the heavy-flavor-jet p_T.

Measurements of the production of a W boson and charm quarks are carried out by determining the charge sign of
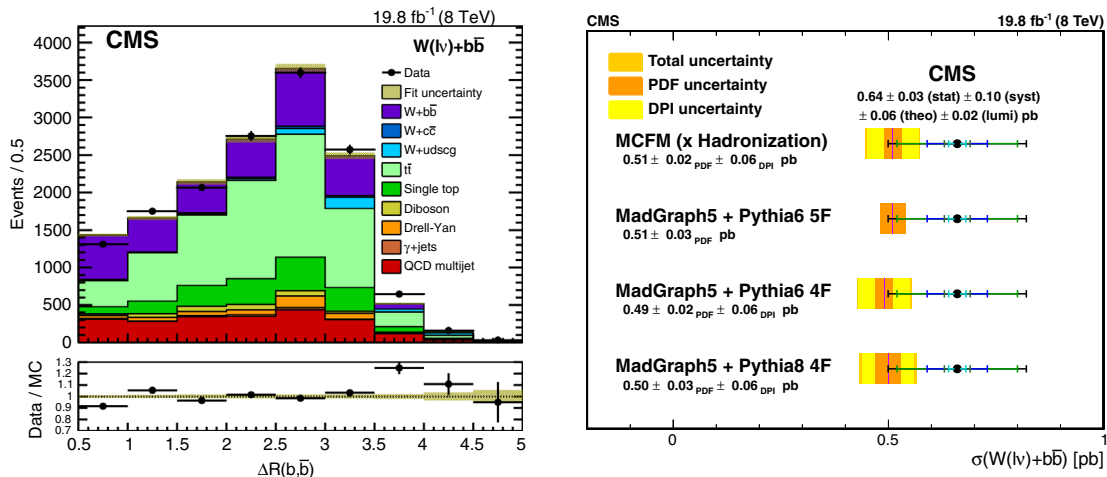

FIG. 60. Measurements of the $W + bb$ production at 8 TeV. Left panels: postfit $\Delta R(b, b)$ distribution. Right panel: comparison between the measured cross section and various QCD predictions. From CMS Collaboration, 2014d, 2017f.
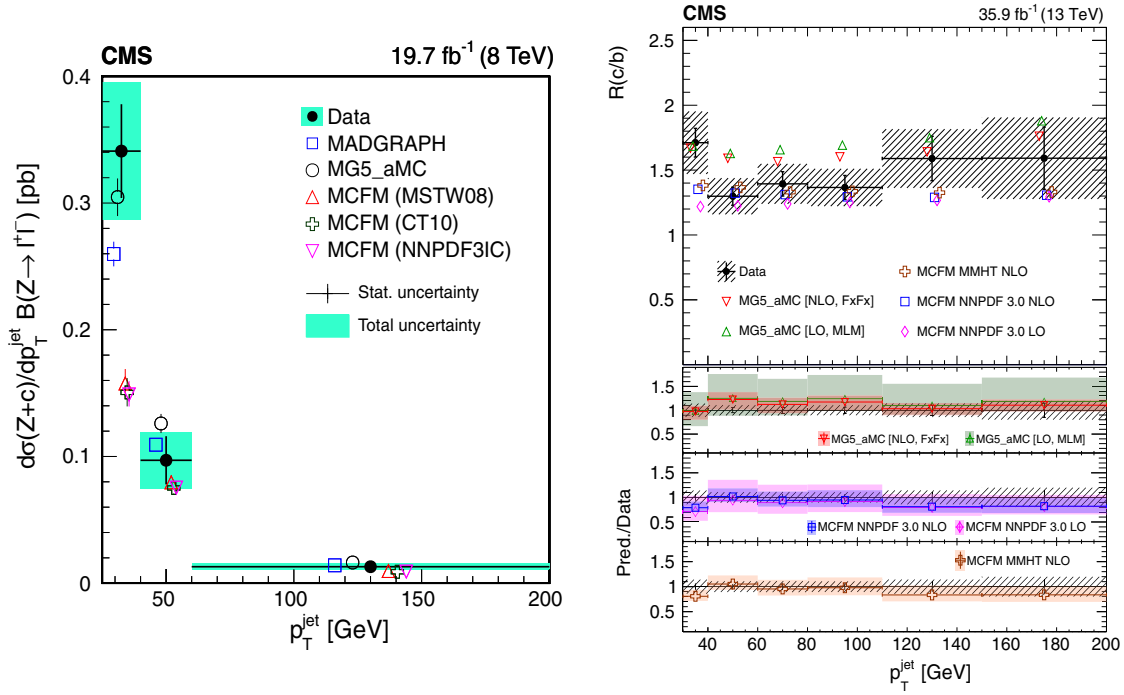
FIG. 61. Left panel: differential $Z + c$ cross section as a function of the transverse momentum of the c jet at 8 TeV. From CMS Collaboration, 2018c. Right panels: $(Z + c)/(Z + b)$ cross-section ratio as a function of the transverse momentum of the jet at 13 TeV. From CMS Collaboration, 2020c.

the W boson and the charm quark and separating events with same-sign (SS) and opposite-sign (OS) charges. Contributions from $W + c$ processes are inferred after performing a subtraction of SS events from OS ones, that effectively removes most background sources.

Initial $W + c$ measurements were performed by CDF Collaboration (2008a) and subsequently reached a 20% overall precision (CDF Collaboration, 2013c), with results compatible with existing theoretical expectations. A 15% constraint on the $|V_{cs}|$ Cabibbo-Kobayashi-Maskawa quark mixing matrix element was also derived from these results.

The first measurements of $W + c$ productions at the LHC were performed with 7 TeV proton collision data by CMS Collaboration (2014a), where hadronic and inclusive semi-leptonic decays of charm hadrons are used to select the presence of c jets. Cross sections and cross-section ratios were measured inclusively to precisions of 3%–7%, and differentially with respect to the absolute value of the pseudorapidity of the charged lepton from the W-boson decay, shown in Fig. 62. Results are directly sensitive to the strange-quark content of the proton and are consistent with the predictions based on global fits of parton distribution functions; see Sec. V.

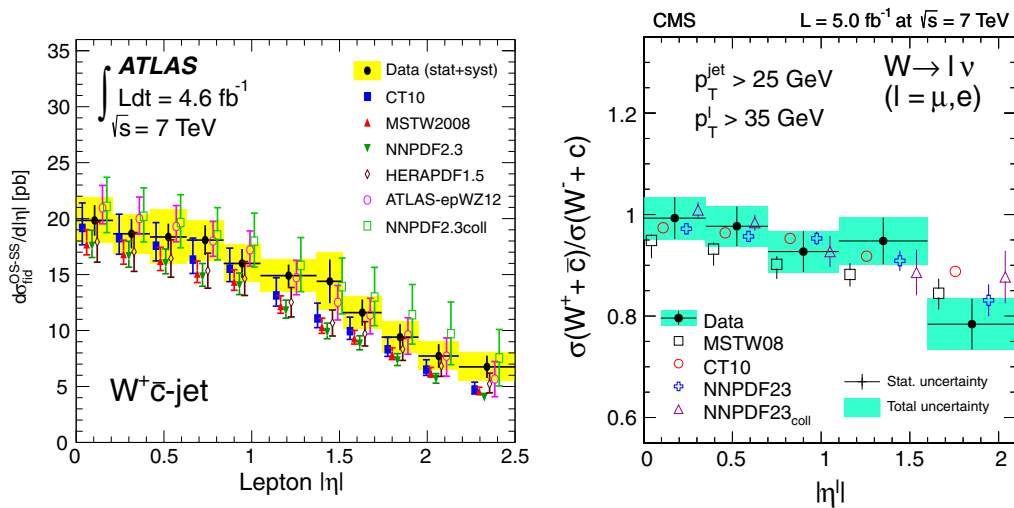FIG. 62. Measurements of $W + c$ production in proton collisions at 7 TeV compared to predictions obtained using various PDF sets. Left panel: measured differential cross section as a function of the charged lepton $|\eta|$. From ATLAS Collaboration, 2014f. Right panel: cross-section ratio $\sigma(W^+ + c)/\sigma(W^- + c)$ as a function of the charged lepton $|\eta|$. From CMS Collaboration, 2014a.
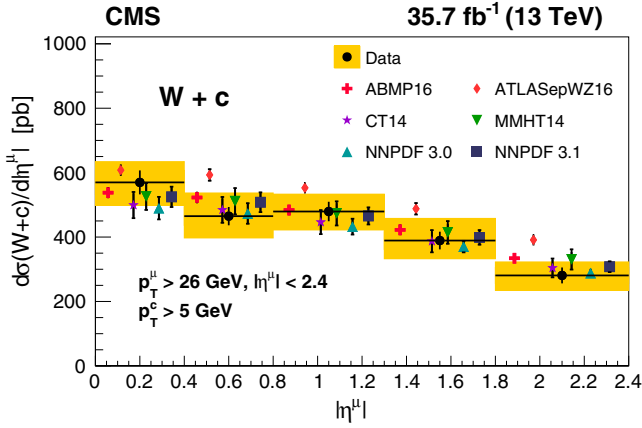
FIG. 63. Differential cross section of $W + c$ production, measured as a function of the charged-lepton pseudorapidity at 13 TeV. The measurement is compared to the QCD predictions at NLO using different PDF sets. From CMS Collaboration, 2019b.

The ATLAS Collaboration (2014f) performed measurements of $W + c$ production at 7 TeV where the charm quark is similarly tagged either by a semileptonic decay or by the presence of a charmed meson. Results where also found to be in good agreement with theoretical predictions for the cross sections with different choices of the PDF set, with a preference for PDFs with an SU(3)-symmetric light-quark sea, as discussed in Sec. V.

The CMS Collaboration (2019b) has also produced $W + c$ measurements with 13 TeV collision data using only charm quarks tagged via the full reconstruction of D mesons. Figure 63 shows differential $W + c$ cross sections measured at 13 TeV by CMS.

Measurements of W boson productions associated with b and c quarks have also been carried out in the forward regions of proton collisions at 7 and 8 TeV by LHCb Collaboration (2015d). A dedicated secondary-vertex tagger is used to identify and separate the presence of heavy-flavor jets. Results are generally in agreement with QCD predictions and do not support a large contribution from intrinsic b-quark content in the proton, but the precision is not sufficient to rule out such a contribution at O(10%).

V. THEORETICAL INTERPRETATIONS OF DATA FROM VECTOR BOSON PRODUCTION WITH ASSOCIATED JETS

The production of high-statistics $V +$ jet Monte Carlo samples is key to many of the Tevatron and LHC physics programs. The validation of MC event generators available with different levels of approximations in pQCD and different nonperturbative QCD model implementations require careful comparisons between predictions and with data. Several investigations into the tuning of related MC parameters and evaluations of uncertainties on their predictions have been carried out by communities of both experimentalists and theorists based on $V +$ jet processes. Examples of validation and tuning studies of $V +$ jet MC

event generators were given by ATLAS Collaboration (2014g, 2016a, 2016c, 2016h; 2017a) and Cooper et al. (2012).

An example is the comparison of the MC generators used by LHC experiments in run 2 analyses with $V +$ jet measurements performed at 7 TeV center-of mass energy in run 1 (ATLAS Collaboration, 2016c). The same generators were then used to simulate events at the run 2 center-of-mass energy of 13 TeV to further investigate the differences between the predictions and assess the theoretical uncertainties. Given the increase in cross section for the $W/Z +$ jet production processes in run 2 with respect to run 1, it was important to carefully assess the accuracy of the MC generators in the new kinematic regime. Predicted differential cross sections were compared to unfolded distributions in data using the RIVET package (Buckley et al., 2013; Bierlich et al., 2020). Although a good overall description of the data is provided by all considered generators, as Fig. 64 shows, some differences between prediction and data at 7 TeV were visible in some observables. This type of study has prompted a new tuning of model parameters (ATLAS Collaboration, 2014g) and improvements in the calculations. Comparisons were also made in phase-space regions and for processes that became more relevant for run 2 analyses due to the larger statistics, such as the production of vector bosons associated with heavy-flavor jets and for electroweak $V + 2$ jets production (ATLAS Collaboration, 2017a). As a result of these studies the uncertainties associated with the normalization and shapes of the predictions of the MC generators for $V +$ jet processes have been routinely assessed on different MC event generators, including variations of matching and merging schemes, parton-shower realizations as well as fragmentation and underlying event models, the strong coupling constant, and PDFs.

An understanding of the proton PDF, and specifically the flavor composition of the quark sea, is important for the
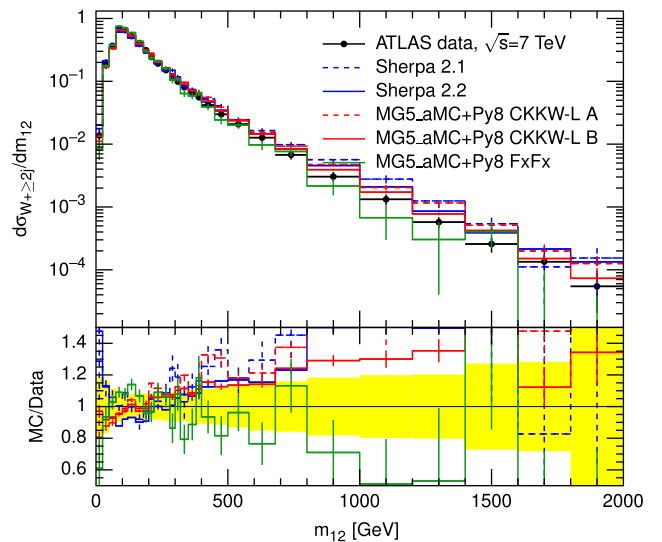

FIG. 64. Comparison between different MC generator models and data for events with a W and at least two jets, in the distribution of the invariant mass of the two leading jets, at 7 TeV pp collisions. From ATLAS Collaboration, 2016c.
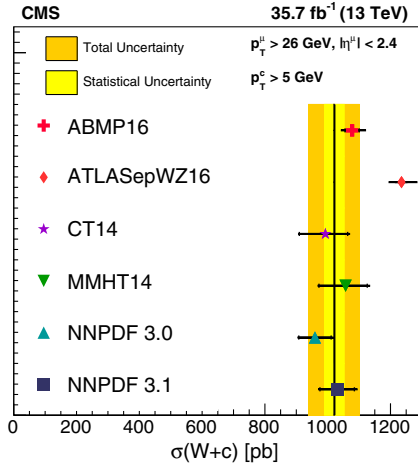
FIG. 65. The fiducial cross section for $W + c$ production at 13 TeV with the CMS detector at the LHC. The measurement is compared to predictions using several PDF sets. With the exception of ATLASepWZ16, which was obtained at NNLO in pQCD, all other PDF sets were obtained at NLO. From CMS Collaboration, 2019b.

LHC physics program as a whole. The strange-quark PDF has a direct impact on the measurement of the W-boson mass. In addition to measurements of charm production in deep-inelastic scattering experiments with neutrinos, the strange-quark content of the nucleon can be obtained from the measurements of inclusive differential W- and Z-boson cross sections, $W+$ charm production as well as $W/Z +$ jets. Inclusive differential W- and Z-boson cross sections at $\sqrt{s} = 7$ TeV (ATLAS Collaboration, 2012d, 2017i; CMS Collaboration, 2012d, 2014b) allowed the strange content of the sea to be measured rather than assumed to be a fixed fraction of the light sea quarks. A QCD interpretation of inclusive W- and Z-boson production data by the ATLAS Collaboration together with data from deep-inelastic scattering at HERA (ATLAS Collaboration, 2012a) showed the sensitivity to the light-quark sea composition of the proton at the LHC. The ratio of the strange-to-down sea-quark distributions was determined to be consistent with one at momentum transfer squared $Q^2 = 1.9$ GeV^2 and Bjorken $x = 0.023$, therefore supporting a symmetric composition of the light-quark sea at low x. The CMS $W + c$ measurement at $\sqrt{s} = 7$ TeV (CMS Collaboration, 2014a) identified processes where a c quark is produced in association with a W boson and was used for the determination of the strange-quark distribution in the proton. This analysis was followed recently by a measurement at 13 TeV center-of-mass energy (CMS Collaboration, 2019b). The CMS results point toward a strangeness suppression with respect to light sea-quark densities in agreement with measurements in neutrino scattering experiments. These results are hence in tension with ATLAS studies based on the analysis of inclusive W- and Z-boson production (ATLAS Collaboration, 2017i) and $W+$ charm production at $\sqrt{s} = 7$ TeV (ATLAS Collaboration, 2014f), which were found to be consistently and significantly better described by an unsuppressed strange sea at low-x values. Figure 65 shows the cross section measured by the CMS experiment for the production of
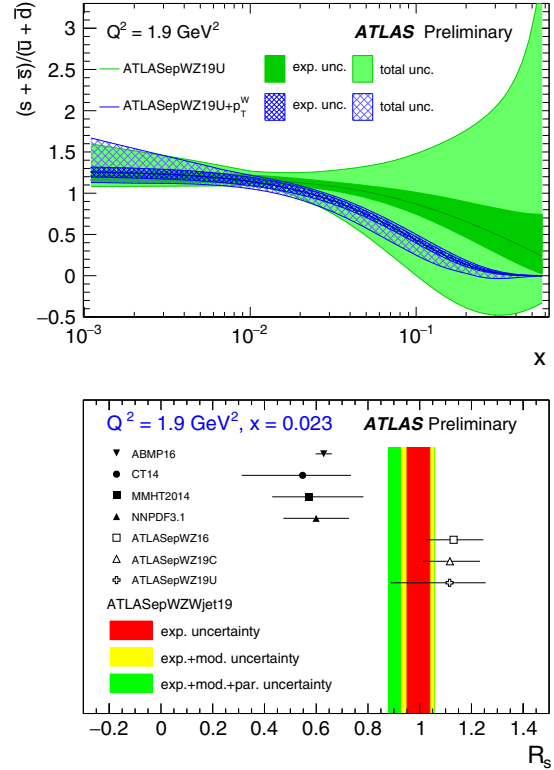
FIG. 66. Top panel: R_s distribution evaluated at $Q^2 = 1.9$ GeV^2, as determined from a fit that includes $W +$ jet data as a function of W p_T, compared to a similar fit without $W +$ jet data as the input. Bottom panel: R_s ratio evaluated at $x = 0.023$ and $Q^2 = 1.9$ GeV^2, for the ATLAS PDF set that includes the $W +$ jet data as the input, compared to other PDF sets. From ATLAS Collaboration, 2019c.

$W + c$ compared to various PDF fits, including one by the ATLAS Collaboration (ATLASepWZ16) that makes use of inclusive W and Z cross-section data as an input.

The cross-section ratio $R_c^\pm = \sigma(W^+ + \bar{c})/\sigma(W^- + c)$ can be sensitive to the $s - \bar{s}$ asymmetry in the PDFs that was suggested by neutrino data (Goncharov et al., 2001). The results by CMS (see Fig. 62) and ATLAS [see Fig. 12 of ATLAS Collaboration (2014f)] are compatible, within 1 standard deviation, with predictions obtained using PDF parametrizations with no asymmetry or a small asymmetry of the order of few percent. Those LHC measurements of the $R_c^\pm$ ratio at 7 TeV were limited by statistical uncertainties. Given the far larger dataset collected by LHC experiments at higher center-of-mass energies, it will be interesting to see such measurements repeated at greater precision.

As discussed in Sec. II.B.4 the study of W- or Z-boson production with jets allows one to access the high-x region of the parton phase space that is of great importance for PDF fitting, as it is currently poorly constrained by data and subject to nonperturbative effects with large uncertainties from phenomenological models. The Tevatron $W^\pm$ asymmetry data are not subject to such uncertainties; however, the results from CDF and D0 experiments are in tension (CDF Collaboration, 2009a; D0 Collaboration, 2015). The production of $W/Z +$ jets at the LHC provides a new and independent dataset that can be used as input to PDF fits to access partons at high x.

Given the ATLAS and CMS tension on the strange-quark PDF, it is therefore of particular interest to check the impact of the new $W + \text{jet}$ data on the strange-quark density. Figure 66 shows the results of the PDF analysis of the ATLAS measurement of the W-boson p_T spectrum (ATLAS Collaboration, 2018b) in $W + \text{jet}$ events at a center-of-mass energy of 8 TeV. This is shown in Fig. 39 fitted together with ATLAS inclusive W and Z production measurements at 7 TeV and HERA deep-inelastic scattering data. The PDF fit is performed at NNLO in pQCD and was made possible by recent theoretical developments providing NNLO predictions for such processes (Boughezal, Focke, Liu, and Petriello, 2015; Gehrmann-De Ridder *et al.*, 2016b). The fraction of the strange-quark density in the proton can be defined by the quantity $R_s = (s + \bar{s})/(\bar{u} + \bar{d})$, which is shown in Fig. 66. The effect of the $W + \text{jet}$ data is most significant in the kinematic region $x > 0.02$, where the uncertainty is significantly lower and the fit results in a R_s distribution that falls from about 1 at $x \approx 0.01$ to about 0.3 at $x \approx 0.1$. At low x, i.e., $x < 0.023$, the fit with the $W + \text{jet}$ data is compatible with the unsuppressed strange-quark density that was found in previous ATLAS analyses with different datasets.

Further measurements at the LHC with even greater precision (including $W/Z + \text{jets}$) aided by NNLO $W + c$ calculations (Czakon *et al.*, 2020) will help us to understand this apparent tension between different experimental datasets in the determination of the strange-quark content of the proton.

VI. CONCLUSIONS AND OUTLOOK

This review has addressed achievements in the understanding of the production of vector bosons associated with light- or heavy-flavor jets, with a focus on the LHC results. These processes are of great importance to the success of physics programs at hadron colliders since they are major backgrounds to new physics searches and are ideal testing grounds for new calculations and models in the QCD and electroweak sectors of the standard model. This review has summarized theoretical techniques developed to describe experimental results in $p\bar{p}$ collisions at the Tevatron and in pp collisions at the LHC and has highlighted a few of the several measurements that were carried out by the CDF and D0 collaborations at the Tevatron as well as the ATLAS, CMS, and LHCb collaborations at the LHC at different center-of-mass energies. Detailed comparisons between the experimental results and cutting-edge predictions have been presented together with discussions of differences in phase spaces and production mechanisms between the Tevatron and the LHC.

The modeling of $V + \text{jet}$ processes improved significantly at the Tevatron, and measurements of such processes have prompted the development of high-order QCD calculations and new techniques for their modeling in MC generators. Tevatron datasets were used to tune theoretical predictions and MC generators, and those tunes also turned out to be accurate at describing the first $V + \text{jet}$ data results at the LHC run 1 despite the large difference in center-of-mass energy. Tevatron data still provide an important legacy for $V + \text{jet}$ analyses at the LHC. The measurements carried out by the LHC

experimental collaborations, thanks to the greater statistics in $V + \text{jet}$ samples, have led to further developments in the theoretical description of such processes in both the QCD and electroweak sectors. These processes have been at the center of both the so-called next-to-leading-order and next-to-next-to-leading-order revolutions in perturbative QCD calculations and their implementations in MC generators.

In several kinematic regions the experimental uncertainties are significantly smaller than the uncertainties in the predictions. Such a high experimental precision has allowed theoretical predictions and models to be tested and constrained (including parton density functions) in a broad kinematic region (including extreme regions of phase space) that is relevant for new physics searches.

Despite the great theoretical progress in the past decades and the many years of understanding the $V + \text{jet}$ production mechanism, there are still theoretical uncertainties that can be further reduced in future developments, for example, higher-order QCD and electroweak contributions in hard scattering matrix elements, parton showers, and their matching algorithms, or better constrained by data like PDFs and underlying event modeling. Improvements in the understanding of these sources of uncertainties in $V + \text{jet}$ processes are critical for improvements in the precision of measurements and in the reach of searches at the LHC and at future collider experiments.

A. Outlook

Studies of $V + \text{jet}$ physics will necessarily continue in future LHC runs and at possible future colliders, as the success of the physics programs of such experiments will rely on a good understanding of such processes. The higher and higher expected statistics, precision, and extended phase space, such as to higher jet multiplicities or higher energy scales, will challenge theoretical predictions to perform calculations at higher-orders in QCD, i.e., at N^3LO,[9] to systematically include higher-order electroweak corrections in MC generators together with mixed electroweak-QCD terms and to improve MC generators for a more accurate estimation of the various sources of uncertainties in the modeling.

Studies of the QCD production of $V + \text{jets}$ will remain critical to the understanding of QCD dynamics as well as for a better understanding of electroweak corrections, as they will become more significant at higher energy scales. Experimental analyses are expected to become more sophisticated in studying statistical and systematic correlations between differential cross sections in the same and in different $V + \text{jet}$ processes, such that several observables can be used simultaneously as inputs to PDF global fits, MC tunes, and indirect searches for new physics. With more accurate and precise theoretical predictions new measurements will become interesting, such as the extraction of the strong coupling α_s from jet rates in $V + \text{jet}$ events.[10]

---

[9]A first result for lepton-pair production via virtual photon exchange was presented in Duhr, Dulat, and Mistlberger (2020a, 2020b).

[10]A precursor to this was presented by Johnson and Maître (2018).

We expect that electroweak analyses will become predominant in the future for searching for anomalies in the gauge structure of the standard model. A good understanding of vector boson fusion production of $V+$ jets is important for studies of Higgs production, and for a thorough investigation of anomalies in the gauge couplings a comprehensive and simultaneous analysis of several electroweak processes will be beneficial. An example of an electroweak process that has not been investigated due to experimental challenges is the eletroweak production of two jets associated with a photon. This process will provide a new window into the studies of anomalous couplings. Developments in the separation of jets induced by quarks or gluons may have a significant impact in the discrimination of electroweak $V+$ jet processes from QCD-induced background in future analyses and may impact the constraints on quark and gluon PDFs. At higher center-of-mass energies the study of the emission of massive vector bosons collinearly with jets in $W/Z+$ jets will become more important and the development and testing of electroweak showering models more relevant than it has been thus far.

As experimental results become more precise, preservation and sharing of analysis details will become more important. Future studies are expected to include multiple differential cross-section measurements, and such a large amount of experimental results will be a wealth for the understanding of the SM and beyond the SM physics. The analysis algorithms as well as the experimental results must be preserved for current and future generations. The LHC experimental data with their uncertainties are stored in the `HepData` repository (Maguire, Heinrich, and Watt, 2017), which has become an essential tool for archiving detailed experimental results, for comparisons against MC predictions, and for tuning and constraining theoretical models, such as the underlying event and PDFs. In recent years the RIVET project (standing for Robust Independent Validation of Experiment and Theory) (Buckley *et al.*, 2013; Bierlich *et al.*, 2020) has been considered as the most important repository for analysis algorithms (a combination of fiducial phase-space definitions and physics objects). This project was originally intended as a tool kit for the validation of MC event generators; however, thanks to its large and ever growing set of experimental analyses and its link to the `HepData` repository for experimental data points from the collider experiments, it has also become useful as a long-term repository of analysis algorithms. RIVET also provides useful algorithms to extract observable quantities from different MC generators in a model-independent way, i.e., without prior knowledge of specific algorithm implementations or specific event record definitions. Such repositories and analysis tools will become more critical in multiprocess fits such as PDFs and effective field theory, including for storing information about correlations between measurements.

ACKNOWLEDGMENTS

REFERENCES

Aaij, R., *et al.*, 2019, "A comprehensive real-time analysis model at the LHCb experiment," J. Instrum. **14**, P04006.

Actis, S., A. Denner, L. Hofer, A. Scharf, and S. Uccirati, 2013, "Recursive generation of one-loop amplitudes in the standard model," J. High Energy Phys. 04, 037.

Alcaraz Maestre, J., *et al.* (SM and NLO MULTILEG and SM MC Working Groups), 2012, "The SM and NLO Multileg and SM MC Working Groups: Summary report," arXiv:1203.6803.

Alioli, Simone, Christian W. Bauer, Calvin Berggren, Frank J. Tackmann, and Jonathan R. Walsh, 2015, "Drell-Yan production at NNLL′ + NNLO matched to parton showers," Phys. Rev. D **92**, 094020.

Alioli, Simone, Paolo Nason, Carlo Oleari, and Emanuele Re, 2008, "NLO vector-boson production matched with shower in POWHEG," J. High Energy Phys. 07, 060.

Alioli, Simone, Paolo Nason, Carlo Oleari, and Emanuele Re, 2011, "Vector boson plus one jet production in POWHEG," J. High Energy Phys. 01, 095.

Altarelli, Guido, R. Keith Ellis, and G. Martinelli, 1979, "Large perturbative corrections to the Drell-Yan process in QCD," Nucl. Phys. **B157**, 461–497.

Alwall, J., R. Frederix, S. Frixione, V. Hirschi, F. Maltoni, O. Mattelaer, H. S. Shao, T. Stelzer, P. Torrielli, and M. Zaro, 2014, "The automated computation of tree-level and next-to-leading order differential cross sections, and their matching to parton shower simulations," J. High Energy Phys. 07, 079.

Alwall, Johan, *et al.*, 2008, "Comparative study of various algorithms for the merging of parton showers and matrix elements in hadronic collisions," Eur. Phys. J. C **53**, 473–500.

Anastasiou, Charalampos, Lance J. Dixon, Kirill Melnikov, and Frank Petriello, 2004, "High precision QCD at hadron colliders: Electroweak gauge boson rapidity distributions at NNLO," Phys. Rev. D **69**, 094008.

Andersson, Bo, G. Gustafson, G. Ingelman, and T. Sjöstrand, 1983, "Parton fragmentation and string dynamics," Phys. Rep. **97**, 31–145.

Appel, J. A., *et al.*, 1986, "Measurement of $W^{\pm}$ and Z^0 properties at the CERN $\bar{p}p$ collider," Z. Phys. C **30**, 1–22.

Arnison, G., *et al.*, 1983a, "Experimental observation of isolated large transverse energy electrons with associated missing energy at $s = 540$ GeV," Phys. Lett. **122B**, 103–116.

Arnison, G., *et al.*, 1983b, "Experimental observation of lepton pairs of invariant mass around 95 GeV/c^2 at the CERN SPS collider," Phys. Lett. **126B**, 398–410.

Arnison, G., *et al.*, 1983c, "Further evidence for charged intermediate vector bosons at the SPS Collider," Phys. Lett. **129B**, 273–282.

Arnison, G., *et al.*, 1984a, "Observation of muonic Z^0-decay at the $\bar{p}p$ collider," Phys. Lett. **147B**, 241–248.

Arnison, G., *et al.*, 1984b, "Observation of the muonic decay of the charged intermediate vector boson," Phys. Lett. **134B**, 469–476.

ATLAS Collaboration, 2011a, "Measurement of the inclusive isolated prompt photon cross-section in pp collisions at $\sqrt{s} = 7$ TeV using 35 pb^{-1} of ATLAS data," Phys. Lett. B **706**, 150–167.

ATLAS Collaboration, 2011b, "Measurement of the inclusive isolated prompt photon cross section in pp collisions at $\sqrt{s} = 7$ TeV with the ATLAS detector," Phys. Rev. D **83**, 052005.

ATLAS Collaboration, 2011c, "Measurement of the production cross section for W-bosons in association with jets in pp collisions at $\sqrt{s} = 7$ TeV with the ATLAS detector," Phys. Lett. B **698**, 325–345.

ATLAS Collaboration, 2012a, "Determination of the Strange Quark Density of the Proton from ATLAS Measurements of the $W \to \ell\nu$ and $Z \to \ell\ell$ Cross Sections," Phys. Rev. Lett. **109**, 012001.

ATLAS Collaboration, 2012b, "Measurement of the cross-section for b-jets produced in association with a Z boson at $\sqrt{s} = 7$ TeV with the ATLAS detector," Phys. Lett. B **706**, 295–313.

ATLAS Collaboration, 2012c, "Measurement of the cross section for the production of a W boson in association with b-jets in pp collisions at $\sqrt{s} = 7$ TeV with the ATLAS detector," Phys. Lett. B **707**, 418.

ATLAS Collaboration, 2012d, "Measurement of the inclusive $W^{\pm}$ and Z/γ^* cross sections in the e and μ decay channels in pp collisions at $\sqrt{s} = 7$ TeV with the ATLAS detector," Phys. Rev. D **85**, 072004.

ATLAS Collaboration, 2012e, "Measurement of the polarisation of W bosons produced with large transverse momentum in pp collisions at $\sqrt{s} = 7$ TeV with the ATLAS experiment," Eur. Phys. J. C **72**, 2001.

ATLAS Collaboration, 2012f, "Measurement of the production cross section for Z/γ^* in association with jets in pp collisions at $\sqrt{s} = 7$ TeV with the ATLAS detector," Phys. Rev. D **85**, 032009.

ATLAS Collaboration, 2012g, "Measurement of the production cross section of an isolated photon associated with jets in proton-proton collisions at $\sqrt{s} = 7$ TeV with the ATLAS detector," Phys. Rev. D **85**, 092014.

ATLAS Collaboration, 2012h, "Study of jets produced in association with a W boson in pp collisions at $\sqrt{s} = 7$ TeV with the ATLAS detector," Phys. Rev. D **85**, 092002.

ATLAS Collaboration, 2013a, "Dynamics of isolated-photon plus jet production in pp collisions at $\sqrt{s} = 7$ TeV with the ATLAS detector," Nucl. Phys. **B875**, 483–535.

ATLAS Collaboration, 2013b, "Measurement of hard double-parton interactions in $W(\to l\nu) + 2$ jet events at $\sqrt{s} = 7$ TeV with the ATLAS detector," New J. Phys. **15**, 033038.

ATLAS Collaboration, 2013c, "Measurement of k_t splitting scales in $W \to \ell\nu$ events at $\sqrt{s} = 7$ TeV with the ATLAS detector," Eur. Phys. J. C **73**, 2432.

ATLAS Collaboration, 2013d, "Measurement of the cross-section for W boson production in association with b-jets in pp collisions at $\sqrt{s} = 7$ TeV with the ATLAS detector," J. High Energy Phys. 06, 084.

ATLAS Collaboration, 2013e, "Measurement of the production cross section of jets in association with a Z boson in pp collisions at $\sqrt{s} = 7$ TeV with the ATLAS detector," J. High Energy Phys. 07, 032.

ATLAS Collaboration, 2014a, "A measurement of the ratio of the production cross sections for W and Z bosons in association with jets with the ATLAS detector," Eur. Phys. J. C **74**, 3168.

ATLAS Collaboration, 2014b, "Measurement of the inclusive isolated prompt photons cross section in pp collisions at $\sqrt{s} = 7$ TeV with the ATLAS detector using 4.6 fb^{-1}," Phys. Rev. D **89**, 052004.

ATLAS Collaboration, 2014c, "Measurement of differential production cross-sections for a Z boson in association with b-jets in 7 TeV proton-proton collisions with the ATLAS detector," J. High Energy Phys. 10, 141.

ATLAS Collaboration, 2014d, "Search for pair-produced third-generation squarks decaying via charm quarks or in compressed supersymmetric scenarios in pp collisions at $\sqrt{s} = 8$ TeV with the ATLAS detector," Phys. Rev. D **90**, 052008.

ATLAS Collaboration, 2014e, "Measurement of the electroweak production of dijets in association with a Z boson and distributions sensitive to vector boson fusion in proton-proton collisions at $\sqrt{s} = 8$ TeV using the ATLAS detector," J. High Energy Phys. 04, 031.

ATLAS Collaboration, 2014f, "Measurement of the production of a W boson in association with a charm quark in pp collisions at $\sqrt{s} = 7$ TeV with the ATLAS detector," J. High Energy Phys. 05, 068.

ATLAS Collaboration, 2014g, "Measurement of the Z/γ^* boson transverse momentum distribution in pp collisions at $\sqrt{s} = 7$ TeV with the ATLAS detector," J. High Energy Phys. 09, 145.

ATLAS Collaboration, 2014h, "Search for strong production of supersymmetric particles in final states with missing transverse momentum and at least three b-jets at $\sqrt{s} = 8$ TeV proton-proton collisions with the ATLAS detector," J. High Energy Phys. 10, 024.

ATLAS Collaboration, 2015a, "Measurements of the W production cross sections in association with jets with the ATLAS detector," Eur. Phys. J. C **75**, 82.

ATLAS Collaboration, 2015b, "Measurement of the forward-backward asymmetry of electron and muon pair-production in pp collisions at $\sqrt{s} = 7$ TeV with the ATLAS detector," J. High Energy Phys. 09, 049.

ATLAS Collaboration, 2015c, "Proposal for truth particle observable definitions in physics measurements," Technical Report No. ATL-PHYS-PUB-2015-013.

ATLAS Collaboration, 2016a, "Measurement of event-shape observables in $Z \to \ell^+\ell^-$ events in pp collisions at $\sqrt{s} = 7$ TeV with the ATLAS detector at the LHC," Eur. Phys. J. C **76**, 375.

ATLAS Collaboration, 2016b, "Measurement of the angular coefficients in Z-boson events using electron and muon pairs from data taken at $\sqrt{s} = 8$ TeV with the ATLAS detector," J. High Energy Phys. 08, 159.

ATLAS Collaboration, 2016c, "Monte Carlo generators for the production of a W or Z/γ^* boson in association with jets at ATLAS in run 2," Technical Report No. ATL-PHYS-PUB-2016-003.

ATLAS Collaboration, 2016d, "Muon reconstruction performance of the ATLAS detector in proton-proton collision data at $\sqrt{s} = 13$ TeV," Eur. Phys. J. C **76**, 292.

ATLAS Collaboration, 2016e, "Measurement of the inclusive isolated prompt photon cross section in pp collisions at $\sqrt{s} = 8$ TeV with the ATLAS detector," J. High Energy Phys. 08, 005.

ATLAS Collaboration, 2016f, "Performance of b-jet identification in the ATLAS Experiment," J. Instrum. **11**, P04008.

ATLAS Collaboration, 2016g, "Performance of pile-up mitigation techniques for jets in pp collisions at $\sqrt{s} = 8$ TeV using the ATLAS detector," Eur. Phys. J. C **76**, 581.

ATLAS Collaboration, 2016h, "Validation of Monte Carlo event generators in the ATLAS Collaboration for LHC run 2," Technical Report No. ATL-PHYS-PUB-2016-001.

ATLAS Collaboration, 2016i, "Search for invisible decays of a Higgs boson using vector-boson fusion in pp collisions at $\sqrt{s} = 8$ TeV with the ATLAS detector," J. High Energy Phys. 01, 172.

ATLAS Collaboration, 2017a, "ATLAS simulation of boson plus jets processes in run 2," Technical Report No. ATL-PHYS-PUB-2017-006.

ATLAS Collaboration, 2017b, "High-E_{T} isolated-photon plus jets production in pp collisions at $\sqrt{s} = 8$ TeV with the ATLAS detector," Nucl. Phys. **B918**, 257–316.

ATLAS Collaboration, 2017c, "Measurement of the cross-section for electroweak production of dijets in association with a Z boson in pp collisions at $\sqrt{s} = 13$ TeV with the ATLAS detector," Phys. Lett. B **775**, 206.

ATLAS Collaboration, 2017d, "Measurement of the cross section for inclusive isolated-photon production in pp collisions at $\sqrt{s} = 13$ TeV using the ATLAS detector," Phys. Lett. B **770**, 473–493.

ATLAS Collaboration, 2017e, "Measurement of W boson angular distributions in events with high transverse momentum jets at $\sqrt{s} = 8$ TeV using the ATLAS detector," Phys. Lett. B **765**, 132–153.

ATLAS Collaboration, 2017f, "Measurement of the k_t splitting scales in $Z \rightarrow \ell\ell$ events in pp collisions at $\sqrt{s} = 8$ TeV with the ATLAS detector," J. High Energy Phys. 08, 026.

ATLAS Collaboration, 2017g, "Measurements of electroweak Wjj production and constraints on anomalous gauge couplings with the ATLAS detector," Eur. Phys. J. C **77**, 474.

ATLAS Collaboration,, 2017h, "Measurements of the production cross section of a Z boson in association with jets in pp collisions at $\sqrt{s} = 13$ TeV with the ATLAS detector," Eur. Phys. J. C **77**, 361.

ATLAS Collaboration, 2017i, "Precision measurement and interpretation of inclusive W^+, W^- and Z/γ^* production cross sections with the ATLAS detector," Eur. Phys. J. C **77**, 367.

ATLAS Collaboration, 2018a, "Measurement of differential cross sections of isolated-photon plus heavy-flavour jet production in pp collisions at $\sqrt{s} = 8$ TeV using the ATLAS detector," Phys. Lett. B **776**, 295–317.

ATLAS Collaboration, 2018b, "Measurement of differential cross sections and W^+/W^- cross-section ratios for W boson production in association with jets at $\sqrt{s} = 8$ TeV with the ATLAS detector," J. High Energy Phys. 05, 077.

ATLAS Collaboration, 2018c, "Measurement of the cross section for isolated-photon plus jet production in pp collisions at $\sqrt{s} = 13$ TeV using the ATLAS detector," Phys. Lett. B **780**, 578–602.

ATLAS Collaboration, 2018d, "Measurement of the effective leptonic weak mixing angle using electron and muon pairs from Z-boson decay in the ATLAS experiment at $\sqrt{s} = 8$ TeV," Technical Report No. ATLAS-CONF-2018-037.

ATLAS Collaboration, 2018d, "Observation of $H \rightarrow b\bar{b}$ decays and VH production with the ATLAS detector," Phys. Lett. B **786**, 59–86.

ATLAS Collaboration,, 2018e, "Performance of missing transverse momentum reconstruction with the ATLAS detector using proton-proton collisions at $\sqrt{s} = 13$ TeV," Eur. Phys. J. C **78**, 903.

ATLAS Collaboration,, 2018f, "Measurements of b-jet tagging efficiency with the ATLAS detector using $t\bar{t}$ events at $\sqrt{s} = 13$ TeV," J. High Energy Phys. 08, 089.

ATLAS Collaboration, 2019a, "Electron and photon performance measurements with the ATLAS detector using the 2015–2017 LHC proton-proton collision data," J. Instrum. **14**, P12006.

ATLAS Collaboration, 2019b, "Measurement of the inclusive cross-section for the production of jets in association with a Z boson in proton-proton collisions at 8 TeV using the ATLAS detector," Eur. Phys. J. C **79**, 847.

ATLAS Collaboration, 2019c, "QCD analysis of ATLAS $W^{\pm}$ boson production data in association with jets," Technical Report No. ATL-PHYS-PUB-2019-016.

ATLAS Collaboration, 2019d, "Measurement of the inclusive isolated-photon cross section in pp collisions at $\sqrt{s} = 13$ TeV using 36 fb^{-1} of ATLAS data," J. High Energy Phys. 10, 203.

ATLAS Collaboration, 2019e, "Standard model summary plots summer 2019", Technical Report No. ATL-PHYS-PUB-2019-024.

ATLAS Collaboration, 2019f, "Measurement of the ratio of cross sections for inclusive isolated-photon production in pp collisions at $\sqrt{s} = 13$ and 8 TeV with the ATLAS detector," J. High Energy Phys. 04, 093.

ATLAS Collaboration, 2020a, "Jet energy scale and resolution measured in proton-proton collisions at $\sqrt{s} = 13$ TeV with the ATLAS detector," Report No. CERN-EP-2020-083 [arXiv:2007.02645].

ATLAS Collaboration, 2020b, "Performance of electron and photon triggers in ATLAS during LHC run 2," Eur. Phys. J. C **80**, 47.

ATLAS Collaboration, 2020c, "Measurement of isolated-photon plus two-jet production in pp collisions at $\sqrt{s} = 13$ TeV with the ATLAS detector," J. High Energy Phys. 03, 179.

ATLAS Collaboration, 2020d, "Measurements of the production cross-section for a Z boson in association with b-jets in proton-proton collisions at $\sqrt{s} = 13$ TeV with the ATLAS detector," J. High Energy Phys. 07, 044.

ATLAS Collaboration, 2021, "Differential cross-section measurements for the electroweak production of dijets in association with a Z boson in proton-proton collisions at ATLAS," Eur. Phys. J. C **81**, 163.

Aurenche, Patrick, Michel Fontannaz, Jean-Philippe Guillet, Eric Pilon, and Monique Werlen, 2006, "Recent critical study of photon production in hadronic collisions," Phys. Rev. D **73**, 094007.

Bacchetta, Alessandro, Valerio Bertone, Chiara Bissolotti, Giuseppe Bozzi, Filippo Delcarro, Fulvio Piacenza, and Marco Radici, 2020, "Transverse-momentum-dependent parton distributions up to N^{3}LL from Drell-Yan data," J. High Energy Phys. 07, 117.

Baglio, J., et al., 2014, "Release note—VBFNLO 2.7.0.," arXiv:1404.3940.

Bagnaia, P., et al., 1983, "Evidence for $Z^0 \rightarrow e^+e^-$ at the CERN $\bar{p}p$ collider," Phys. Lett. **129B**, 130–140.

Bagnaia, P., et al., 1984, "A study of high transverse momentum electrons produced in $\bar{p}p$ collisions at 540 GeV," Z. Phys. C **24**, 1–17.

Bähr, M., et al., 2008, "HERWIG++ physics and manual," Eur. Phys. J. C **58**, 639.

Bähr, Manuel, Stefan Gieseke, and Michael H. Seymour, 2008, "Simulation of multiple partonic interactions in HERWIG++," J. High Energy Phys. 07, 076.

Balazs, C., and C. P. Yuan, 1997, "Soft gluon effects on lepton pairs at hadron colliders," Phys. Rev. D **56**, 5558–5583.

Ball, Richard D., Valerio Bertone, Marco Bonvini, Stefano Forte, Patrick Groth Merrild, Juan Rojo, and Luca Rottoli, 2016, "Intrinsic charm in a matched general-mass scheme," Phys. Lett. B **754**, 49–58.

Banfi, A., S. Redford, M. Vesterinen, P. Waller, and T. R. Wyatt, 2011, "Optimisation of variables for studying dilepton transverse momentum distributions at hadron colliders," Eur. Phys. J. C **71**, 1600.

Banfi, Andrea, Mrinal Dasgupta, and Simone Marzani, 2011, "QCD predictions for new variables to study dilepton transverse momenta at hadron colliders," Phys. Lett. B **701**, 75–81.

Banfi, Andrea, Pier Francesco Monni, Gavin P. Salam, and Giulia Zanderighi, 2012, "Higgs and Z-Boson Production with a Jet Veto," Phys. Rev. Lett. **109**, 202001.

Banfi, Andrea, Gavin P. Salam, and Giulia Zanderighi, 2006, "Infrared safe definition of jet flavor," Eur. Phys. J. C **47**, 113–124.

Banner, M., et al., 1983, "Observation of single isolated electrons of high transverse momentum in events with missing transverse energy at the CERN $\bar{p}p$ collider," Phys. Lett. **122B**, 476–485.

Barberio, Elisabetta, Bob van Eijk, and Zbigniew Wąs, 1991, "PHOTOS: A universal Monte Carlo for QED radiative corrections in decays," Comput. Phys. Commun. **66**, 115–128.

Barzè, Luca, Guido Montagna, Paolo Nason, Oreste Nicrosini, and Fulvio Piccinini, 2012, "Implementation of electroweak corrections in the POWHEG BOX: Single W production," J. High Energy Phys. 04, 037.

Barzè, Luca, Guido Montagna, Paolo Nason, Oreste Nicrosini, Fulvio Piccinini, and Alessandro Vicini, 2013, "Neutral current Drell-Yan with combined QCD and electroweak corrections in the POWHEG BOX," Eur. Phys. J. C **73**, 2474.

Becher, Thomas, and Matthias Neubert, 2011, "Drell-Yan production at small q_T, transverse parton distributions and the collinear anomaly," Eur. Phys. J. C **71**, 1665.

Bellm, Johannes, Stefan Gieseke, and Simon Plätzer, 2018, "Merging NLO multi-jet calculations with improved unitarization," Eur. Phys. J. C **78**, 244.

Bellm, Johannes, et al., 2016, "HERWIG 7.0/HERWIG++ 3.0 release note," Eur. Phys. J. C **76**, 196.

Berends, Frits A., W. T. Giele, H. Kuijf, R. Kleiss, and W. James Stirling, 1989, "Multi-jet production in W, Z events at $p\bar{p}$ colliders," Phys. Lett. B **224**, 237–242.

Berger, C. F., Z. Bern, L. J. Dixon, F. Febres Cordero, D. Forde, H. Ita, D. A. Kosower, and D. Maître, 2008, "Automated implementation of on-shell methods for one-loop amplitudes," Phys. Rev. D **78**, 036003.

Berger, C. F., Z. Bern, Lance J. Dixon, Fernando Febres Cordero, D. Forde, T. Gleisberg, H. Ita, D. A. Kosower, and D. Maître, 2009, "Precise Predictions for W + 3 Jet Production at Hadron Colliders," Phys. Rev. Lett. **102**, 222001.

Berger, C. F., Z. Bern, Lance J. Dixon, F. Febres Cordero, D. Forde, T. Gleisberg, H. Ita, D. A. Kosower, and D. Maître, 2010, "Next-to-leading order QCD predictions for Z, γ^* + 3-jet distributions at the Tevatron," Phys. Rev. D **82**, 074002.

Berger, C. F., Z. Bern, Lance J. Dixon, F. Febres Cordero, D. Forde, T. Gleisberg, H. Ita, D. A. Kosower, and D. Maître, 2011, "Precise Predictions for W + 4-Jet Production at the Large Hadron Collider," Phys. Rev. Lett. **106**, 092001.

Bermudez Martinez, A., et al., 2019, "Production of Z-bosons in the parton branching method," Phys. Rev. D **100**, 074027.

Bern, Z., G. Diana, L. J. Dixon, F. Febres Cordero, S. Höche, H. Ita, D. A. Kosower, D. Maître, and K. J. Ozeren, 2011, "Driving missing data at next-to-leading order," Phys. Rev. D **84**, 114002.

Bern, Z., L. J. Dixon, F. Febres Cordero, S. Höche, H. Ita, D. A. Kosower, D. Maître, and K. J. Ozeren, 2013, "Next-to-leading order W + 5-jet production at the LHC," Phys. Rev. D **88**, 014025.

Bernaciak, C., and D. Wackeroth, 2012, "Combining NLO QCD and electroweak radiative corrections to W boson production at hadron colliders in the POWHEG framework," Phys. Rev. D **85**, 093003.

Bertone, Valerio, Stefano Carrazza, and Juan Rojo, 2015, "Doped parton distributions," arXiv:1509.04022.

Bierlich, Christian, et al., 2020, "Robust independent validation of experiment and theory: RIVET version 3," SciPost Phys. **8**, 026.

Binoth, T., et al. (SM and NLO Multileg Working Group), 2010, "The SM and NLO Multileg Working Group: Summary report," arXiv:1003.1241.

Bizoń, Wojciech, Xuan Chen, Aude Gehrmann-De Ridder, Thomas Gehrmann, Nigel Glover, Alexander Huss, Pier Francesco Monni, Emanuele Re, Luca Rottoli, and Paolo Torrielli, 2018, "Fiducial distributions in Higgs and Drell-Yan production at N^{3}LL+NNLO," J. High Energy Phys. 12, 132.

Bizoń, Wojciech, Aude Gehrmann-De Ridder, Thomas Gehrmann, Nigel Glover, Alexander Huss, Pier Francesco Monni, Emanuele

Re, Luca Rottoli, and Duncan M. Walker, 2019, "The transverse momentum spectrum of weak gauge bosons at N^{3}LL + NNLO," Eur. Phys. J. C **79**, 868.

Blazey, Gerald C., et al., 2000, "Run II jet physics," arXiv:hep-ex/0005012.

Bloch, F., and A. Nordsieck, 1937, "Note on the radiation field of the electron," Phys. Rev. **52**, 54–59.

Bothmann, Enrico, et al., 2019, "Event generation with SHERPA 2.2," SciPost Phys. **7**, 34.

Boughezal, Radja, John M. Campbell, R. Keith Ellis, Christfried Focke, Walter T. Giele, Xiaohui Liu, and Frank Petriello, 2016, "Z-Boson Production in Association with a Jet at Next-to-Next-to-Leading Order in Perturbative QCD," Phys. Rev. Lett. **116**, 152001.

Boughezal, Radja, Christfried Focke, Walter Giele, Xiaohui Liu, and Frank Petriello, 2015, "Higgs boson production in association with a jet at NNLO using jettiness subtraction," Phys. Lett. B **748**, 5–8.

Boughezal, Radja, Christfried Focke, Xiaohui Liu, and Frank Petriello, 2015, "W-Boson Production in Association with a Jet at Next-to-Next-to-Leading Order in Perturbative QCD," Phys. Rev. Lett. **115**, 062002.

Boughezal, Radja, Xiaohui Liu, and Frank Petriello, 2016a, "Phenomenology of the Z-boson plus jet process at NNLO," Phys. Rev. D **94**, 074015.

Boughezal, Radja, Xiaohui Liu, and Frank Petriello, 2016b, "W-boson plus jet differential distributions at NNLO in QCD," Phys. Rev. D **94**, 113009.

Bozzi, Giuseppe, Stefano Catani, Giancarlo Ferrera, Daniel de Florian, and Massimiliano Grazzini, 2011, "Production of Drell-Yan lepton pairs in hadron collisions: Transverse-momentum resummation at next-to-next-to-leading logarithmic accuracy," Phys. Lett. B **696**, 207–213.

Buckley, Andy, Jonathan Butterworth, Leif Lonnblad, David Grellscheid, Hendrik Hoeth, James Monk, Holger Schulz, and Frank Siegert, 2013, "RIVET user manual," Comput. Phys. Commun. **184**, 2803–2819.

Butterworth, J. M., Jeffrey R. Forshaw, and M. H. Seymour, 1996, "Multiparton interactions in photoproduction at HERA," Z. Phys. C **72**, 637–646.

Cacciari, Matteo, Mario Greco, and Paolo Nason, 1998, "The p_T spectrum in heavy flavor hadroproduction," J. High Energy Phys. 05, 007.

Cacciari, Matteo, and Gavin P. Salam, 2008, "Pileup subtraction using jet areas," Phys. Lett. B **659**, 119–126.

Cacciari, Matteo, Gavin P. Salam, and Gregory Soyez, 2008, "The anti-k_t jet clustering algorithm," J. High Energy Phys. 04, 063.

Campbell, J. M., F. Caola, F. Febres Cordero, L. Reina, and D. Wackeroth, 2012, "NLO QCD predictions for W + 1 jet and W + 2 jet production with at least one b jet at the 7 TeV LHC," Phys. Rev. D **86**, 034021.

Campbell, John M., and R. K. Ellis, 2010, "MCFM for the Tevatron and the LHC," Nucl. Phys. B, Proc. Suppl. **205-206**, 10–15.

Campbell, John M., and R. Keith Ellis, 2002, "Next-to-leading order corrections to W + 2 jet and Z + 2 jet production at hadron colliders," Phys. Rev. D **65**, 113007.

Campbell, John M., R. Keith Ellis, F. Febres Cordero, F. Maltoni, L. Reina, D. Wackeroth, and S. Willenbrock, 2009, "Associated production of a W boson and one b jet," Phys. Rev. D **79**, 034023.

Campbell, John M., R. Keith Ellis, F. Maltoni, and S. Willenbrock, 2004, "Associated production of a Z boson and a single heavy quark jet," Phys. Rev. D **69**, 074021.

Campbell, John M., R. Keith Ellis, F. Maltoni, and S. Willenbrock, 2006, "Production of a Z boson and two jets with one heavy-quark tag," Phys. Rev. D **73**, 054007; **77**, 019903(E) (2008).

Campbell, John M., R. Keith Ellis, F. Maltoni, and S. Willenbrock, 2007, "Production of a W boson and two jets with one b-quark tag," Phys. Rev. D **75**, 054015.

Campbell, John M., R. Keith Ellis, Paolo Nason, and Giulia Zanderighi, 2013, "W and Z bosons in association with two jets using the POWHEG method," J. High Energy Phys. 08, 005.

Campbell, John M., R. Keith Ellis, and Ciaran Williams, 2017a, "Direct Photon Production at Next-to-Next-to-Leading Order," Phys. Rev. Lett. **118**, 222001.

Campbell, John M., R. Keith Ellis, and Ciaran Williams, 2017b, "Driving missing data at the LHC: NNLO predictions for the ratio of $\gamma + j$ and $Z + j$," Phys. Rev. D **96**, 014037.

Campbell, John M., Juan Rojo, Emma Slade, and Ciaran Williams, 2018, "Direct photon production and PDF fits reloaded," Eur. Phys. J. C **78**, 470.

Catani, S., Yuri L. Dokshitzer, M. H. Seymour, and B. R. Webber, 1993, "Longitudinally invariant K_t clustering algorithms for hadron hadron collisions," Nucl. Phys. **B406**, 187–224.

Catani, S., M. Fontannaz, J. P. Guillet, and E. Pilon, 2002, "Cross-section of isolated prompt photons in hadron-hadron collisions," J. High Energy Phys. 05, 028.

Catani, S., F. Krauss, R. Kuhn, and B. R. Webber, 2001, "QCD matrix elements + parton showers," J. High Energy Phys. 11, 063.

Catani, Stefano, Leandro Cieri, Giancarlo Ferrera, Daniel de Florian, and Massimiliano Grazzini, 2009, "Vector Boson Production at Hadron Colliders: A Fully Exclusive QCD Calculation at NNLO," Phys. Rev. Lett. **103**, 082001.

Catani, Stefano, Leandro Cieri, Daniel de Florian, Giancarlo Ferrera, and Massimiliano Grazzini, 2014, "Universality of transverse-momentum resummation and hard factors at the NNLO," Nucl. Phys. **B881**, 414–443.

Catani, Stefano, Simone Devoto, Massimiliano Grazzini, Stefan Kallweit, Javier Mazzitelli, and Hayk Sargsyan, 2019, "Top-quark pair hadroproduction at next-to-next-to-leading order in QCD," Phys. Rev. D **99**, 051501.

Catani, Stefano, and Massimiliano Grazzini, 2007, "Next-to-Next-to-Leading-Order Subtraction Formalism in Hadron Collisions and Its Application to Higgs-Boson Production at the Large Hadron Collider," Phys. Rev. Lett. **98**, 222002.

CDF Collaboration, 2006, "Measurement of the b jet cross-section in events with a Z boson in $p\bar{p}$ collisions at $\sqrt{s} = 1.96$ TeV," Phys. Rev. D **74**, 032008.

CDF Collaboration, 2008a, "First Measurement of the Production of a W Boson in Association with a Single Charm Quark in $p\bar{p}$ Collisions at $\sqrt{s} = 1.96$ TeV," Phys. Rev. Lett. **100**, 091803.

CDF Collaboration, 2008b, "Measurement of Inclusive Jet Cross Sections in $Z/\gamma^* \to e^+e^-$ + jets Production in $p\bar{p}$ Collisions at $\sqrt{s} = 1.96$ TeV," Phys. Rev. Lett. **100**, 102001.

CDF Collaboration, 2008c, "Measurement of the cross section for W-boson production in association with jets in $p\bar{p}$ collisions at $\sqrt{s} = 1.96$ TeV," Phys. Rev. D **77**, 011108.

CDF Collaboration, 2009a, "Direct Measurement of the W Production Charge Asymmetry in $p\bar{p}$ Collisions at $\sqrt{s} = 1.96$ TeV," Phys. Rev. Lett. **102**, 181801.

CDF Collaboration, 2009b, "Measurement of cross sections for b jet production in events with a Z boson in $p\bar{p}$ collisions at $\sqrt{s} = 1.96$ TeV," Phys. Rev. D **79**, 052008.

CDF Collaboration, 2010a, "Study of the associated production of photons and b-quark jets in $p\bar{p}$ collisions at $\sqrt{s} = 1.96$ TeV," Phys. Rev. D **81**, 052006.

CDF Collaboration, 2010b, "First Measurement of the b-Jet Cross Section in Events with a W Boson in $p\bar{p}$ Collisions at $\sqrt{s} = 1.96$ TeV," Phys. Rev. Lett. **104**, 131801.

CDF Collaboration, 2011, "First Measurement of the Angular Coefficients of Drell-Yan e^+e^- Pairs in the Z Mass Region from $p\bar{p}$ Collisions at $\sqrt{s} = 1.96$ TeV," Phys. Rev. Lett. **106**, 241801.

CDF Collaboration, 2013a, "Indirect measurement of $\sin^2 \theta_W$ (M_W) using e^+e^- pairs in the Z-boson region with $p\bar{p}$ collisions at a center-of-momentum energy of 1.96 TeV," Phys. Rev. D **88**, 072002; **88**, 079905(E) (2013).

CDF Collaboration, 2013b, "Measurement of the Cross Section for Direct-Photon Production in Association with a Heavy Quark in $p\bar{p}$ Collisions at $\sqrt{s} = 1.96$ TeV," Phys. Rev. Lett. **111**, 042003.

CDF Collaboration, 2013c, "Observation of the Production of a W Boson in Association with a Single Charm Quark," Phys. Rev. Lett. **110**, 071801.

CDF Collaboration, 2015, "Measurement of differential production cross section for Z/γ^* bosons in association with jets in $p\bar{p}$ collisions at $\sqrt{s} = 1.96$ TeV," Phys. Rev. D **91**, 012002.

CDF and D0 Collaborations, 2018, "Tevatron run II combination of the effective leptonic electroweak mixing angle," Phys. Rev. D **97**, 112007.

Chen, Xuan, Thomas Gehrmann, Nigel Glover, Marius Höfer, and Alexander Huss, 2020, "Isolated photon and photon + jet production at NNLO QCD accuracy," J. High Energy Phys. 04, 166.

Chiesa, Mauro, Nicolas Greiner, and Francesco Tramontano, 2016, "Automation of electroweak corrections for LHC processes," J. Phys. G **43**, 013002.

Chiesa, Mauro, Guido Montagna, Luca Barzè, Mauro Moretti, Oreste Nicrosini, Fulvio Piccinini, and Francesco Tramontano, 2013, "Electroweak Sudakov Corrections to New Physics Searches at the LHC," Phys. Rev. Lett. **111**, 121801.

Christiansen, Jesper Roy, and Torbjörn Sjöstrand, 2014, "Weak gauge boson radiation in parton showers," J. High Energy Phys. 04, 115.

Cieri, Leandro, Giancarlo Ferrera, and German F. R. Sborlini, 2018, "Combining QED and QCD transverse-momentum resummation for Z boson production at hadron colliders," J. High Energy Phys. 08, 165.

CMS Collaboration, 2009, "Performance of jet reconstruction with charged tracks only," Technical Report No. CMS-PAS-JME-08-001.

CMS Collaboration, 2010, Commissioning of trackjets in pp collisions at 7 TeV, Technical Report No. CMS-PAS-JME-10-006.

CMS Collaboration, 2011a, "Measurement of the differential cross section for isolated prompt photon production in pp collisions at 7 TeV," Phys. Rev. D **84**, 052011.

CMS Collaboration, 2011b, "Measurement of the Isolated Prompt Photon Production Cross Section in pp Collisions at $\sqrt{s} = 7$ TeV," Phys. Rev. Lett. **106**, 082001.

CMS Collaboration, 2011c, "Measurement of the Polarization of W Bosons with Large Transverse Momenta in W + jets Events at the LHC," Phys. Rev. Lett. **107**, 021802.

CMS Collaboration, 2011d, "Measurement of the weak mixing angle with the Drell-Yan process in proton-proton collisions at the LHC," Phys. Rev. D **84**, 112002.

CMS Collaboration, 2012a, "Jet production rates in association with W and Z bosons in pp collisions at $\sqrt{s} = 7$ TeV," J. High Energy Phys. 01, 010.

CMS Collaboration, 2012b, "Measurement of the Z/γ^* + b-jet cross section in pp collisions at $\sqrt{s} = 7$ TeV," J. High Energy Phys. 06, 126.

CMS Collaboration, 2012c, "Search for supersymmetry in hadronic final states using M_{T2} in pp collisions at $\sqrt{s} = 7$ TeV," J. High Energy Phys. 10, 018.

CMS Collaboration, 2012d, "Measurement of the Electron Charge Asymmetry in Inclusive W Production in pp Collisions at $\sqrt{s} = 7$ TeV," Phys. Rev. Lett. **109**, 111806.

CMS Collaboration, 2013a, "Measurement of the cross section and angular correlations for associated production of a Z boson with b hadrons in pp collisions at $\sqrt{s} = 7$ TeV," J. High Energy Phys. 12, 039.

CMS Collaboration, 2013b, "Measurement of the hadronic activity in events with a Z and two jets and extraction of the cross section for the electroweak production of a Z with two jets in pp collisions at $\sqrt{s} = 7$ TeV," J. High Energy Phys. 10, 062.

CMS Collaboration, 2013c, "Event shapes and azimuthal correlations in $Z +$ jets events in pp collisions at $\sqrt{s} = 7$ TeV," Phys. Lett. B **722**, 238–261.

CMS Collaboration, 2013d, "Identification of b-quark jets with the CMS experiment," J. Instrum. **8**, P04013.

CMS Collaboration, 2013e, "Performance of quark/gluon discrimination in 8 TeV pp data," Technical Report No. CMS-PAS-JME-13-002.

CMS Collaboration, 2013f, "Rapidity distributions in exclusive $Z +$ jet and $\gamma +$ jet events in pp collisions at $\sqrt{s} = 7$ TeV," Phys. Rev. D **88**, 112009.

CMS Collaboration, 2014a, "Measurement of associated $W +$ charm production in pp collisions at $\sqrt{s} = 7$ TeV," J. High Energy Phys. 02, 013.

CMS Collaboration, 2014b, "Measurement of the muon charge asymmetry in inclusive $pp \to W + X$ production at $\sqrt{s} = 7$ TeV and an improved determination of light parton distribution functions," Phys. Rev. D **90**, 032004.

CMS Collaboration, 2014c, "Measurement of the production cross sections for a Z boson and one or more b jets in pp collisions at $\sqrt{s} = 7$ TeV," J. High Energy Phys. 06, 120.

CMS Collaboration, 2014d, "Measurement of the production cross section for a W boson and two b jets in pp collisions at $\sqrt{s} = 7$ TeV," Phys. Lett. B **735**, 204–225.

CMS Collaboration, 2014e, "Measurement of the triple-differential cross section for photon + jets production in proton-proton collisions at $\sqrt{s} = 7$ TeV," J. High Energy Phys. 06, 009.

CMS Collaboration, 2014f, "Study of double parton scattering using $W +$ 2-jet events in proton-proton collisions at $\sqrt{s} = 7$ TeV, J. High Energy Phys. 03, 032.

CMS Collaboration, 2015a, "Comparison of the $Z/\gamma^* +$ jets to $\gamma +$ jets cross sections in pp collisions at $\sqrt{s} = 8$ TeV," J. High Energy Phys. 10, 128.

CMS Collaboration, 2015b, "Angular coefficients of Z bosons produced in pp collisions at $\sqrt{s} = 8$ TeV and decaying to $\mu^+\mu^-$ as a function of transverse momentum and rapidity," Phys. Lett. B **750**, 154–175.

CMS Collaboration, 2015c, "Differential cross section measurements for the production of a W boson in association with jets in proton-proton collisions at $\sqrt{s} = 7$ TeV," Phys. Lett. B **741**, 12–37.

CMS Collaboration, 2015d, "Measurement of electroweak production of two jets in association with a Z boson in proton-proton collisions at $\sqrt{s} = 8$ TeV," Eur. Phys. J. C **75**, 66.

CMS Collaboration, 2015e, "Measurements of jet multiplicity and differential production cross sections of $Z +$ jets events in proton-proton collisions at $\sqrt{s} = 7$ TeV," Phys. Rev. D **91**, 052008.

CMS Collaboration, 2015f, "Performance of electron reconstruction and selection with the CMS detector in proton-proton collisions at $\sqrt{s} = 8$ TeV," J. Instrum. **10**, P06005.

CMS Collaboration, 2015g, "Performance of photon reconstruction and identification with the CMS detector in proton-proton collisions at $\sqrt{s} = 8$ TeV," J. Instrum. **10**, P08010.

CMS Collaboration, 2016, "Measurement of electroweak production of a W boson and two forward jets in proton-proton collisions at $\sqrt{s} = 8$ TeV," J. High Energy Phys. 11, 147.

CMS Collaboration, 2017a, "Measurements of differential production cross sections for a Z boson in association with jets in pp collisions at $\sqrt{s} = 8$ TeV," J. High Energy Phys. 04, 022.

CMS Collaboration, 2017b, Jet algorithms performance in 13 TeV data, Technical Report No. CMS-PAS-JME-16-003.

CMS Collaboration, 2017c, "Searches for invisible decays of the Higgs boson in pp collisions at $\sqrt{s} = 7$, 8, and 13 TeV," J. High Energy Phys. 02, 135.

CMS Collaboration, 2017d, "Jet energy scale and resolution in the CMS experiment in pp collisions at 8 TeV," J. Instrum. **12**, P02014.

CMS Collaboration, 2017e, "Measurement of the differential cross sections for the associated production of a W boson and jets in proton-proton collisions at $\sqrt{s} = 13$ TeV," Phys. Rev. D **96**, 072005.

CMS Collaboration, 2017f, "Measurement of the production cross section of a W boson in association with two b jets in pp collisions at $\sqrt{s} = 8$ TeV," Eur. Phys. J. C **77**, 92.

CMS Collaboration, 2017g, "Measurements of differential cross sections for associated production of a W boson and jets in proton-proton collisions at $\sqrt{s} = 8$ TeV," Phys. Rev. D **95**, 052002.

CMS Collaboration, 2017h, "Measurements of the associated production of a Z boson and b jets in pp collisions at $\sqrt{s} = 8$ TeV," Eur. Phys. J. C **77**, 751.

CMS Collaboration, 2017i, "Particle-flow reconstruction and global event description with the CMS detector," J. Instrum. **12**, P10003–P10003.

CMS Collaboration, 2017j, "The CMS trigger system," J. Instrum. **12**, P01020.

CMS Collaboration, 2018a, "Electroweak production of two jets in association with a Z boson in proton-proton collisions at $\sqrt{s} = 13$ TeV," Eur. Phys. J. C **78**, 589.

CMS Collaboration, 2018b, "Identification of heavy-flavour jets with the CMS detector in pp collisions at 13 TeV," J. Instrum. **13**, P05011.

CMS Collaboration, 2018c, "Measurement of associated $Z +$ charm production in proton-proton collisions at $\sqrt{s} = 8$ TeV," Eur. Phys. J. C **78**, 287.

CMS Collaboration, 2018d, "Measurement of differential cross sections for Z boson production in association with jets in proton-proton collisions at $\sqrt{s} = 13$ TeV," Eur. Phys. J. C **78**, 965.

CMS Collaboration, 2018e, "Measurement of the weak mixing angle using the forward-backward asymmetry of Drell-Yan events in pp collisions at 8 TeV," Eur. Phys. J. C **78**, 701.

CMS Collaboration, 2018f, "Observation of Higgs Boson Decay to Bottom Quarks," Phys. Rev. Lett. **121**, 121801.

CMS Collaboration, 2019a, "Displays of candidate VHcc events," Report No. CMS-PHO-EVENTS-2019-006.

CMS Collaboration, 2019b, "Measurement of associated production of a W boson and a charm quark in proton-proton collisions at $\sqrt{s} = 13$ TeV," Eur. Phys. J. C **79**, 269.

CMS Collaboration, 2019c, "Measurement of differential cross sections for inclusive isolated-photon and photon + jet production in proton-proton collisions at $\sqrt{s} = 13$ TeV," Eur. Phys. J. C **79**, 20.

CMS Collaboration, 2019d, "Measurements of triple-differential cross sections for inclusive isolated-photon + jet events in pp collisions at $\sqrt{s} = 8$ TeV," Eur. Phys. J. C **79**, 969.

CMS Collaboration, 2019e "Performance of missing transverse momentum reconstruction in proton-proton collisions at $\sqrt{s} = $ 13 TeV using the CMS detector," J. Instrum. **14**, P07004.

CMS Collaboration, 2019f, "Search for invisible decays of a Higgs boson produced through vector boson fusion in proton-proton collisions at $\sqrt{s} = 13$ TeV," Phys. Lett. B **793**, 520–551.

CMS Collaboration, 2020a, "Measurement of differential cross sections for Z bosons produced in association with charm jets in pp collisions at $\sqrt{s} = 13$ TeV," arXiv:2012.04119.

CMS Collaboration, 2020b, "Measurement of electroweak production of a W boson in association with two jets in proton-proton collisions at $\sqrt{s} = 13$ TeV," Eur. Phys. J. C **80**, 43.

CMS Collaboration, 2020c, "Measurement of the associated production of a Z boson with charm or bottom quark jets in proton-proton collisions at $\sqrt{s} = 13$ TeV," Phys. Rev. D **102**, 032007.

CMS Collaboration, 2020d, "Performance of the reconstruction and identification of high-momentum muons in proton-proton collisions at $\sqrt{s} = 13$ TeV," J. Instrum. **15**, P02027.

CMS Collaboration, 2020e, "Pileup mitigation at CMS in 13 TeV data," J. Instrum. **15**, P09018.

CMS Collaboration, 2020f, "Summaries of CMS cross section measurements," https://twiki.cern.ch/twiki/bin/view/CMSPublic/PhysicsResultsCombined.

Collins, John C., Davison E. Soper, and George F. Sterman, 1985, "Transverse momentum distribution in Drell-Yan pair and W and Z boson production," Nucl. Phys. **B250**, 199–224.

Cooper, B., J. Katzy, M. L. Mangano, A. Messina, L. Mijović, and P. Skands, 2012, "Importance of a consistent choice of α_S in the matching of AlpGen and PYTHIA," Eur. Phys. J. C **72**, 2078.

Coradeschi, Francesco, and Thomas Cridge, 2019, "reSolve—A transverse momentum resummation tool," Comput. Phys. Commun. **238**, 262–294.

Corke, Richard, and Torbjorn Sjostrand, 2010, "Multiparton interactions and rescattering," J. High Energy Phys. 01, 035.

Currie, James, E. W. N. Glover, and Steven Wells, 2013, "Infrared structure at NNLO using antenna subtraction," J. High Energy Phys. 04, 066.

Czakon, Michał, Alexander Mitov, Mathieu Pellen, and Rene Poncelet, 2020, "NNLO QCD predictions for $W + c$-jet production at the LHC," arXiv:2011.01011.

D0 Collaboration, 2005, "Measurement of the Ratio of Inclusive Cross Sections $\sigma(pp \rightarrow Z + b$-jet$)/\sigma(pp \rightarrow Z +jet)$ at $\sqrt{s} = 1.96$ TeV," Phys. Rev. Lett. **94**, 161801.

D0 Collaboration, 2008a, "Measurement of differential $Z/\gamma^* +$ jet $+ X$ cross sections in $p\bar{p}$ collisions at $\sqrt{s} = 1.96$ TeV," Phys. Lett. B **669**, 278–286.

D0 Collaboration, 2008b, "Measurement of the differential cross-section for the production of an isolated photon with associated jet in $p\bar{p}$ collisions at $\sqrt{s} = 1.96$ TeV," Phys. Lett. B **666**, 435–445.

D0 Collaboration, 2009c, "Measurement of $\gamma + b + X$ and $\gamma + c + X$ Production Cross Sections in p Anti-p Collisions at $\sqrt{s} = 1.96$ TeV," Phys. Rev. Lett. **102**, 192002.

D0 Collaboration, 2009d, "Measurements of differential cross sections of $Z/\gamma^* +$ jets $+ X$ events in proton anti-proton collisions at $\sqrt{s} = 1.96$ TeV," Phys. Lett. B **678**, 45–54.

D0 Collaboration, 2010a, "Double parton interactions in $\gamma + 3$ jet events in $p\bar{p}$ bar collisions $\sqrt{s} = 1.96$ TeV," Phys. Rev. D **81**, 052012.

D0 Collaboration, 2010b, "Measurement of $Z/\gamma^* +$ jet $+ X$ angular distributions in $\bar{p}p$ collisions at $\sqrt{s} = 1.96$ TeV," Phys. Lett. B **682**, 370–380.

D0 Collaboration, 2011a, "A measurement of the ratio of inclusive cross sections $\sigma(p\bar{p} \rightarrow Z + b$-quark jet$)/\sigma(p\bar{p} \rightarrow Z +jet)$ at $\sqrt{s} = 1.96$ TeV," Phys. Rev. D **83**, 031105.

D0 Collaboration, 2011b, "Azimuthal decorrelations and multiple parton interactions in $\gamma + 2$ jet and $\gamma + 3$ jet events in $p\bar{p}$ collisions at $\sqrt{s} = 1.96$ TeV," Phys. Rev. D **83**, 052008.

D0 Collaboration, 2011c, "Measurements of inclusive $W +$ jets production rates as a function of jet transverse momentum in $p\bar{p}$ collisions at $\sqrt{s} = 1.96$ TeV," Phys. Lett. B **705**, 200–207.

D0 Collaboration, 2012, "Measurement of the photon+b-jet production differential cross section in $p\bar{p}$ collisions at $\sqrt{s} = 1.96$ TeV," Phys. Lett. B **714**, 32–39.

D0 Collaboration, 2013a, "Measurement of the differential photon + c-jet cross section and the ratio of differential photon + c and photon + b cross sections in proton-antiproton collisions at $\sqrt{s} = 1.96$ TeV," Phys. Lett. B **719**, 354–361.

D0 Collaboration, 2013b, "Measurement of the $p\bar{p} \rightarrow W + b + X$ production cross section at $\sqrt{s} = 1.96$ TeV," Phys. Lett. B **718**, 1314–1320.

D0 Collaboration, 2013c, "Measurement of the ratio of differential cross sections $\sigma(p\bar{p} \rightarrow Z + bjet)/\sigma(p\bar{p} \rightarrow Z +$ jet$)$ in $p\bar{p}$ collisions at $\sqrt{s} = 1.96$ TeV," Phys. Rev. D **87**, 092010.

D0 Collaboration, 2013d, "Studies of W boson plus jets production in $p\bar{p}$ collisions at $\sqrt{s} = 1.96$ TeV," Phys. Rev. D **88**, 092001.

D0 Collaboration, 2014, "Measurement of Associated Production of Z Bosons with Charm Quark Jets in $\bar{p}p$ Collisions at $\sqrt{s} = 1.96$ TeV," Phys. Rev. Lett. **112**, 042001.

D0 Collaboration, 2015, "Measurement of the electron charge asymmetry in $p\bar{p} \rightarrow W + X \rightarrow e\nu + X$ decays in $p\bar{p}$ collisions at $\sqrt{s} = 1.96$ TeV," Phys. Rev. D **91**, 032007.

Davidson, N., T. Przedzinski, and Z. Wąs, 2016, "PHOTOS interface in C++: Technical and physics documentation," Comput. Phys. Commun. **199**, 86–101.

de Florian, Daniel, Manuel Der, and Ignacio Fabre, 2018, "QCD ⊕ QED NNLO corrections to Drell-Yan production," Phys. Rev. D **98**, 094008.

Denner, Ansgar, Stefan Dittmaier, Tobias Kasprzik, and Alexander Mück, 2011, "Electroweak corrections to dilepton + jet production at hadron colliders," J. High Energy Phys. 06, 069.

Denner, Ansgar, Stefan Dittmaier, Tobias Kasprzik, and Alexander Mück, 2013, "Electroweak corrections to monojet production at the LHC," Eur. Phys. J. C **73**, 2297.

Denner, Ansgar, Lars Hofer, Andreas Scharf, and Sandro Uccirati, 2015, "Electroweak corrections to lepton pair production in association with two hard jets at the LHC," J. High Energy Phys. 01, 094.

Denner, Ansgar, and Stefano Pozzorini, 2001a, "One-loop leading logarithms in electroweak radiative corrections. I. Results," Eur. Phys. J. C **18**, 461–480.

Denner, Ansgar, and Stefano Pozzorini, 2001b, "One-loop leading logarithms in electroweak radiative corrections. II. Factorization of collinear singularities," Eur. Phys. J. C **21**, 63–79.

Dittmaier, Stefan, Alexander Huss, and Christian Schwinn, 2014, "Mixed QCD-electroweak $\mathcal{O}(\alpha_s \alpha)$ corrections to Drell-Yan processes in the resonance region: Pole approximation and non-factorizable corrections," Nucl. Phys. **B885**, 318–372.

Dittmaier, Stefan, Alois Kabelschacht, and Tobias Kasprzik, 2008, "Polarized QED splittings of massive fermions and dipole subtraction for non-collinear-safe observables," Nucl. Phys. **B800**, 146–189.

Dokshitzer, Yuri L., G. D. Leder, S. Moretti, and B. R. Webber, 1997, "Better jet clustering algorithms," J. High Energy Phys. 08, 001.

Duhr, Claude, Falko Dulat, and Bernhard Mistlberger, 2020a, "Charged current Drell-Yan production at N^{3}LO," J. High Energy Phys. 11, 143.

Duhr, Claude, Falko Dulat, and Bernhard Mistlberger, 2020b, "Drell-Yan Cross Section to Third Order in the Strong Coupling Constant," Phys. Rev. Lett. 125, 172001.

Ebert, Markus A., and Frank J. Tackmann, 2017, "Resummation of transverse momentum distributions in distribution space," J. High Energy Phys. 02, 110.

Ellis, R. Keith, Kirill Melnikov, and Giulia Zanderighi, 2009, "$W + 3$ jet production at the Tevatron," Phys. Rev. D 80, 094002.

Ellis, Stephen D., and Davison E. Soper, 1993, "Successive combination jet algorithm for hadron collisions," Phys. Rev. D 48, 3160–3166.

Febres Cordero, F., and L. Reina, 2015, "Electroweak gauge-boson production in association with b jets at hadron colliders," Int. J. Mod. Phys. A 30, 1530042.

Febres Cordero, F., L. Reina, and D. Wackeroth, 2006, "NLO QCD corrections to W boson production with a massive b-quark jet pair at the Tevatron p anti-p collider," Phys. Rev. D 74, 034007.

Febres Cordero, F., Fernando L. Reina, and D. Wackeroth, 2009, "W- and Z-boson production with a massive bottom-quark pair at the Large Hadron Collider," Phys. Rev. D 80, 034015.

Field, R. D., and R. P. Feynman, 1977, "Quark elastic scattering as a source of high transverse momentum mesons," Phys. Rev. D 15, 2590–2616.

Field, Richard D, and Stephen Wolfram, 1983, "A QCD model for $e + e-$ annihilation," Nucl. Phys. B213, 65–84.

Figueroa, D., S. Honeywell, S. Quackenbush, L. Reina, C. Reuschle, and D. Wackeroth, 2018, "Electroweak and QCD corrections to Z-boson production with one b jet in a massive five-flavor scheme," Phys. Rev. D 98, 093002.

Forte, Stefano, Eric Laenen, Paolo Nason, and Juan Rojo, 2010, "Heavy quarks in deep-inelastic scattering," Nucl. Phys. B834, 116–162.

Frederix, Rikkert, Stefano Frixione, Valentin Hirschi, Fabio Maltoni, Roberto Pittau, and Paolo Torrielli, 2011, "W and Z/γ^* boson production in association with a bottom-antibottom pair," J. High Energy Phys. 09, 061.

Frederix, Rikkert, Stefano Frixione, Valentin Hirschi, Fabio Maltoni, Roberto Pittau, and Paolo Torrielli, 2012, "aMC@NLO predictions for Wjj production at the Tevatron," J. High Energy Phys. 02, 048.

Frederix, Rikkert, and Stefano Frixione, 2012, "Merging meets matching in MC@NLO," J. High Energy Phys. 12, 061.

Frederix, Rikkert, Stefano Frixione, Andreas Papaefstathiou, Stefan Prestel, and Paolo Torrielli, 2016, "A study of multi-jet production in association with an electroweak vector boson," J. High Energy Phys. 02, 131.

Frixione, Stefano, 1998, "Isolated photons in perturbative QCD," Phys. Lett. B 429, 369–374.

Frixione, Stefano, Paolo Nason, and Carlo Oleari, 2007, "Matching NLO QCD computations with parton shower simulations: The POWHEG method," J. High Energy Phys. 11, 070.

Frixione, Stefano, and Bryan R. Webber, 2002, "Matching NLO QCD computations and parton shower simulations," J. High Energy Phys. 06, 029.

Frixione, Stefano, and Bryan R. Webber, 2004, "The MC@NLO 2.3 event generator," arXiv:hep-ph/0402116.

Garland, L. W., T. Gehrmann, E. W. Nigel Glover, A. Koukoutsakis, and E. Remiddi, 2002a, "The two loop QCD matrix element for $e^+e^- \to 3$ jets," Nucl. Phys. B627, 107–188.

Garland, L. W., T. Gehrmann, E. W. Nigel Glover, A. Koukoutsakis, and E. Remiddi, 2002b, "Two loop QCD helicity amplitudes for $e^+e^- \to 3$ jets," Nucl. Phys. B642, 227–262.

Gauld, R., A. Gehrmann-De Ridder, T. Gehrmann, E. W. N. Glover, and A. Huss, 2017, "Precise predictions for the angular coefficients in Z-boson production at the LHC," J. High Energy Phys. 11, 003.

Gauld, R., A. Gehrmann-De Ridder, E. W. N. Glover, A. Huss, and I. Majer, 2020, "Predictions for Z-boson production in association with a b-jet at $\mathcal{O}(\alpha_s^3)$," arXiv:2005.03016.

Gaunt, Jonathan, Maximilian Stahlhofen, Frank J. Tackmann, and Jonathan R. Walsh, 2015, "N-jettiness subtractions for NNLO QCD calculations," J. High Energy Phys. 09, 058.

Gavin, Ryan, Ye Li, Frank Petriello, and Seth Quackenbush, 2011, "FEWZ 2.0: A code for hadronic Z production at next-to-next-to-leading order," Comput. Phys. Commun. 182, 2388–2403.

Gehrmann, Thomas, Stefan Höche, Frank Krauss, Marek Schönherr, and Frank Siegert, 2013, "NLO QCD matrix elements + parton showers in $e^+e^- \to$ hadrons," J. High Energy Phys. 01, 144.

Gehrmann-De Ridder, A., T. Gehrmann, and E. W. N. Glover, 2005, "Antenna subtraction at NNLO," J. High Energy Phys. 09, 056.

Gehrmann-De Ridder, A., T. Gehrmann, E. W. N. Glover, A. Huss, and T. A. Morgan, 2016a, "NNLO QCD corrections for Drell-Yan p_T^Z and ϕ^* observables at the LHC," J. High Energy Phys. 11, 094.

Gehrmann-De Ridder, A., T. Gehrmann, E. W. N. Glover, A. Huss, and T. A. Morgan, 2016b, "Precise QCD Predictions for the Production of a Z Boson in Association with a Hadronic Jet," Phys. Rev. Lett. 117, 022001.

Gehrmann-De Ridder, A., T. Gehrmann, E. W. N. Glover, A. Huss, and T. A. Morgan, 2016c, "The NNLO QCD corrections to Z boson production at large transverse momentum," J. High Energy Phys. 07, 133.

Gehrmann-De Ridder, A., T. Gehrmann, E. W. N. Glover, A. Huss, and D. M. Walker, 2018, "Next-to-Next-to-Leading-Order QCD Corrections to the Transverse Momentum Distribution of Weak Gauge Bosons," Phys. Rev. Lett. 120, 122001.

Gehrmann-De Ridder, A., T. Gehrmann, E. W. N. Glover, A. Huss, and D. M. Walker, 2019, "Vector boson production in association with a jet at forward rapidities," Eur. Phys. J. C 79, 526.

Gerwick, Erik, Tilman Plehn, Steffen Schumann, and Peter Schichtel, 2012, "Scaling patterns for QCD jets," J. High Energy Phys. 10, 162.

Gieseke, Stefan, Frasher Loshaj, and Patrick Kirchgäßer, 2017, "Soft and diffractive scattering with the cluster model in Herwig," Eur. Phys. J. C 77, 156.

Glück, M., L. E. Gordon, E. Reya, and W. Vogelsang, 1994, "High p_T Photon Production at $p\bar{p}$ Collider," Phys. Rev. Lett. 73, 388–391.

Goncharov, M., et al. (NuTeV Collaboration), 2001, "Precise measurement of dimuon production cross sections in ν_μ Fe and $\bar{\nu}_\mu$ Fe deep inelastic scattering at the Tevatron," Phys. Rev. D 64, 112006.

Hagiwara, Kaoru, S. Ishihara, R. Szalapski, and D. Zeppenfeld, 1993, "Low-energy effects of new interactions in the electroweak boson sector," Phys. Rev. D 48, 2182–2203.

Hagiwara, Kaoru, T. Kuruma, and Y. Yamada, 1992, "Probing the one loop Zgg vertex at hadron colliders," Nucl. Phys. B369, 171–188.

Hagiwara, Kaoru, R. D. Peccei, D. Zeppenfeld, and K. Hikasa, 1987, "Probing the weak boson sector in $e^+e^- \to W^+W^-$," Nucl. Phys. B282, 253–307.

Hamberg, R., W. L. van Neerven, and T. Matsuura, 1991, "A complete calculation of the order α_s^2 correction to the Drell-Yan K factor," Nucl. Phys. B359, 343–405.

Hamilton, Keith, and Paolo Nason, 2010, "Improving NLO-parton shower matched simulations with higher order matrix elements," J. High Energy Phys. 06, 039.

Hamilton, Keith, Paolo Nason, Carlo Oleari, and Giulia Zanderighi, 2013, "Merging $H/W/Z + 0$ and 1 jet at NLO with no merging scale: A path to parton shower + NNLO matching," J. High Energy Phys. 05, 082.

Hamilton, Keith, Paolo Nason, and Giulia Zanderighi, 2012, "MINLO: Multi-scale improved NLO," J. High Energy Phys. 10, 155.

Hamilton, Keith, and Peter Richardson, 2006, "Simulation of QED radiation in particle decays using the YFS formalism," J. High Energy Phys. 07, 010.

Hamilton, Keith, Peter Richardson, and Jon Tully, 2008, "A positive-weight next-to-leading order Monte Carlo simulation of Drell-Yan vector boson production," J. High Energy Phys. 10, 015.

Hamilton, Keith, Peter Richardson, and Jon Tully, 2009, "A Modified CKKW matrix element merging approach to angular-ordered parton showers," J. High Energy Phys. 11, 038.

Hartanto, H. B., and L. Reina, 2014, "Hard-photon production with b jets at hadron colliders," Phys. Rev. D 89, 074001.

Höche, S., F. Krauss, S. Pozzorini, M. Schönherr, J. M. Thompson, and K. C. Zapp, 2014, "Triple vector boson production through Higgs-Strahlung with NLO multijet merging," Phys. Rev. D 89, 093015.

Höche, Stefan, Johannes Krause, and Frank Siegert, 2019, "Multijet merging in a variable flavor number scheme," Phys. Rev. D 100, 014011.

Höche, Stefan, Frank Krauss, Marek Schönherr, and Frank Siegert, 2011a, "Automating the POWHEG method in SHERPA," J. High Energy Phys. 04, 024.

Höche, Stefan, Frank Krauss, Marek Schönherr, and Frank Siegert, 2011b, "NLO matrix elements and truncated showers," J. High Energy Phys. 08, 123.

Höche, Stefan, Frank Krauss, Marek Schönherr, and Frank Siegert, 2012, "A critical appraisal of NLO + PS matching methods," J. High Energy Phys. 09, 049.

Höche, Stefan, Frank Krauss, Marek Schönherr, and Frank Siegert, 2013a, "QCD matrix elements + parton showers: The NLO case," J. High Energy Phys. 04, 027.

Höche, Stefan, Frank Krauss, Marek Schönherr, and Frank Siegert, 2013b, "$W + n$-Jet Predictions at the Large Hadron Collider at Next-to-Leading Order Matched with a Parton Shower," Phys. Rev. Lett. 110, 052001.

Höche, Stefan, Frank Krauss, Steffen Schumann, and Frank Siegert, 2009, "QCD matrix elements and truncated showers," J. High Energy Phys. 05, 053.

Höche, Stefan, Ye Li, and Stefan Prestel, 2015, "Drell-Yan lepton pair production at NNLO QCD with parton showers," Phys. Rev. D 91, 074015.

Höche, Stefan, Stefan Prestel, and Holger Schulz, 2019, "Simulation of vector boson plus many jet final states at the high luminosity LHC," Phys. Rev. D 100, 014024.

Hollik, W., B. A. Kniehl, E. S. Scherbakova, and O. L. Veretin, 2015, "Electroweak corrections to Z-boson hadroproduction at finite transverse momentum," Nucl. Phys. B900, 576–602.

Ita, H., Z. Bern, L. J. Dixon, Fernando Febres Cordero, D. A. Kosower, and D. Maître, 2012, "Precise predictions for $Z + 4$ jets at hadron colliders," Phys. Rev. D 85, 031501.

Jäger, B., 2010, "Next-to-leading order QCD corrections to photon production via weak-boson fusion," Phys. Rev. D 81, 114016.

Jäger, Barbara, Steven Schneider, and Giulia Zanderighi, 2012, "Next-to-leading order QCD corrections to electroweak Zjj production in the POWHEG BOX," J. High Energy Phys. 09, 083.

Ježo, Tomas, Michael Klasen, and Florian König, 2016, "Prompt photon production and photon-hadron jet correlations with POWHEG BOX," J. High Energy Phys. 11, 033.

Johnson, Mark, and Daniel Maître, 2018, "Strong coupling constant extraction from high-multiplicity $Z + $ jets observables," Phys. Rev. D 97, 054013.

Kallweit, Stefan, Jonas M. Lindert, Philipp Maierhöfer, Stefano Pozzorini, and Marek Schönherr, 2015, "NLO electroweak automation and precise predictions for $W + $ multijet production at the LHC," J. High Energy Phys. 04, 012.

Kallweit, Stefan, Jonas M. Lindert, Philipp Maierhöfer, Stefano Pozzorini, and Marek Schönherr, 2016, "NLO QCD + EW predictions for $V + $ jets including off-shell vector-boson decays and multijet merging," J. High Energy Phys. 04, 021.

Kallweit, Stefan, Jonas M. Lindert, Stefano Pozzorini, Marek Schönherr, and Philipp Maierhöfer, 2015, "NLO QCD + EW automation and precise predictions for $V + $ multijet production," arXiv:1505.05704.

Karlberg, Alexander, Emanuele Re, and Giulia Zanderighi, 2014, "NNLOPS accurate Drell-Yan production," J. High Energy Phys. 09, 134.

Kom, Chun-Hay, and W. James Stirling, 2010, "Charge asymmetry in $W + $ jets production at the LHC," Eur. Phys. J. C 69, 67–73.

Kosower, David A., 1998, "Antenna factorization of gauge theory amplitudes," Phys. Rev. D 57, 5410–5416.

Krauss, Frank, Petar Petrov, Marek Schönherr, and Michael Spannowsky, 2014, "Measuring collinear W emissions inside jets," Phys. Rev. D 89, 114006.

Kühn, Johann H., A. Kulesza, S. Pozzorini, and M. Schulze, 2005a, "Logarithmic electroweak corrections to hadronic $Z + 1$ jet production at large transverse momentum," Phys. Lett. B 609, 277–285.

Kühn, Johann H., A. Kulesza, S. Pozzorini, and M. Schulze, 2005b, "One-loop weak corrections to hadronic production of Z bosons at large transverse momenta," Nucl. Phys. B727, 368–394.

Kühn, Johann H., A. Kulesza, S. Pozzorini, and M. Schulze, 2006, "Electroweak corrections to hadronic photon production at large transverse momenta," J. High Energy Phys. 03, 059.

Kühn, Johann H., A. Kulesza, S. Pozzorini, and M. Schulze, 2007, "Electroweak corrections to large transverse momentum production of W bosons at the LHC," Phys. Lett. B 651, 160–165.

Kühn, Johann H., A. Kulesza, S. Pozzorini, and M. Schulze, 2008, "Electroweak corrections to hadronic production of W bosons at large transverse momenta," Nucl. Phys. B797, 27–77.

Ladinsky, G. A., and C. P. Yuan, 1994, "Nonperturbative regime in QCD resummation for gauge boson production at hadron colliders," Phys. Rev. D 50, R4239.

Lam, C. S., and Wu-Ki Tung, 1978, "Systematic approach to inclusive lepton pair production in hadronic collisions," Phys. Rev. D 18, 2447.

Lam, C. S., and Wu-Ki Tung, 1980, "Parton-model relation without quantum-chromodynamic modifications in lepton pair production," Phys. Rev. D 21, 2712.

Lavesson, Nils, and Leif Lönnblad, 2008a, "Extending CKKW-merging to one-loop matrix elements," J. High Energy Phys. 12, 070.

Lavesson, Nils, and Leif Lönnblad, 2008b, "Merging parton showers and matrix elements: Back to basics," J. High Energy Phys. 04, 085.

LHCb Collaboration, 2014a, "Observation of associated production of a Z boson with a D meson in the forward region," J. High Energy Phys. 04, 091.

LHCb Collaboration, 2014b, "Study of forward Z + jet production in pp collisions at √s = 7 TeV," J. High Energy Phys. 01, 033.

LHCb Collaboration, 2015a, "Measurement of the forward-backward asymmetry in Z/γ* → μ⁺μ⁻ decays and determination of the effective weak mixing angle," J. High Energy Phys. 11, 190.

LHCb Collaboration, 2015b, "Measurement of the Z + b-jet cross-section in pp collisions at √s = 7 TeV in the forward region," J. High Energy Phys. 01, 064.

LHCb Collaboration, 2015c, "LHCb detector performance," Int. J. Mod. Phys. A 30, 1530022.

LHCb Collaboration, 2015d, "Study of W boson production in association with beauty and charm," Phys. Rev. D 92, 052001.

LHCb Collaboration, 2016, "Measurement of forward W and Z boson production in association with jets in proton-proton collisions at √s = 8 TeV," J. High Energy Phys. 05, 131.

LHCb Collaboration, 2019a, "Design and performance of the LHCb trigger and full real-time reconstruction in run 2 of the LHC," J. Instrum. 14, P04013.

LHCb Collaboration, 2019b, "Measurement of Charged Hadron Production in Z-Tagged Jets in Proton-Proton Collisions at √s = 8 TeV," Phys. Rev. Lett. 123, 232001.

LHCb Collaboration, 2019c, "Measurement of the electron reconstruction efficiency at LHCb," J. Instrum. 14, P11023.

Li, Ye, and Frank Petriello, 2012, "Combining QCD and electroweak corrections to dilepton production in the framework of the FEWZ simulation code," Phys. Rev. D 86, 094034.

Lindert, J. M., et al., 2017, "Precise predictions for V + jets dark matter backgrounds," Eur. Phys. J. C 77, 829.

Lönnblad, Leif, 2002, "Correcting the color dipole cascade model with fixed order matrix elements," J. High Energy Phys. 05, 046.

Lönnblad, Leif, and Stefan Prestel, 2012, "Matching tree-level matrix elements with interleaved showers," J. High Energy Phys. 03, 019.

Lönnblad, Leif, and Stefan Prestel, 2013a, "Merging multi-leg NLO matrix elements with parton showers," J. High Energy Phys. 03, 166.

Lönnblad, Leif, and Stefan Prestel, 2013b, "Unitarising matrix element + parton shower merging," J. High Energy Phys. 02, 094.

Maguire, Eamonn, Lukas Heinrich, and Graeme Watt, 2017, "HEP-Data: A repository for high energy physics data," J. Phys. Conf. Ser. 898, 102006.

Maître, Daniel, and Sebastian Sapeta, 2013, "Simulated NNLO for high-p_T observables in vector boson + jets production at the LHC," Eur. Phys. J. C 73, 2663.

Mangano, Michelangelo L., Mauro Moretti, and Roberto Pittau, 2002, "Multijet matrix elements and shower evolution in hadronic collisions: $Wb\bar{b}$ + n jets as a case study," Nucl. Phys. B632, 343–362.

Mantry, Sonny, and Frank Petriello, 2011, "Transverse momentum distributions in the nonperturbative region," Phys. Rev. D 84, 014030.

Melnikov, Kirill, and Frank Petriello, 2006a, "Electroweak gauge boson production at hadron colliders through $O(\alpha_s^2)$," Phys. Rev. D 74, 114017.

Melnikov, Kirill, and Frank Petriello, 2006b, "The W Boson Production Cross Section at the LHC through $O(\alpha_s^2)$," Phys. Rev. Lett. 96, 231803.

Mirkes, E., 1992, "Angular decay distribution of leptons from W bosons at NLO in hadronic collisions," Nucl. Phys. B387, 3–85.

Mirkes, E., and J. Ohnemus, 1994, "W and Z polarization effects in hadronic collisions," Phys. Rev. D 50, 5692–5703.

Moch, Sven, Peter Uwer, and Stefan Weinzierl, 2002, "Two loop amplitudes with nested sums: Fermionic contributions to $e^+e^- \to q\bar{q}g$," Phys. Rev. D 66, 114001.

Monni, Pier Francesco, Paolo Nason, Emanuele Re, Marius Wiesemann, and Giulia Zanderighi, 2020, "MiNNLO_PS: A new method to match NNLO QCD to parton showers," J. High Energy Phys. 05, 143.

Monni, Pier Francesco, Emanuele Re, and Paolo Torrielli, 2016, "Higgs Transverse-Momentum Resummation in Direct Space," Phys. Rev. Lett. 116, 242001.

Mück, Alexander, and Lennart Oymanns, 2017, "Resonace-improved parton-shower matching for the Drell-Yan process including electroweak corrections," J. High Energy Phys. 05, 090.

Nason, Paolo, 2004, "A New method for combining NLO QCD with shower Monte Carlo algorithms," J. High Energy Phys. 11, 040.

Oleari, Carlo, and Laura Reina, 2011, "$W^{\pm} b\bar{b}$ production in POWHEG," J. High Energy Phys. 08, 061.

Oleari, Carlo, and Dieter Zeppenfeld, 2004, "QCD corrections to electroweak $l\nu_l jj$ and $l^+l^- jj$ production," Phys. Rev. D 69, 093004.

Plätzer, Simon, 2013, "Controlling inclusive cross sections in parton shower + matrix element merging," J. High Energy Phys. 08, 114.

Re, Emanuele, 2012, "NLO corrections merged with parton showers for Z + 2 jets production using the POWHEG method," J. High Energy Phys. 10, 031.

Rubin, Mathieu, Gavin P. Salam, and Sebastian Sapeta, 2010, "Giant QCD K-factors beyond NLO," J. High Energy Phys. 09, 084.

Schissler, Franziska, and Dieter Zeppenfeld, 2013, "Parton shower effects on W and Z production via vector boson fusion at NLO QCD," J. High Energy Phys. 04, 057.

Schönherr, Marek, and Frank Krauss, 2008, "Soft photon radiation in particle decays in SHERPA," J. High Energy Phys. 12, 018.

Seymour, Michael H., 1992, "Photon radiation in final state parton showering," Z. Phys. C 56, 161–170.

Siegert, Frank, 2017, "A practical guide to event generation for prompt photon production with SHERPA," J. Phys. G 44, 044007.

Sjöstrand, T., and Peter Z. Skands, 2004, "Multiple interactions and the structure of beam remnants," J. High Energy Phys. 03, 053.

Sjöstrand, Torbjörn, Stefan Ask, Jesper R. Christiansen, Richard Corke, Nishita Desai, Philip Ilten, Stephen Mrenna, Stefan Prestel, Christine O. Rasmussen, and Peter Z. Skands, 2015, "An introduction to PYTHIA 8.2," Comput. Phys. Commun. 191, 159.

Sjöstrand, Torbjörn, and Maria van Zijl, 1987, "A multiple interaction model for the event structure in hadron collisions," Phys. Rev. D 36, 2019.

Stavreva, T. P., and J. F. Owens, 2009, "Direct photon production in association with a heavy quark at hadron colliders," Phys. Rev. D 79, 054017.

Stewart, Iain W., Frank J. Tackmann, and Wouter J. Waalewijn, 2011, "Beam Thrust Cross Section for Drell-Yan Production at Next-to-Next-to-Leading-Logarithmic Order," Phys. Rev. Lett. 106, 032001.

Tackmann, Frank J., Jonathan R. Walsh, and Saba Zuberi, 2012, "Resummation properties of jet vetoes at the LHC," Phys. Rev. D **86**, 053011.

Vesterinen, M., and T. R. Wyatt, 2009, "A novel technique for studying the Z boson transverse momentum distribution at hadron colliders," Nucl. Instrum. Methods Phys. Res., Sect. A **602**, 432–437.

Webber, B. R., 1984, "A QCD model for jet fragmentation including soft gluon interference," Nucl. Phys. **B238**, 492–528.

Winter, Jan-Christopher, Frank Krauss, and Gerhard Soff, 2004, "A modified cluster hadronization model," Eur. Phys. J. C **36**, 381–395.

Yennie, D. R., Steven C. Frautschi, and H. Suura, 1961, "The infrared divergence phenomena and high-energy processes," Ann. Phys. (N.Y.) **13**, 379–452.